공학박사 학위논문

APPLICATIONS OF MICROFLUIDIC CHIPS WITH POLYELECTROLYTIC GEL ELECTRODES

고분자 전해질 전극이 집적된 마이크로 유동칩 응용 연구

2013 년 2 월

서울대학교 대학원

협동과정 바이오엔지니어링 전공

김 광 복

APPLICATIONS OF MICROFLUIDIC CHIPS WITH POLYELECTROLYTIC GEL ELECTRODES

고분자 전해질 전극이 집적된 마이크로 유동칩 응용 연구

지도교수 김 희 찬

이 논문을 공학박사 학위논문으로 제출함

2013 년 **1** 월

서울대학교 대학원

협동과정 바이오엔지니어링 전공

김 광 복

김광복의 박사 학위논문을 인준함

2013 년 **1** 월

위 원 장 정 택 동 (인)

부위원장 김 희 찬 (인)

위 원 허 동 은 (인)

위 원 천 홍 구 (인)

위 원 주 세 경 (인)

Ph.D. Dissertation

APPLICATIONS OF MICROFLUIDIC CHIPS WITH POLYELECTROLYTIC GEL ELECTRODES

BY

KWANG BOK KIM

FEBRUARY 2013

INTERDISCIPLINARY PROGRAM FOR BIOENGINEERING

THE GRADUATE SCHOOL

SEOUL NATIONAL UNIVERSITY

APPLICATIONS OF MICROFLUIDIC CHIPS WITH POLYELECTROLYTIC GEL ELECTRODES

BY

KWANG BOK KIM

INTERDISCIPLINARY PROGRAM FOR BIOENGINEERING

THE GRADUATE SCHOOL

SEOUL NATIONAL UNIVERSITY

THIS DISSERTATION IS APPROVED FOR

THE DEGREE OF DOCTOR OF PHILOSOPHY

FEBRUARY 2013

DOCTORAL COMMITTEE :

Chairman _____ *Taek Dong Chung, Ph.D.*

Vice Chairman _____ *Hee Chan Kim. Ph.D.*

Member _____ *Dongeun Huh, Ph.D.*

Member _____ *Honggu Chun, Ph.D.*

Member _____ *Segyeong Joo, Ph.D.*

Abstract

APPLICATIONS OF MICROFLUIDIC CHIPS WITH POLYELECTROLYTIC GEL ELECTRODES

By

Kwang Bok Kim

Interdisciplinary Program for Bioengineering
The Graduate School
Seoul National University

This dissertation is focused on a variety of designs, fabrication processes, and innovative biomedical, electrical, and analytical chemistry applications of microfluidic systems with polyelectrolytic gel electrodes (PGEs) including poly-diallyldimethylammonium chloride (pDADMAC) and poly-2-acrylamido-2-methyl-1-propanesulfonic acid (pAMPSA) as positively and negatively charged polymer, respectively.

First, to rapidly count the number of red blood cells (RBCs), we developed a novel microfluidic chip-based cell counter with positively

charged PGEs. The proposed microdevice is based on the principle that the impedance across a microchannel between two PGEs varies sensitively as RBCs pass through it. The number and amplitude of impedance peaks provide the information about the number and size of RBCs, respectively. The performance of this PGEs-based system was evaluated in three steps. First, in order to observe the size-only dependence of the impedance signal, three different sizes of fluorescent microbeads (7.2, 10.0, and 15.0 μm) were used in the experiment. Second, the cell counting performance was evaluated by using 7.2 μm fluorescent microbeads, similar in size to RBCs, in various concentrations and comparing the results with an animal hematoanalyzer. Finally, in human blood sample tests, intravenously collected whole blood was just diluted in a PBS without centrifuge or other pretreatments. The PGE-based system produced almost identical number of RBCs in over 800 fold diluted samples to the results from a commercialized human hematoanalyzer.

Second, using the oppositely charged pDADMAC and pAMPSA polyelectrolytes, we elaborate controlled the ionic current in polyelectrolyte junction field effect transistor (pJFET). The polyelectrolyte plugs were formed at two spots in the microchannel network. The positively charged pDADMAC and negatively charged pAMPSA polyelectrolytes allow the selective passage of anions and cations, respectively. The ionic current of the mainchannel is sensitively affected by the extent of ion depletion that is caused by intensive ion extraction through the polyelectrolyte plugs under a gate

voltage.

Finally, we developed a reversible preconcentration of gold nanoparticles (AuNPs) for chemical analysis based on surface-enhanced Raman scattering (SERS) in a microfluidic system. AuNPs homogeneously dispersed in solution were locally preconcentrated by charge-selective ion extraction through a pair of negatively charged polyelectrolyte plugs. This phenomenon created dynamic hot spots among the preconcentrated AuNPs that could be redispersed as required. Hugely intensified SERS signals from the concentrated AuNPs plug in the microfluidic system provided the fingerprint information about the molecules that were adsorbed on the AuNP surfaces or dissolved in the solution phase in reproducible manner. This unique behavior of nanoparticles handled by microfluidics suggests new opportunities for non-invasive and non-destructive monitoring of molecular species in chemical or biological samples, possibly for use during sequential processes on massively integrated chips.

Keywords : Polyelectrolyte, Electrokinetics, Microfluidics, Cell counter, Polyelectrolyte Junction Field Effect Transistor (pJFET), Surface-enhanced Raman Scattering (SERS)

Student Number : 2007-21272

CONTENTS

List of Figures

Chapter 1.

Introduction

Polyelectrolytes are polymers which have positively and negatively charged ionizable groups along the polymer chain. They are generally soluble in polar solvents, such as water, whose solubility is caused by the electrostatic interactions between water and the charged monomer. The polyelectrolytes are classified into natural polyelectrolytes, synthetic polyelectrolytes, and chemically modified biopolymers. In electrochemistry, they are classified as polyacids (polyanions), polybase (polycations), and polyampholytes. The anionic polyelectrolytes are generally homo- and copolymers of sodium salt of acrylic acid with acrylamide, which are called polyacrylamides. The most representative examples of anionic polyelectrolytes are poly styrene sulfonic acids (PSSA) and

poly-2-acrylamido-2-methyl-1-propanesulfonic acid (pAMPSA). The cationic polyelectrolytes are homo- or copolymers with acrylamide, which can be generally produced by copolymerising acrylamide with different ratio of amino-derivatives of acrylic acid or methacrylic acid esters. For example, diallyldimethylammonium chloride (DADMAC) is synthesised from allyl chloride and dimethylamine. Poly-DADMAC (pDADMAC) can be formed from radical polymerization of DADMAC. The ampholytic polyelectrolytes are crosslinked polymers containing both positively and negatively charged repeat units, such as acidic and basic vinyl monomers, sulfobetaine monomers, ion-pair comonomers, and charged anionic and cationic monomers. The polyampholytes have a balanced stoichiometry that means same number of negative and positive monomers, which is essentially controlled by attractive electrostatic interactions. In general, the polyampholytes are usually insoluble in water. To dissolve in water, it is necessary to add salts which screen and weaken the chemical interaction [1].

The recent advances in the preparation and characterization of polymeric materials have been adopted in biological systems due to their potential applications, for example membranes, coating on films and fibers, isolation of protein and DNA, microcapsules for drug delivery [2]. In addition, to recreate the complex cell structures, the soft and wet nature of polyelectrolytes have provided a proper adhesion to cells, elasticity, and mechanical strength. For instance, a functional endothelial cells on the artificial blood vascular can adhere

and proliferate to charged polyelectrolyte gels, such as pAMPSA [3]. The polyelectrolyte plugs also have unique electrical responses. When an AC current with certain amplitude and frequency is applied, the polyelectrolyte plugs have similar dynamic movement of biological systems, such as muscle, leading to creation artificial organs [4].

Recently, many researchers have developed a faster and easier way to fabricate electrodes in microfluidic systems. Metallic microelectrodes have been used for numerous microdevices, such as heaters, biosensors, mixers, pumps, actuators, and sorters based on electrokinetic phenomena. A common way for fabrication of metallic electrodes is thermal or e-beam evaporation, electrochemical deposition and sputtering. However, these methods require multiple fabrication steps and it is difficult to accurately align the electrodes with the desired microchannels. As one of the alternative way to replace the metallic electrodes, polymer plugs are created in the microchannel to maintain ionic contact between the microfluidic systems and electrodes. The polymer plugs are easily fabricated by conventional polymerization processes and can electrically connect the electrodes by ionic current in the microchannel.

The major objective of this dissertation is to explore possibility of polyelectrolytes gel electrodes (PGEs) as electrodes in microfluidic systems and certify its properties through various applications. In chapter two, I present a novel microfluidic chip with PGEs used to rapidly count the number of red blood cells (RBCs) in diluted whole blood. The proposed microdevice is based on the principle that the

impedance across a microchannel between two PGEs varies sensitively as RBCs pass through it. The number and amplitude of impedance peaks provide the information about the number and size of RBCs, respectively. This system features a low-voltage dc detection method and noncontact condition between cells and metal electrodes. Major advantages include stable detection under varying cellular flow rate and position in the microchannel, little chance of cell damage due to high electric field gradient and no surface fouling of the metal electrodes.

Chapter three provides the second application for polyelectrolyte junction field effect transistor capable of operating in an aqueous microfluidic network on a chip. In this research, poly-diallyl dimethylammonium chloride and poly-2-acrylamido-2-methyl-1-propanesulfonic acid are used for the elaborate control of the ion flow by selective extraction of anions and cations from the microchannel. The rate of ion extraction can be regulated by simply adjusting the gate voltage, and it results in ion depletion in the vicinity of the polyelectrolyte plugs. The extent of ion depletion between the polyelectrolyte plugs is a sensitive function of the ion resistance of the microchannel; therefore, the current between the source and the drain can be controlled by regulating the gate voltage.

Finally, the fourth chapter presents a reversible preconcentration of gold nanoparticles (AuNPs) for chemical analysis based on surface-enhanced Raman scattering (SERS) in a microfluidic system. AuNPs homogeneously dispersed in solution were locally

preconcentrated by charge-selective ion extraction through a pair of negatively charged polyelectrolyte plugs. This phenomenon created dynamic hot spots among the preconcentrated AuNPs that could be redispersed as required. Hugely intensified SERS signals from the concentrated AuNPs plug in the microfluidic system provided the fingerprint information about the molecules that were adsorbed on the AuNP surfaces or dissolved in the solution phase in reproducible manner. This unique behavior of nanoparticles handled by microfluidics suggests new opportunities for non-invasive and non-destructive monitoring of molecular species in chemical or biological samples, possibly for use during sequential processes on massively integrated chips.

Chapter 2.

Application I

Microfluidic Chip for Red Blood Cell Quantification

2.1 Introduction

2.1.1 Blood Analysis

Blood analysis is used to determine physiological and biochemical state, such as disease, mineral content, drug effectiveness, and organ function. For the blood test, veinpuncture is used to obtain cells and extracellular fluid from human body. Blood commonly drawn from the vein of the arm, finger, and the earlobe, and it is composed of

plasma, red blood cells, white blood cells, and platelets. Blood plays an important role as a medium for providing oxygen and nutrients, and drawing wastes to the excretory systems for disposal. Since blood affects and is affected by many medical condition, blood tests are the most commonly performed medical tests.

Many blood tests are designed to determine the number of red blood cells and white blood cells, together with the volume, sedimentation rate, and hemoglobin concentration of red blood cells. In addition, blood is analyzed on the basis of properties such as the shape and structural details of cells and hemoglobin, total volume, viscosity, clotting and clotting abnormalities, pH, and level of oxygen and carbon dioxide.

Attention is increasingly being paid to live cells in biological research as well as the clinical diagnosis of diseases. The quantity, shape, and size of the cells in human blood are very important factors in the sustained metabolism of a human body. That is why a large part of cell research and clinical diagnosis involves the quantification of blood cells [5-7]. In particular, the red blood cell (RBC) count (the number of RBCs per volume of blood) is a key indication of clinical problems such as anemia, so that the demand for handy, fast, and cost-effective RBC counters is high and continues to grow.

2.1.2 Conventional Methods for Blood Counting

2.1.2.1 Manual Method

The manual method via a hemacytometer is a standard technique in biological and clinical laboratories [Figure 2.1]. The hemacytometer consist of two chamber, each of which is divided into 9 squares. This chamber is engraved with a laser-etched grid of perpendicular lines. The device is delicately crafted so that the area bounded by the lines and the depth of the chamber are known. It is therefore possible to count the number of cells in a specific volume of fluid, and thereby calculate the concentration of cells in the fluid overall. To count the number of cells, the mirror-like polished surface and coverslip for counting chamber are carefully cleaned. The coverslip is placed over the counting surface prior to injection the sample. After introducing the sample into one of the V-shape wells, the counting chamber is placed on the microscope stage and operators count the number of cells in a certain volume visually. The hemacytometer extremely labor intensive and tedious for researchers, because there is so much subjectivity, counts are sometimes unreliable and difficult to reproduce [8, 9].

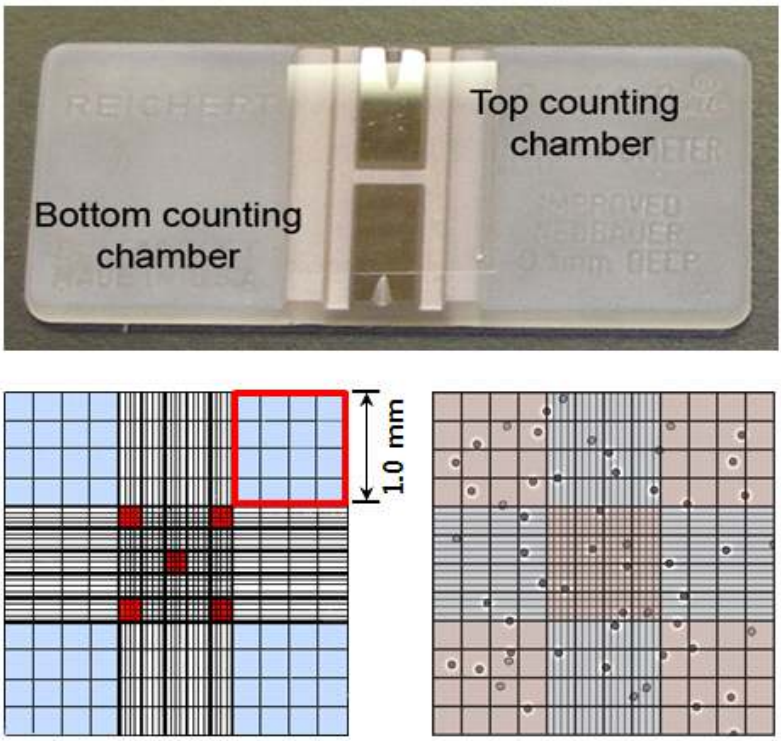

Figure 2.1 Conventional hemacytometer is an enclosed chamber with two V-shape ports for sample introduction. The grid on standard hemacytometer with Neubauer rulings have 9 large squares, and each square has a surface area of 1 mm^2, and the depth of the chamber is 0.1 mm.

2.1.2.2 Optical Method

Fluorescent-activated cell sorters (FACS) is an one of the most useful optical methods for cell counting and sorting in biological research area. FACS was invented in the late 1960s by Bill Bonnerm Rechard Sweet, Russ Hullett, etc., and Becton Dickinson Immunocytometry Systems introduced the commercial machines in the early 1970s. Today, FACS can simultaneously measure 12 fluorescence and 2 scattering light.

As shown in Figure 2.2, FACS consists of sheath fluid, vibrating nozzle, laser, detector, analyzer, and charger. The sheath fluid aligns the cells so that they pass single file through the detecting area, and the vibrating nozzle breaks the cell suspension into fine droplet. FACS generally employ lasers of different wavelengths to extract information about the size, shape, and internal structure from each cell's fluorescence, scattered light, and transmitted light which are detected by photo sensors, such as photomultiplier tube (PMT). The disadvantages of this method include the relatively high cost and difficulty in miniaturization of the optical equipment. The analyzer decides the fluorescence type, such as Lucifer yellow, GFP, Fluorescein, Texas Red, Cascade Blue, Alexa Flour, Ethidium Bromide, Chromomycin A3, Azurite, and Calcein and feedback the charge information of the cells to the charger which gives a specific electric charge for cell sorting [10].

Since FACS acknowledges the now enormous field of flow

cytometry and its many applications in immunology, cell biology, and molecular biology, and its clinical applications in AIDS, leukemia/lymphoma, and cancer detection and analysis, as well as clinical chemistry, this method is relatively high cost and has difficulties in miniaturization of the optical equipment.

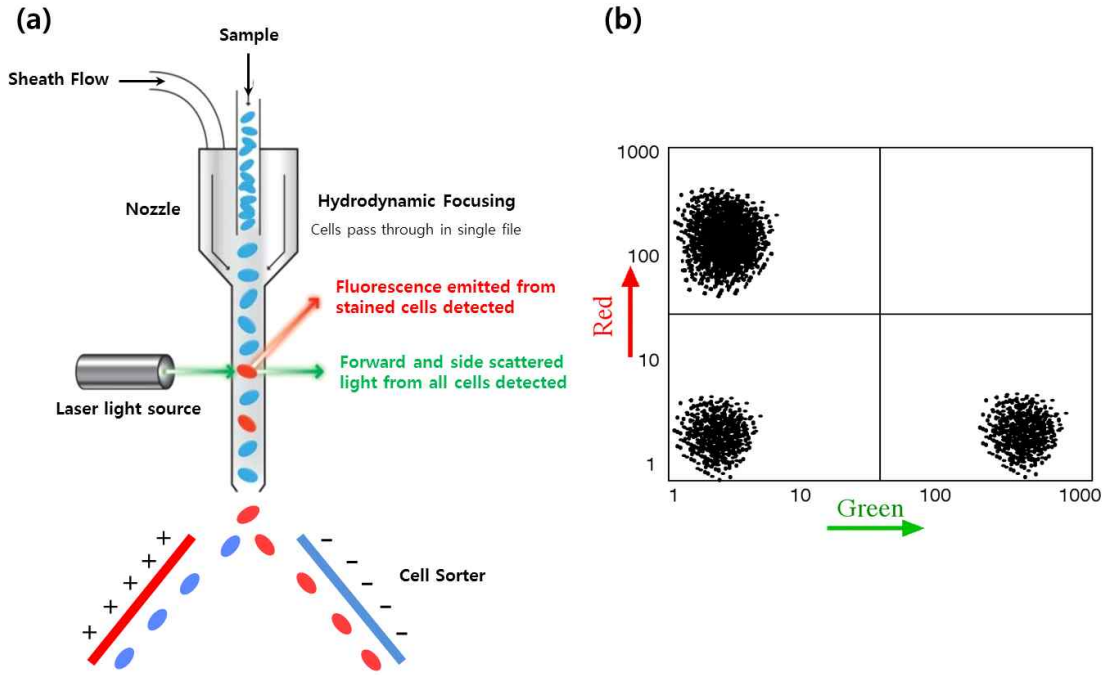

Figure 2.2 Diagram of FACS, (a) The cells labeled with fluorescent dye pass in a single file. Laser excites the dye of the cells and optical sensors detects the emitted light and transduce the optical signals to the electric signals. Finally, cells pass between a pair of charged metal plates. Positively charged cells are attracted by negatively charged plate and vice versa. (b) The intensity of the fluorescence dyes are plotted on X and Y-axis.

2.1.2.3 Coulter Counter Method

The Coulter counter, also referred to as the Aperture-Impedance Method, is commercialized automatic blood cell counter. It was developed initially by Wallace H. Coulter [11]. In this method, a small aperture between two electrodes is under an electric field and the momentary changes of current by cells which pass through the current carrying aperture are counted and classified according to amplitude, as shown in Figure 2.3 [12, 13].

Because Coulter counter method is simple and accurate method for cell or particle counting, many hospital laboratories adopt the method to replace the conventional manual method that manually count each cells under a microscope and typically took a half hour. Furthermore, Coulter method is useful for biological analysis about DNA and virus, and industrial application, such as paint, ceramics, glass, molten metals and food manufacture. They are also routinely employed for quality control. Recently, as reducing the size and adopting multiple channels in the coulter counter, their measurement times are saved.

The Coulter counter is more cost-effective, less time-consuming, and easier to miniaturize than other methods, even though it is not as informative or accurate as the optical method.

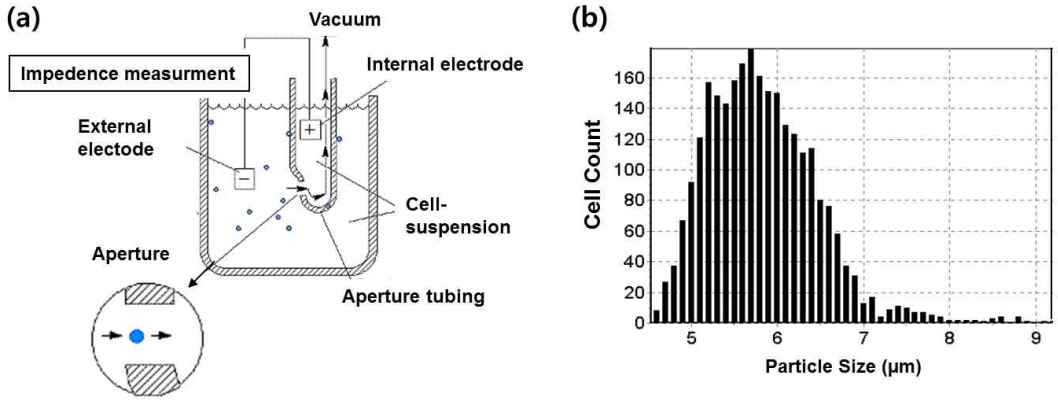

Figure 2.3 Diagram of the basics of the Coulter principle. (a) A tube with a small aperture on the wall is immersed into a beaker that contains particles suspended in a low concentration electrolyte. Two electrodes, one inside the aperture tube and one outside the aperture tube but inside the beaker, are placed and a current path is provided by the electrolyte when an electric field is applied. The impedance between the electrodes is then measured. The pulse height is proportional to the volume of the sensed particle. (b) The total number of the cells for a variety of particle sizes.

2.1.3 Microfluidic Chip-based Cell Counters

Microfluidics was defined as the science and technology of systems to manipulate small amount of fluids (10^{-9} to 10^{-18} liters) in microchannels, and micromachining technologies, such as photo- and softlithography, and microcontact printing allowed microfluidic chip to have the ability to control very small quantities of samples and reagents in the microchannels. Using these technologies, microfluidic chips have wide range of applications, such as chemical analyses (pH, ionic strength, and concentration), high-throughput screening in drug development, examination and manipulation of a single cell and molecule, synthesis of organic compounds, generation and manipulation of monodisperse bubbles and droplets, and microchip-based organ models [14].

The most highly developed of their applications is microfluidic chip-based cell counters for clinical and biological use. As shown in Figure 2.4, in these chip-based systems, the impedance change is monitored in the same way as for macro-scale systems, using a pair of metal electrodes across an aperture fabricated inside a microfluidic chip [15-17]. Miniaturized flow cytometers are also being attempted based on the fact that the scattered laser light [18-20] and fluorescent emissions provide valuable information about the objects, such as size, number, protein expression, etc. [21]. Recently, we have been seeing an acceleration in the development of microfluidic chip flow cytometry [22-24].

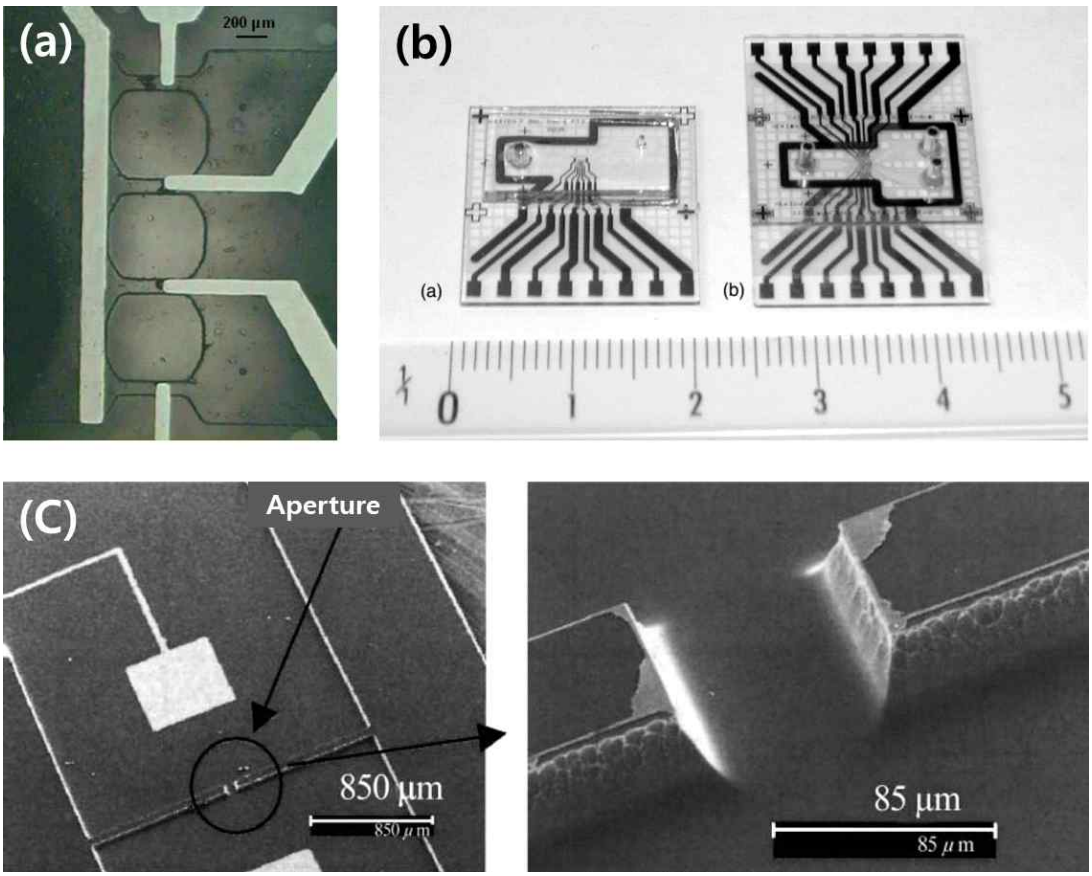

Figure 2.4 Microfluific chip-based cell counters. (a) Four-channel micromachined Coulter counter with gold electrodes. (b) Micro Coulter particle counter (uCPC) with Titanium and Platinum electrodes. (c) A sensor device with Platinum electrodes for blood cell counting using microelectromechanical systems (MEMS) technology.

2.1.4 Goals of This Study

Despite an enormous accomplishment of microfluidic chips-based cell counter, metal electrodes were still adopted as one of the major components, which is causing several problems. The developed microfluidic Coulter counter obtain the impedance signals between the coplanar or from two facing metal electrodes. When electric field is applied to the electrodes via a narrow orifice in the reservoir, single cell or particle passing through the microchannel causes the impedance change of the electrodes. However, when high concentrations of cells are present, the cells will be closer together and two or more cells will pass through the detection region at one time. Therefore, the coulter counter counts them as one and larger particle, the so-called Coincidence Lose. To overcome this problem, a pair of electrodes facing each other was fabricated on the orifice wall. However, as shown by many reports, it is difficult to fabricate the well-defined solid-state electrodes in such an arrangement. Even if such electrodes can be made, only ac current with high frequency is allowed to obtain the data for impedance analysis because the largest part of electric dc or low-frequency potential drops across the electrode surface and thus the presence of a cell between the electrodes does not bring about significant change in impedometry.

The present study proposes a simple system to rapidly count the number of red blood cells (RBCs) by creating polyelectrolytic gel electrodes (PGEs) on a microfluidic chip. When an electric field is

applied across a pair of PGEs spaced from each other by the width of the microchannel, the counter ions of the polyelectrolytes carry the charge. This unique system was utilized to implement cytometry and velocimetry in the microchannels of a microfluidic chip [25], and an effective micro-mixer was constructed based on ion depletion between PGEs [26]. The PGEs let the microchannel separated from the electrodes in the reservoirs so that there is no contact between metal electrodes and diluted blood and aggregation of blood cells or bubbles at electrodes is prevented at electrode. As a result, cells passing between the PGEs produce significant impedance that varies very sensitively with their size. Furthermore, this method is expected to work with even lower dilution factor and thus to require a far smaller volume of whole blood (2 μl) and phosphate buffered saline (PBS) than the Aperture-Impedance Method, in which the electrodes are immersed in the inlet and outlet with samples that are whole blood diluted by 20,000 times or more to reduce the coincident effect.

2.2 Experimental Section

2.2.1 Microfluidic Chip Fabrication

Microfluidic chip is fabricated by standard photolithography and the microchannel has 70 μm wide and 30 μm deep [Figure 2.5]. A Corning 2947 (7.5 x 2.5 x 0.1 cm^3) glass was soaked in a piranha solution (H_2O_2 : H_2SO_4 = 1:3) and cleaned for 45 min. After cleaning

with the piranha solution, it was washed with deionized (DI)-water (NANOpure Diamond, Barnstead), and then with acetone (CMOS grade, J.T.Baker, USA) and methanol (CMOS grade, J.T.Baker, USA). This process was repeated three times. Moisture was completely removed from the glass with clean air, and the glass was put on a hot plate of 150 ℃ for 100 min. The glass was cooled at room temperature for 90 s. Then, the glass was coated with HMDS (Hexa methyl di silazane, Clariant, Switzerland) using a spin-coater (Won Corp.) at 6000 rpm for 30 s. HMDS helps stronger adherence of photoresist (PR) to glass. The glass coated with HMDS was placed on a hot plate of 120 ℃ for 3 min and cooled at room temperature for 90 s. Photoresist (PR) AZ4620 (Clariant) was spreaded on the glass using a spin coater. The spin coater was activated at 500 rpm for 7.5 s and at 6000 rpm for 30 s. The PR-coated glass was soft baked on a hot plate of 100 ℃ for 90 s and cooled at room temperature for 90 s. Then the pattern designed using Silverwriter (Mania barco) was drawn on a mask film (accumax photoplotter film, Kodak). These mask film and glass were aligned by using a UV aligner (MDA-400M, Midas) and exposed to UV light for 10 s. From the exposed glass, the PR in the pattern part which would be etched by AZ400K (Clariant) developer was removed. The developer is repetitively replaced in every 90 s. Before soaking the glass in a new developer solution, the glass surface was cleaned with DI-water and dried with clean air, and this process was repeated three times. The degree of development was checked through a microscope, and then

the glass was hard baked with a hot plate of 150 ℃ for 15 min. After sufficiently cooling at room temperature, the glass surface other than the pattern was protected from exposure to etchant. The glass etched for 45 min using 6:1 buffered oxide etch solution (J.T.Baker) was washed with DI-water and a ultrasonic cleaner (351OE-DTH, Brasonic, USA) for 15 min to remove impurities remaining on the pattern. Then reservoirs and holes were drilled where necessary. For bonding, a Corning2947 glass with the same size as the patterned glass was prepared and washed in a piranha solution for 45 min. Washing sequentially with DI-water, acetone, and methanol was followed by complete removal of moisture. The cover glass was placed on the patterned glass, which were kept in a 600 ℃ furnace (CRF-M15, CEBER, Korea) for 5 h. The glass chip after bonding was stored in a desiccator at constant temperature and humidity.

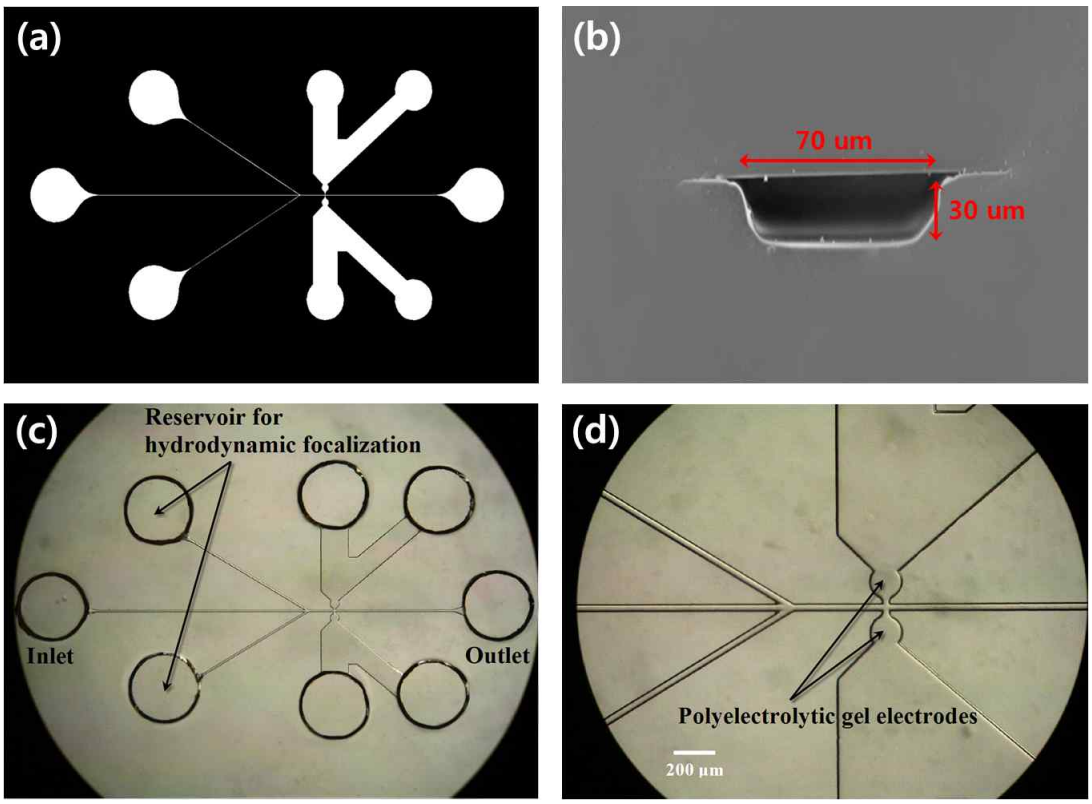

Figure 2.5 The fabricated microfluidic chip. (a) Mask design with AutoCAD. (b) Cross-sectional image of microchannel. (c) The microfluidic chip is comprised of inlet, outlet and reservoirs for hydrodynamic focusing and electrode connection. (d) A pair of PGEs facing each other are fabricated on the microchannel wall.

2.2.2 Positive Charged Polyelectrolytic Gel Electrodes Fabrication

The PGEs system was fabricated by illuminating ultraviolet beam on the specific parts of the glass chip filled with a monomer solution and rinsing [Figure 2.6]. Before photopolymerization, for solid adherence between microchannel and polymers formed in the glass chip, the microchannels were coated with TMSMA(3-(Tri methoxysilyl)propyl methacrylate) in a dark condition at room temperature for 1 h. The TMSMA-coated surface in the channel was washed with methanol (J.T.Baker). An aqueous diallyldimethylammonium chloride (DADMAC, 65 wt%, Sigma-Aldrich) solution was mixed with photoinitiator(2-hydroxy - 4′-(2-hydroxyethoxy)-2-methylpropiophenone) and cross-linker(N,N′ -Methylene-bisacrylamide) to be 2% of the DADMAC content. The aqueous DADMAC solution was infused into the microchannel through the reservoirs of the microfluidic chip. The mask and chip were aligned using a UV aligner (MDA-400M, Midas) to determine the desired position of PGEs formation, and the intensity of UV light exposure was 20 mW cm^{-2} for 4 s. Then the PGEs and microchannel were washed with 1 M KCl electrolyte solution, and stored in 1 M KCl before use.

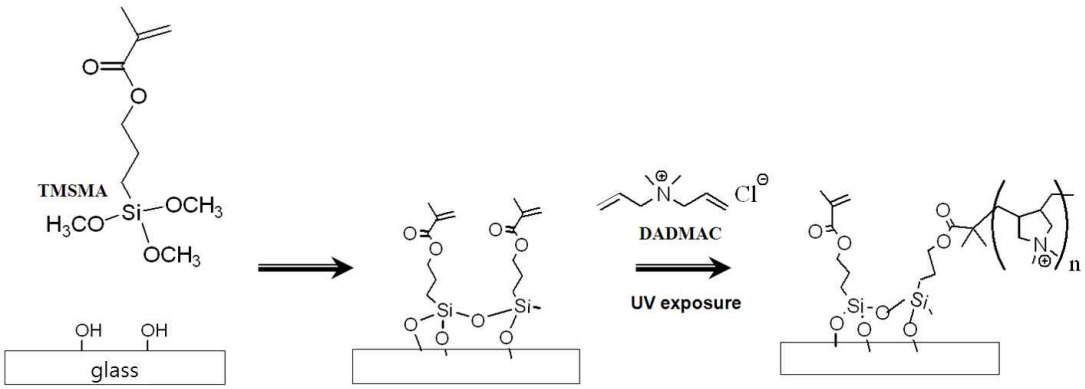

Figure 2.6 Structure diagrams and chemical reaction processes of TMSMA and DADMAC.

2.2.3 Instrumentation

DC impedance analyzer converted the impedance change into voltage pulses. 0.4 V DC bias produced around 13 μA dc current, which was applied between the Ag/AgCl electrodes immersed into the internal filling solutions in the reservoirs on the microfluidic chip [Figure 2.7]. The voltage pulses generated by microbeads or cells were amplified by 2000 folds. The number of microbeads or blood cells were counted by using the LabVIEW (National Instrument, LabVIEW 8.2). The sampling rate for data acquisition was 50 kHz and the flow rate of the syringe pump (KDS100, KD Scientific) was l0 μl/h.

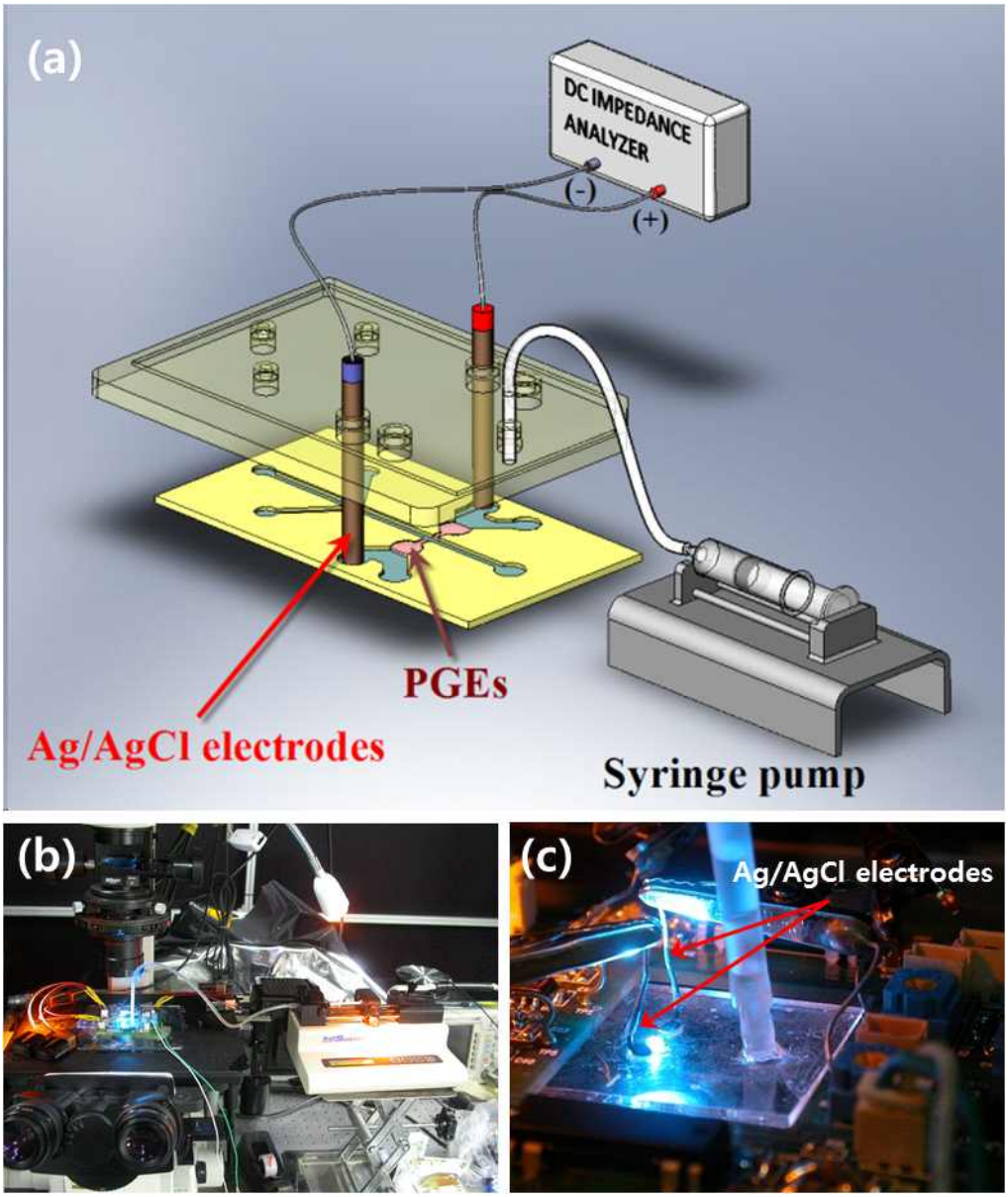

Figure 2.7 (a) Illustration of the proposed microfluidic chip cell counter. (b) Using fluorescence microscope, microbeads and cells passing through the microchannel can be observed. (c) DC impedance analyzer amplifies the impedance changes between the PGEs and transmits the signals to a laptop computer for peak detection.

2.2.4 Sample Preparation

To validate the performance of the PGEs system, we used the fluorescent microbeads that were dispersed in PBS at pH 7.4 and well individually recognized by optical microscope. The average diameters of the beads were 7.2, 10.0 and 15.0 m whose coefficients of variation were less then 10%, to calibrate the changes of impedance peak amplitude as a function of their size. The performance of the PGEs system and animal hematoanalyzer was compared by employing 7.2 m fluorescent microbeads that are similar to RBCs in size. The whole blood samples, which were gratefully donated by the volunteers, were mixed with a solution of ethylenediamine tetraammonium salt (EDTA) to prevent from coagulation. It was diluted with PBS after blood sampling and directly injected into the microfluidic chip.

2.3 Results and Discussion

2.3.1 Amplitude Calibration of Impedance Change

The correlation between impedance change and the size of fluorescent microbeads was examined using the fluorescent microbeads in three different sizes (7.2, 10.0 and 15.0 μm in diameter). As shown in Figure 2.5, there is the main microchannel between one pair of PGEs facing each other and perpendicular to the flow direction. The PGEs separate the internal filling solution of 1 M KCl from the sample solution in the main microchannel so that the microbeads to be measured are not directly exposed to the Ag/AgCl electrodes. This is an advantage because it can perfectly protect the cells from possible damage on the metal electrode surface, which is often found during using the conventional particle or cell counters based on the Coulter principle. Cl^- ions carry the charge through the PGEs, which is driven by the DC biased Ag/AgCl electrodes. When a beads or a blood cell passes the region between the two PGEs, a pulse signal appears due to the impedance change as shown in Figure 2.8(a). Because the impedance between PGEs is proportional to the microbead size, larger microbeads bring about greater pulse amplitudes as shown in Figure 2.8(b). This PGEs system is based on a low voltage DC impedance analysis so that the impedance change is regardless the bead position between the electrodes but only a function of the bead size.

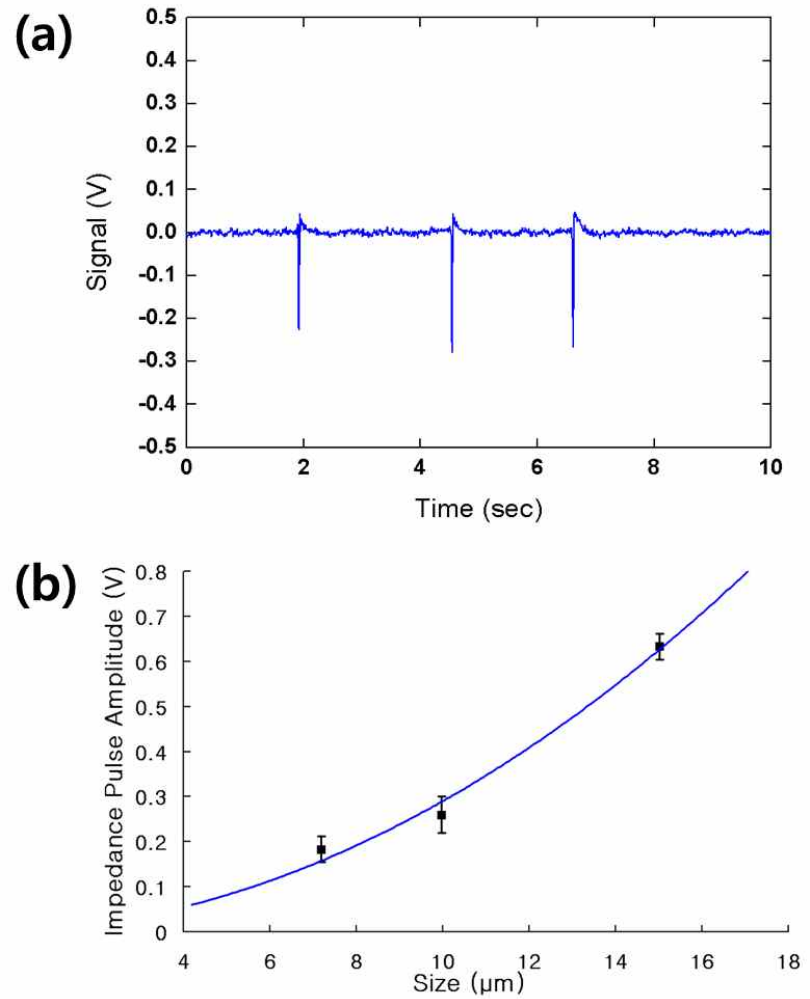

Figure 2.8 (a) Measured impedance signal between a pair of PGEs induced by 10.0 mm fluorescent microbead. (b) The impedance pulse amplitude was affected by the cell size regardless of the flow rate or the distance between electrodes and cells, and each point was tested eight times.

2.3.2 Performance Evaluation Using Fluorescent Microbeads

A blood sample of normal people contains 4,200,000 to 6,300,000 RBCs per microliter in average and the diameter of human RBCs is 6 to 8 μm. To evaluate the performance of the PGE-based cell counter, we conducted a model experiment using fluorescent microbeads with the diameter of 7.2 μm, which is similar to that of RBCs in a variety of concentrations. The counting result from PGE-based blood cell counter was compared with an animal hematoanalyzer (MS 9-5; Melet schloesing laboratories, France) As shown in Figure 2.9(a), the count results match each other well and have a reasonable error range.

The PGEs system can produce very stable data even at a high concentration because more probable coincident effect due to the high concentration is suppressed by the narrow sample flow of ~20 μm induced by hydrodynamic focusing as shown in Figure 2.9(b). The sample solution and the plain PBS are filled in the inlet reservoir of the main microchannel and those of the two side channels, respectively. Suction at the outlet of the main microchannel leads to the sheath flow without using any sophisticated flow control by using only one syringe pump. Because the proposed system uses DC impedance analysis, the pulse amplitude is not sensitive to the position of beads between PGEs. Therefore, the sheath flow does not have to be finely controlled.

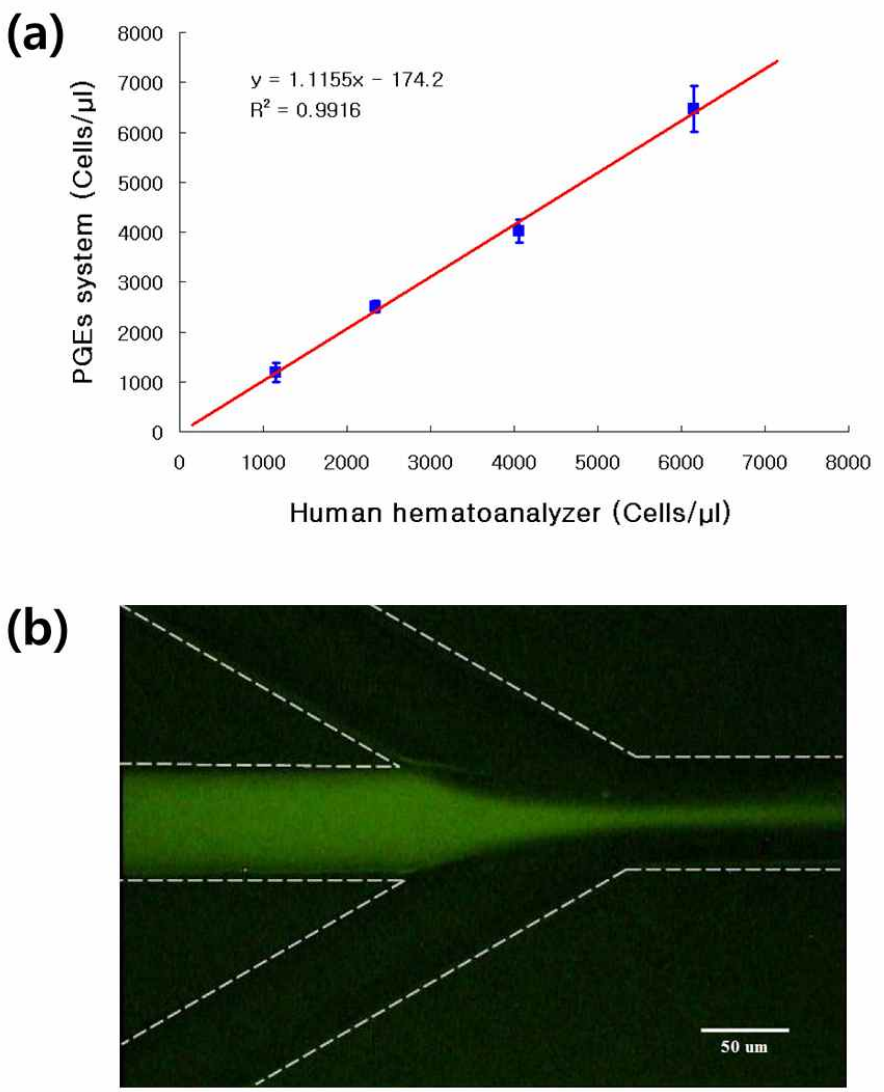

Figure 2.9 (a) The results from the PGEs system (squares) and animal hematoanalyzer for various concentrations of the fluorescent microbeads of 7.2 mm in diameter, which are in similar size to that of RBCs. (b) The sample flow width was narrowed down by 1-D hydrodynamic focusing to reduce coincident effect.

2.3.3 Quantification of Human Red Blood Cells

Commercially available human hematoanalyzers generally conduct RBC counting by diluting whole blood by 20,000 to 40,000 times. The proposed microfluidic chip can count RBCs with a dilution of much lower ratio. Figure 2.10 shows a comparison with a human hematoanalyzer by injecting 2 μL human whole blood that were diluted to different concentrations in PBS containing EDTA anticoagulant. It was found that more dilution led to the RBC cell count closer to that from the clinical hematoanalyzer (HST-N402XE; Sysmex, Japan). For 800-fold or more dilution, the results agree at least 90 % with the human hematoanalyzer. Less dilution than 800-fold results in a lower accuracy than human hematoanalyzer due to the coincident effect.

The PGEs system has the valuable advantage that it requires no additional process to separate blood cells, neither centrifuge nor filtering. Furthermore, it can protect the samples from electrical damage and undesirable aggregation between electrodes and samples because the diluted blood cells are not exposed to metal electrodes. The whole system including external operating circuit as well as microfluidic chip is simple and handy enough to be a promising type of the POCT-type cell counters.

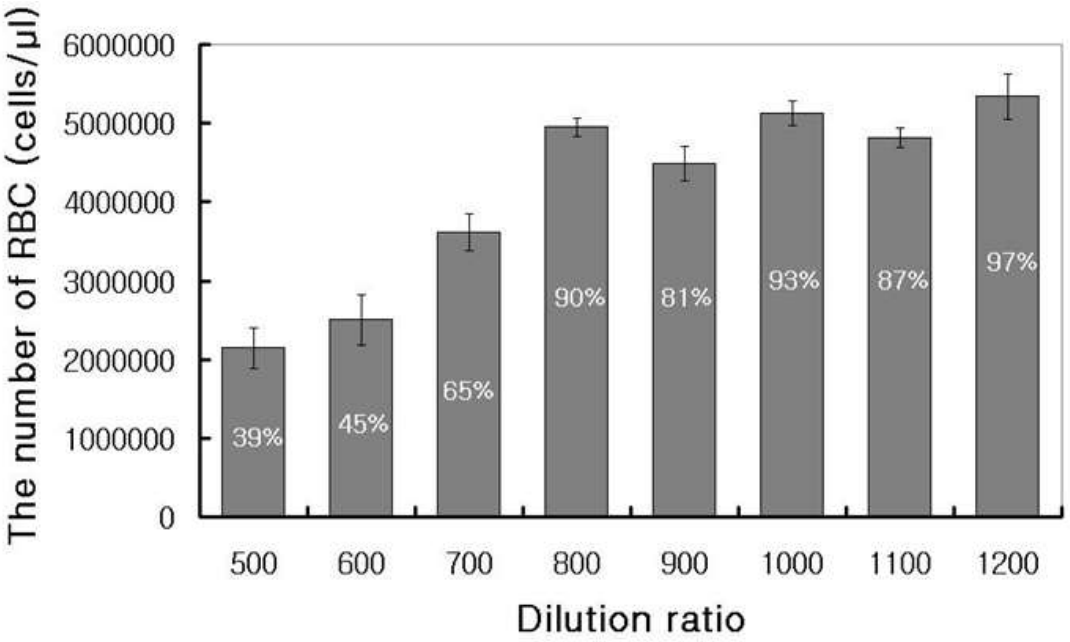

Figure 2.10 The count results of the RBCs in human whole blood diluted with PBS in various ratios. For comparison, a clinical human hematoanalyzer was used to count the number of RBCs in the same sample.

2.4 Conclusion

We suggest a new strategy of DC impedance analysis employing a low voltage and a pair of PGEs on a microfluidic chip. Red blood cells in a human whole blood can be counted fast in a convenient way without involving centrifuge or filtering. The only pretreatment prior to counting is one step of dilution with a buffer and EDTA, which can be readily combined with a microfluidic counting chip. We demonstrated that only 800-fold dilution of 2 μL human whole blood

allows reasonable assess of the RBCs number with higher than 90% accuracy. This is supposedly ascribed to the substantial suppression of coincident effect by introducing a low DC bias applied in perpendicular direction through a pair of PGEs across the microchannel. Furthermore, the proposed system provides another practical advantage of safely protecting the blood samples from metal electrodes with PGEs.

The RBC counting ability of the proposed PGEs system in this study was confirmed by comparing with a commercial hematoanalyzers. Although a number of miniaturized chip-type blood cell counters have been suggested, it is hardly to find the successful case for clinical analysis because their entire systems still require large and expensive optical equipments that often need sophisticated alignment and fine tuning. In these respects, the proposed PGEs system has sufficient potential for clinical applications and development for a point-of-care test (POCT).

Publications

Kwang Bok Kim, Honggu Chun, Hee Chan Kim*, and Taek Dong Chung*, "Red Blood Cell Quantification Microfluidic Chip Using Polyelectrolytic Gel Electrodes", *Electrophoresis*, 2009, 30, 9, 1-6.

Chapter 3.

Application II

Ionic Junction Field Effect Transistor on a Microfluidic System

3.1 Introduction

3.1.1 Electric Double Layer

When in contact with an aqueous solution, most solid surfaces carry electrostatic charge or an electrical surface potential. Generally, the solution is electrically neutral having an equal number of positively and negatively charged ions. But, the electrostatic charges

in the surface will attract the counterions in the liquid, such as an electrolyte solution or a liquid with impurities. Because of the electrostatic attraction, the counterion concentration near the solid surface is higher than that in the bulk liquid far away from the solid surface. However, the coion concentration near the surface is lower than that in the bulk liquid far away from the solid surface, due to the electrical repulsion. Therefore there is a net charge with excess counterions in the region close to the surface. This net charge should balance the charge at the solid surface. The charged surface and the layer of the liquid containing the balancing charges is called the electrical double layer (EDL), as illustrated in Figure 3.1. Immediately next to the charged solid surface, there is a layer of ions that are strongly attracted to solid surface and are immobile. This layer is called the compact layer, normally about several Angstroms thick. The charge and potential distributions in the compact layer are mainly determined by the geometrical restrictions of ion and molecule size and the short-range interactions between ions, the wall and the adjoining dipoles. From the compact layer to the electrically neutral bulk liquid, the net charge density gradually reduces to zero. Ions in this region are affected less strongly by the electrostatic interaction and mobile. This region is called the diffuse layer of the EDL [27].

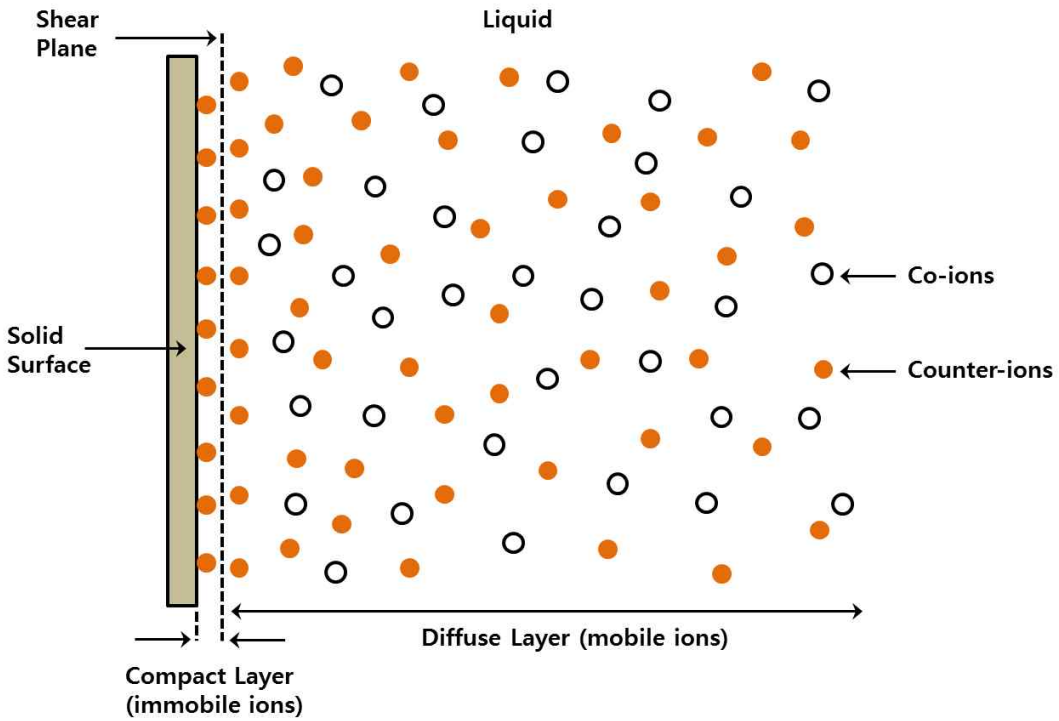

Figure 3.1 Illustration of the electric double layer (EDL) and ion distributions in the liquid.

3.1.2 Electrokinetic Phenomena in Microfluidic Networks

Electrokinetic phenomena in microfluidic networks include electroosmosis (EO), electrophoresis (EP), and streaming potential. Harnessing electrokinetic phenomena in microfluidic devices for moving fluid and particles including cells, bacteria, viruses, and proteins is essential for micro-total analysis systems and lab-on-a-chip applications. When an electric field is applied, the excess counterions in the diffuse layer of the EDL will move under

the applied electrical force. This is called the electroosmosis. As the ions move, they drag the surrounding liquid molecules to move with them due to the viscous effect, resulting in a bulk liquid motion. Such a liquid motion is called the electroosmotic flow [Figure 3.2]. As shown in Figure 3.3, electrophoresis is the motion of an electrostatic charged particle in the bulk liquid by the electrical field. The charged particles accelerates until the electric force is equal to the frictional force. In absence of an applied electric field, when a liquid is forced to flow through a capillary or microchannel under an applied hydrostatic pressure difference, the counterions in the diffuse layer of the EDL are carried towards the downstream end, resulting in an electrical current in the pressure-driven flow direction. This current is called the streaming current. Corresponding to this streaming current, there is an electrokinetic potential called the streaming potential. This flow induced streaming potential is a potential difference that builds up along a microchannel. This streaming potential acts to drive the counterions in the diffuse layer of the EDL to move in the direction opposite to streaming current. The action of the streaming potential will generate an electrical current called the conduction current. At steady state, the streaming current will be balanced by the conduction current, and hence the net current in the microchannel is zero.

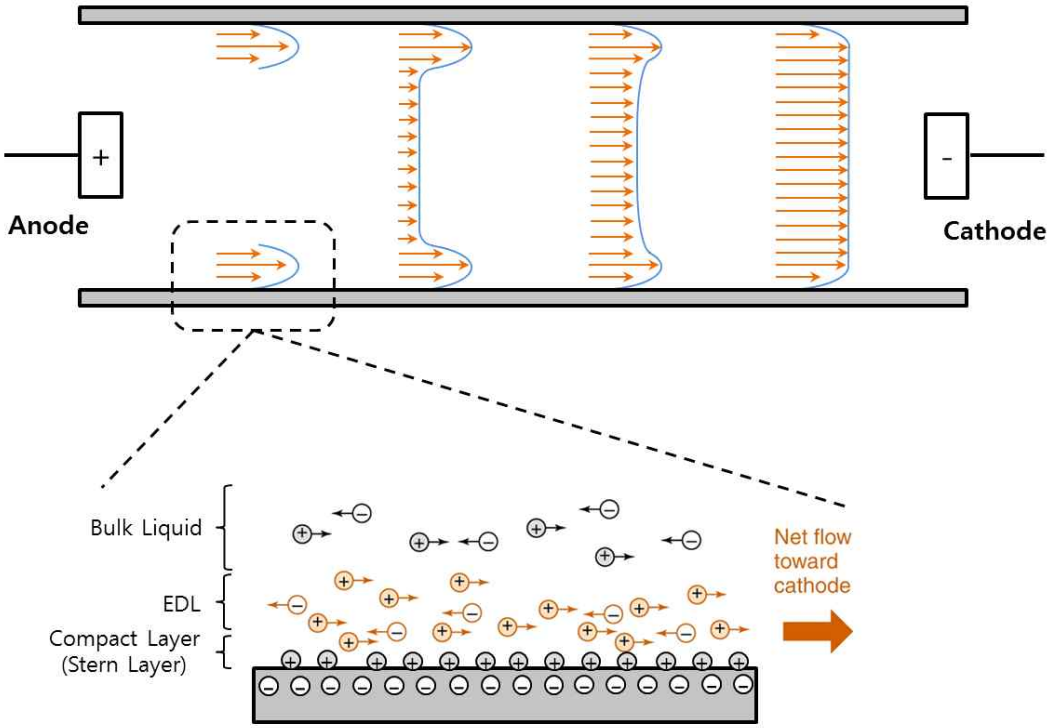

Figure 3.2 Illustration of electroosmotic flow (EOF) in a microchannel.

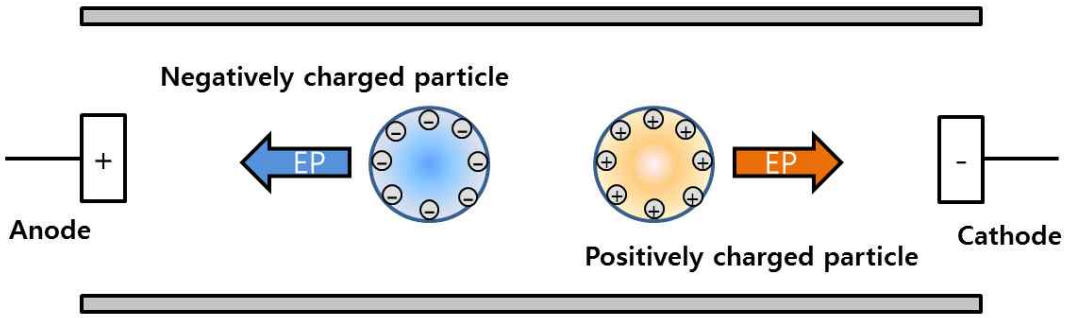

Figure 3.3 The electrophoretic motion of the charged particles in a microchannel.

3.1.3 Applications of Electrokinetic Phenomena

3.1.3.1 Electrophoretic Separation

For chemical and biological analysis, separation is the first step and among the many separation techniques, such as filtration, chromatography, and centrifugation, capillary electrophoresis is the main technique adaptable to separate a wide range of biological samples including DNA, proteins, peptides, and cells. Electrophoresis can be performed much more efficiently on microfluidic platform than that in conventional capillary method. The microfluidic chip-based electrophoresis device have lower sample consumption, portability, and shorter analysis time. In the case of DNA separation, finish-line detection method of capillary electrophoresis is widely used however this method difficult to separate larger-sized fragments due to the longest time to reach the detection area. As shown in Figure 3.4, microchip-based gel electrophoresis device with scanning detector can observe smaller and faster moving fragments in early stages of separation and also allow the larger and slower moving fragments to be observed without the time for the analytes to move the entire capillary channel [28].

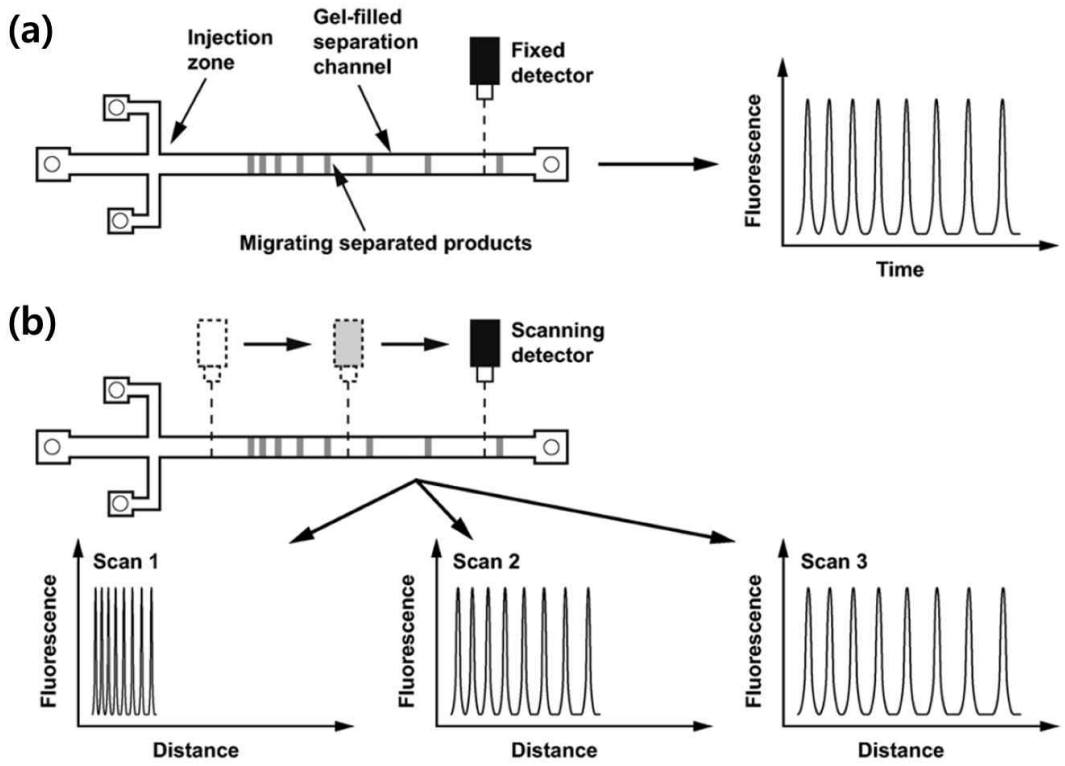

Figure 3.4 (a) Microchip gel electrophoresis with fixed detector. (b) Advanced gel electrophoresis device combined with scanning detector.

3.1.3.2 Electroosmotic Pump

Over the past decades, many fluid pumps have been developed for microfluidics system, and most of the concepts were from mechanical pumps of the industry. The precision, accuracy, and size of the pump are dependent on data sheet of the commercial products, most of which are not available to microsystems, therefore there are necessary to redesign and additional evaluation process for adoption of them. To overcome the these obstacles and as an alternative of

mechanical pump system, electroosmotic (EO) pumps are developed in the microfluidic devices. The EO pumps are particularly useful to microsystems for cell culture and cell sorting, because living cells are not exposed to high electric fields for operating the pump. As shown Figure 3.5(a), th an EO pump an electric field is applied in a limited region generating EOF flow (channel 2). Membranes separate the electrodes from the internal fluid channel allowing for electric current to pass but not the fluid. The internal pressure is generated that pumps the fluid outside the EOF region, vacuum draws the fluid into the pump (channel 1) and a positive pressure drives the fluid out (channel 3). The fluid flow in channel 2 is actually a combination of EOF flow and back pressure flow. The cell chamber can be placed before or after the EO pump allowing for the use of EOF while isolating the cells from the electric field [29]. In Figure 3.5(b), two microchannels are coated with positively and negatively charged polymers, respectively. Therefore, when an electric field is applied to the channels, each channel generates the electroosmotic flow in opposite directions, resulting in field-free flow in the mainchannel for fast living cell sorting [30].

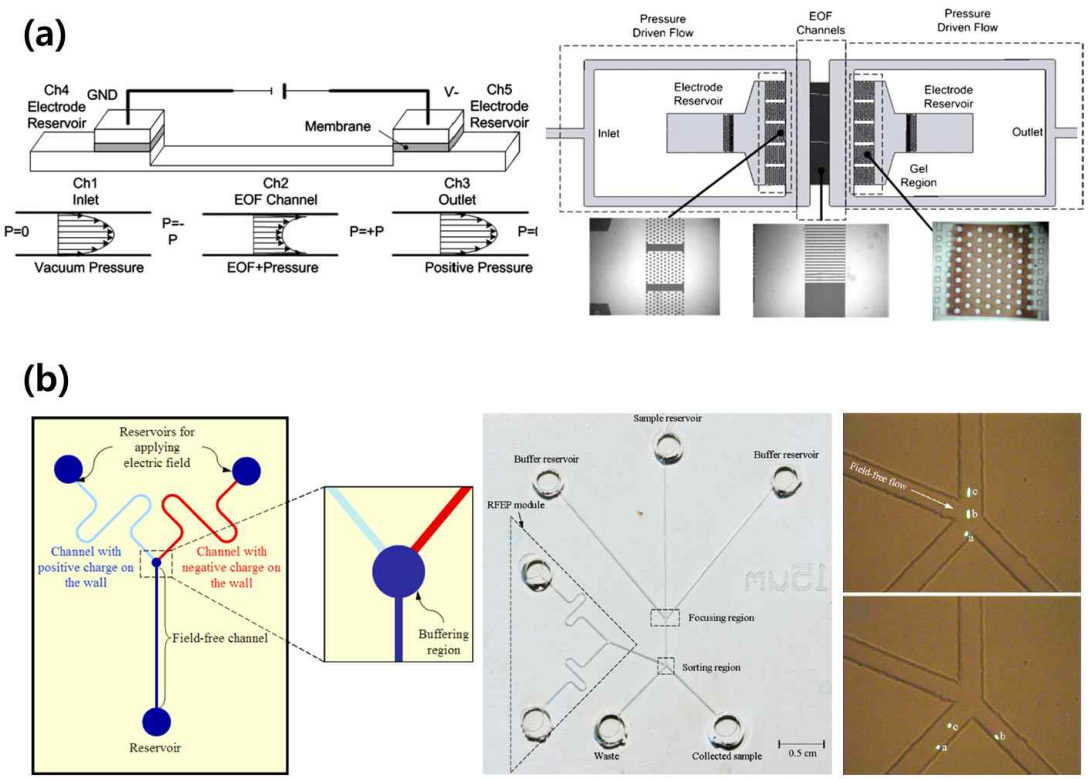

Figure 3.5 Electroosmotic pump for (a) cell culture and (b) cell sorting.

3.1.3.3 Electrokinetic Micromixer

Microfluidic chips designed for biochemical analysis are frequently required a more rapid and effective reaction performance in a microchannel. Micromixer can be categorized in terms of the mixing mechanism into two basic types: active and passive. Active micromixers are associated with the introduction of external energy into the system, such as ultrasound, acoustically induced vibrations, piezoelectrically vibrating, electrokinetic, small impellers, microvalves, and micropumps. On the other hand, passive micromixers rely on the

mass transport phenomena provided by molecular diffusion and chaotic advection. These devices are designed with a channel geometry to increase the surface area between the different fluids and decrease the diffusion path. To enhance chaotic advection, the laminar flow in the microchannel is controlled by channel design.

In the biological research area, passive micromixers are inappropriate because their long and complicated microchannel can cause high sheer stress on cells and make it to difficult to maintain and control their mixing condition. Therefore, researches have focused on active micromixer. Electrokinetic micromixers take advantage of fluctuating electric field to induce mixing in microchannels. The fluctuating electric fields cause rapid stretching and folding of the fluids interfaces to stir the fluid stream [Figure 3.6(a)][31]. As shown in Figure 3.6(b), the positively and negatively charged polyelectrolytic gel electrodes (PGEs) facing each other are fabricated on the microchannel wall. Each PGEs generates ion depletion and enrichment regions between the PGEs at same time. Switching of the electric bias can interchange the ion depleted and enriched regions and also mix the two fluid stream [32].

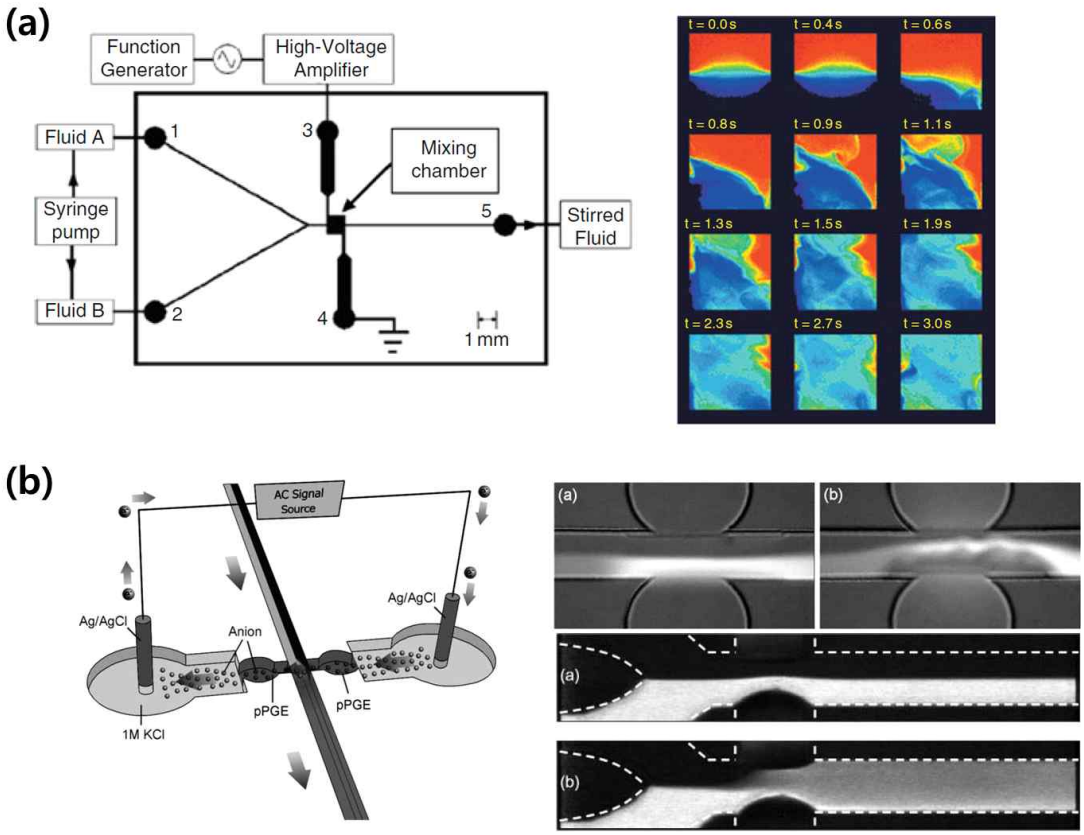

Figure 3.6 (a) Electrokinetic instability micromixer with sinusoidally alternating electric field. (b) Electrokinetic ion control for micromixer.

3.1.3.4 Electrokinetic Preconcentration

Sample preconcentration which concentrates sample analytes to detection and increases the signal-to-noise ratio are integral step of analytical chemistry. In proteomics, the protein have the large dynamic range of the concentration (pg/ml to mg/ml), as well as the large number of the proteins. To enhance the detectivity, several microfluidic chip systems for preconcentration are developed with

electrokinetic trapping technique. As shown in Figure 3.7(a), when electric field is applied across the nanochannel that have ion permselectivity by an electric double layer (EDL) overlapping phenomenon, concentration polarization and ion depletion region are generated by local electric field gradient. Therefore, charged molecules driven by electroosmotic flow are preconcentrated in the microchannel [33]. To improve the preconcentration efficiency, nanochannels are replaced with a negatively charged hydrophilic polymer for electrokinetic ion control [Figure 3.7(b)]. The ion selective polymer increase the counterion selective extraction efficiency due to high surface area, low impedance, and high frequency response. Under the external electric field, only cations are pass through the negatively charged polymer, and anions are expelled at same time. Therefore, ion depletion region is created and expanded in the microchannel, resulting in anionic molecules are trapped and stacked near the ion depletion region [34].

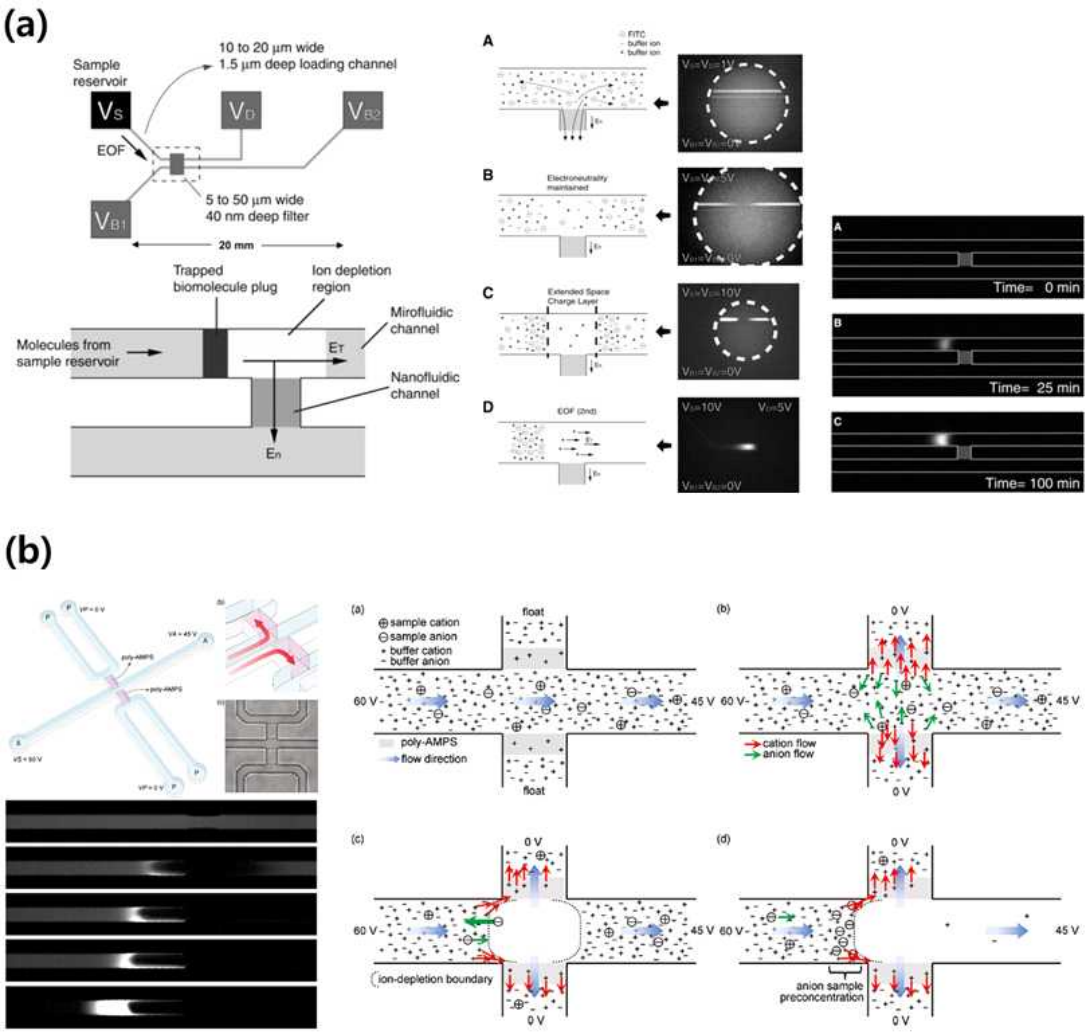

Figure 3.7 (a) Nano-and microfluidic channel-based preconcentration device. (b) Ion selective polymer membranes are fabricated on the microchannel wall for electrokinetic sample trapping.

3.1.3.5 Diode and Transistor

Using electric double layer (EDL) overlapping of the surface on the nanochannel, nanofluidic devices can control the ion flow for mimic the diode characteristics in solid-state electronics. The negatively and positively charged surfaces of the nanochannel have similar properties of electrons and holes in an n-type and p-type semiconductor materials, respectively. A symmetric distribution of cations and anions in the nanochannel generates the uneven ion flow by the applied electric field, which creates ion depletion and enrichment phenomenon for enhancing and reducing the ionic current. The cation and anion distribution ratio in the nanofluidic diode system is affected by ion concentration, nanochannel size, and the polarity and density of the surface charge. The ionic rectification effect in the nanochannel can be established by combination of these parameters. As shown in Figure 3.8, diode-like nanofluidic system have asymmetric charged surface of the channel whose one half of the surface is positively charge while other half one is negatively charge in ionic solution. The positively and negatively charged nanochannel contain more anions and cations, respectively. When a forward bias is applied on the system, the cations in the negative nanochannel and anions in positive nanochannel move toward the junction of the nanochannels. Therefore, the concentration of the junction is increased by ion enrichment, and thereby ionic conductance increases. On the contrary, at reverse bias, cations and

anions are extracted in the junction of the nanochannel, which create the ion depletion region. As enhancing the ion depletion, the ionic conductance of the nanochannel is decreased. These the ion depletion and enrichment in the nanochannel cause the rectifying I-V characteristics [35].

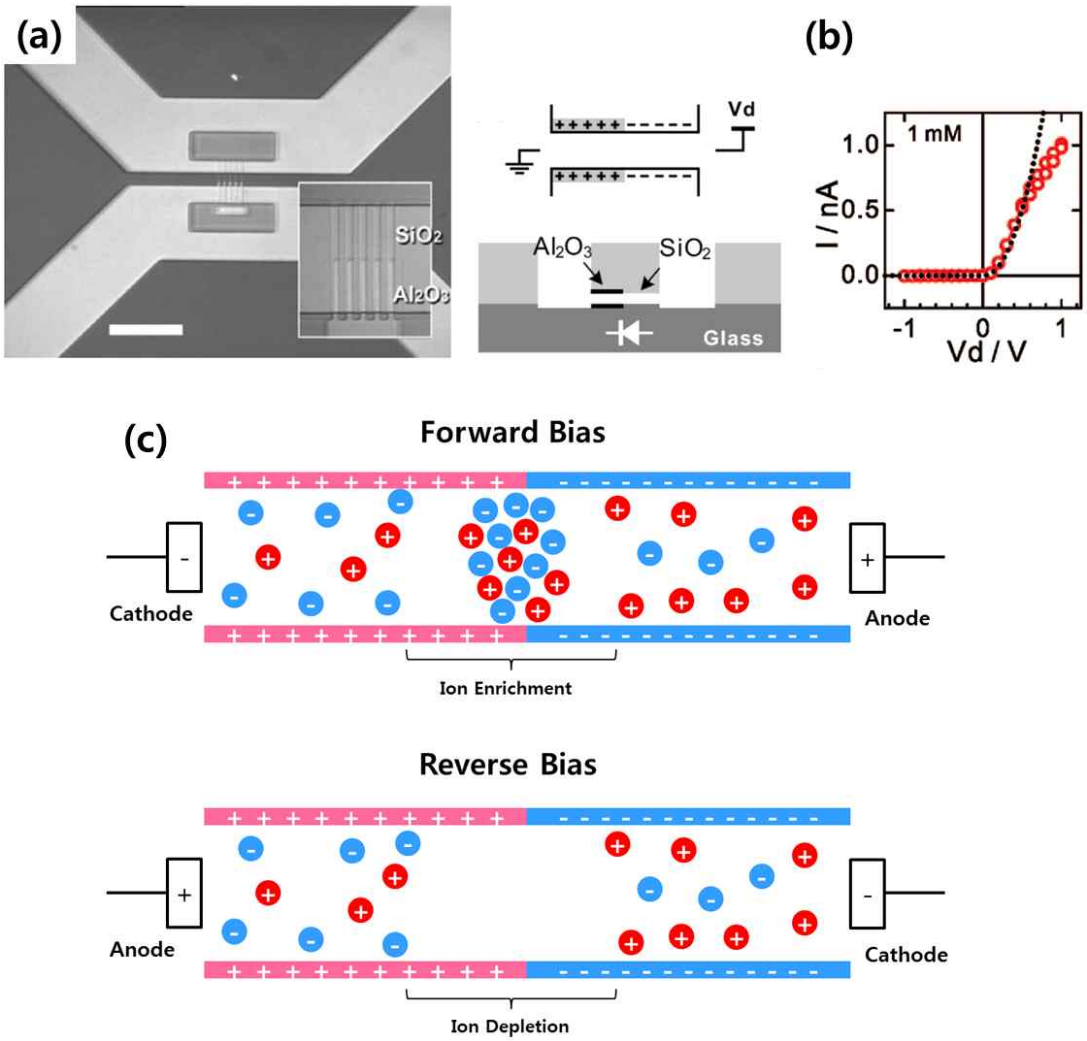

Figure 3.8 (a) Schematics of nanofluidic diode device. (b) Diode I-V characteristic curve. (c) Mechanism of rectifying effect in a nanochannel with opposite charged surface.

This phenomena in nanochannel can also be created in a bipolar membrane junction consisted of positively and negatively charged polymer [Figure 3.9]. Under a forward bias, the ion concentration at the junction of polymer membrane is increased by ion enrichment, resulting in increasing the ionic current. On the other hand, When reverse bias is applied between the membranes, the ion depletion region is created and extended at the junction, therefore the current as applied potential are decreased. Using this polymer membrane-based diode system, a variety of logic gates including AND, OR, and NAND gate, are established with combination of multiple diodes in a single microfluidic chip [36].

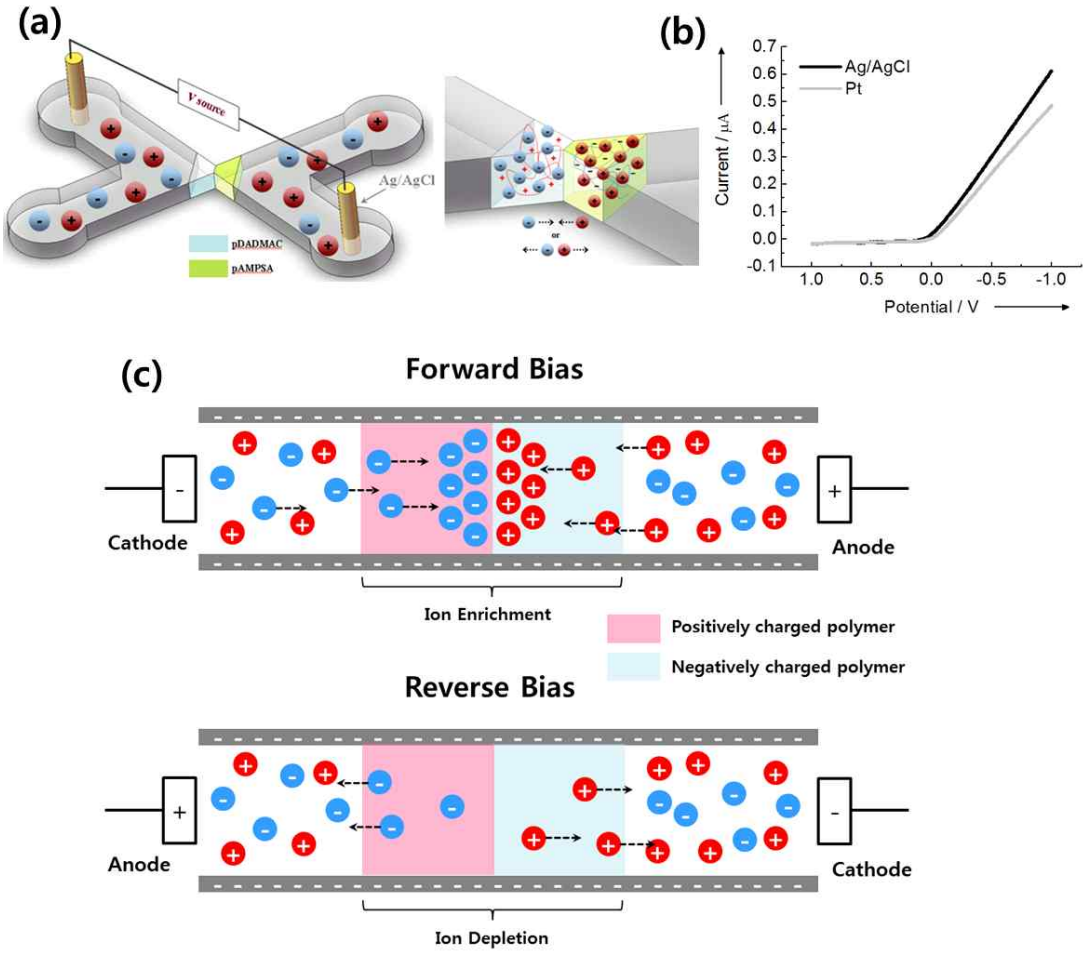

Figure 3.9 (a) Illustration of Bipolar polymer membrane-based diode system. (b) Diode I-V characteristic curve. (c) Mechanism of rectifying effect in a polymer membranes with opposite charged backbone.

With the development of diode-like nanofluidic devices, a nano- and microfluidic transistor system have been used for manipulation of ions and biomolecules in sub-femtoliters volumes. Figure 3.10(a) shows microfluidic transistor with the organic semiconductor pentacene. The organic compound pentacene is consisted of five benzene rings which acts as a p-type semiconductor. The source and drain electrode are defined by the microchannel and are filled with mercury. Although the current-voltage characteristics of the microfluidic transistor show similar properties of conventional transistor that source-drain current is modulated by the gate voltage, it is difficult to use for biological applications due toxicity of mercury, and the gate voltage which control the source-drain current has low sensitivity to use a biosensor [37]. To overcome these limitations, nanofluidic transistors based on a metal-oxide-solution (MOSol) is fabricated for mimicking a metal-oxide-semiconductor field-effect transistor (MOSFET). As shown in Figure 3.10(b), the gate voltage can modulate the ionic conductance in the nanochannel. When a negative gate voltage applied to the system, the cation concentration are increased, thus increasing the source-drain current which is carried by the cations. On the contrary, under a positive gate voltage, the cations are depleted in the nanochannel, resulting in reduce the conductance. The multiple nanofluidic transistors can be integrated in ionic circuit for manipulating extremely small amount of biomolecules [38].

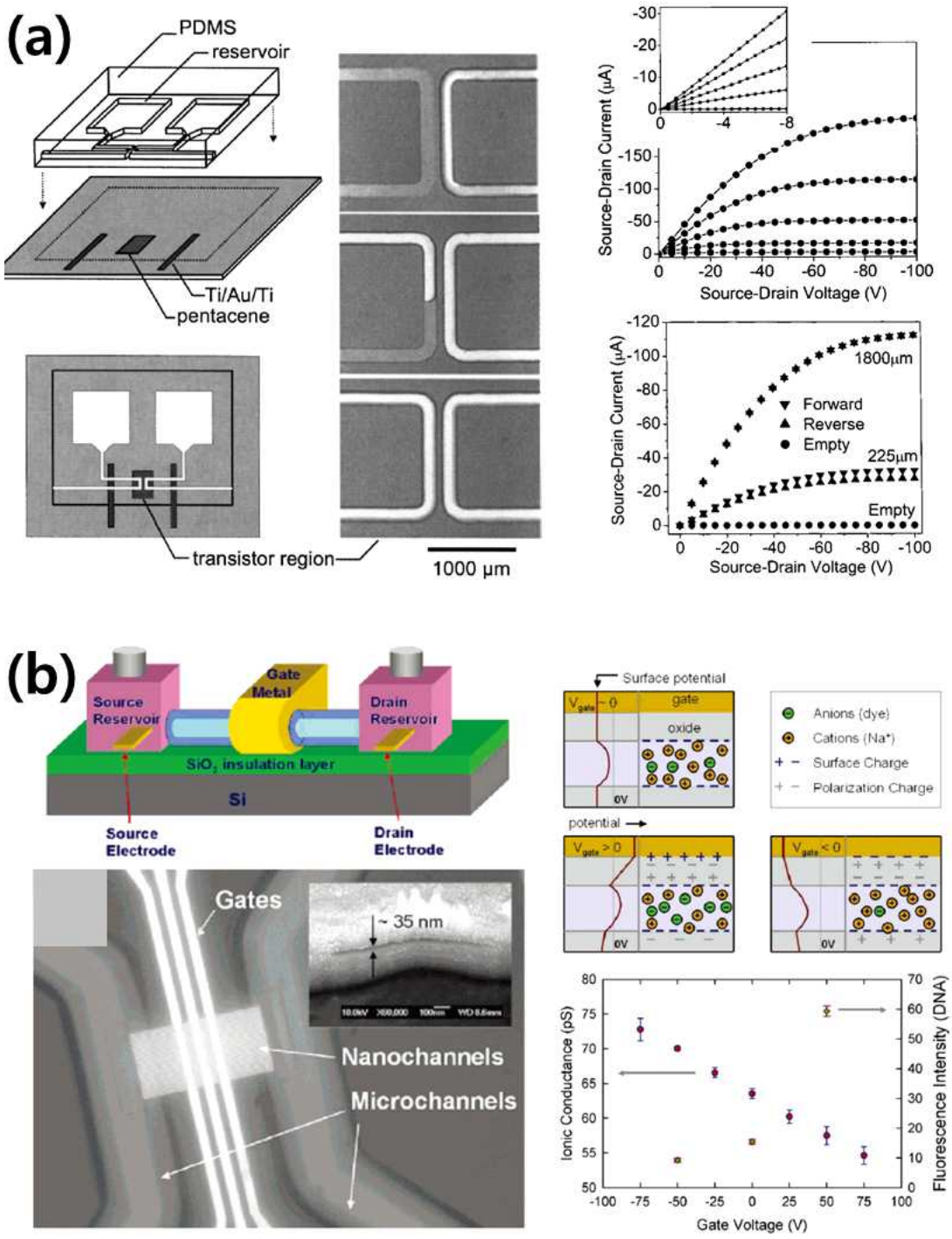

Figure 3.10 (a) Tunable organic transistor on a microfluidic chip. (b) Nanofluidic transistor with electrokinetic ion control.

3.1.4 Goals of This Study

We study a polyelectrolyte junction field effect transistor (pJFET) that is developed on a microfluidic chip, as shown in Figure 3.11(a). The proposed system is the first microfluidic transistor based on polyelectrolytes, which are charge-selective polymers of poly-diallyldimethylammonium chloride (pDADMAC) and poly-2-acrylamido-2-methyl-1-propanesulfonic acid (pAMPSA). The polyelectrolyte plugs were formed at two spots in the microchannel network. Positive and negative charged polyelectrolytes, pDADMAC and pAMPSA, selectively allow anions and cations to pass. As shown in Figure 3.11(b), the ion current of mainchannel is sensitively affected by the extent of ion depletion, which intensive ion extraction through the polyelectrolyte plugs brings about under a gate voltage (V_G), which is similar to solid state JFET operation [Figure 3.11(c)]. The region where ion depletion occurs was visualized by fluorescence images of positively and negatively charged dyes of rhodamine 6G and fluorescein. The characteristics of the proposed pJFET were demonstrated by I_D versus V_G curves, where I_D and V_G are the current between the source and drain and the gate voltage, respectively.

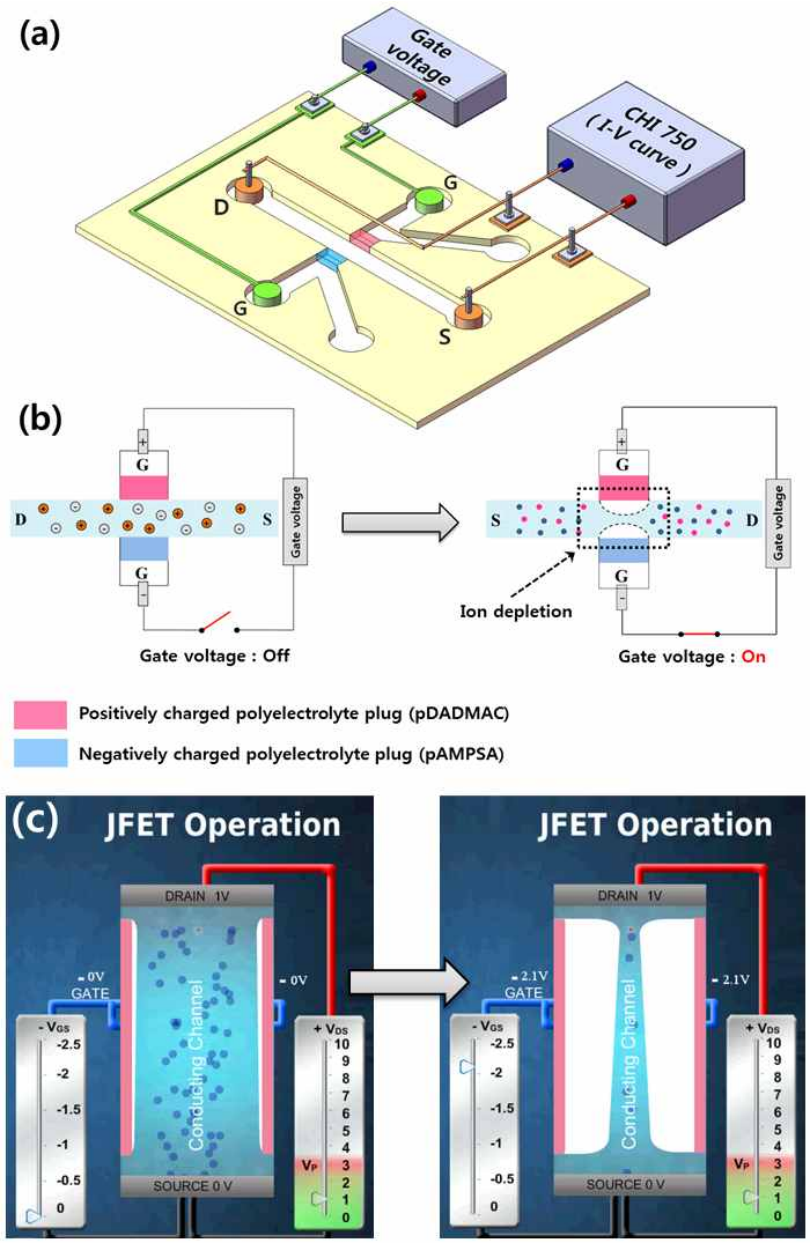

Figure 3.11 (a) Illustration of the polyelectrolyte junction field effect transistor (pJFET). (b) A pair of oppositely facing polyelectrolytes, pDADMAC, and pAMPSA, is positioned on the microchannel wall. The plugs extract both cations and anions to generate local ion depletion region. (c) Operation schematic of the solid state JFET.

3.2 Experimental Section

3.2.1 Microfluidic Chip Fabrication

A microfluidic chip with width of 70 μm and depth of 30 μm was fabricated adopting the standard photolithography method. The surface of Corning 2927 slide glass was washed with piranha solution (H_2O_2 : H_2SO_4 = 1:3), and hexamethyldisilazane (HMDS) was coated on the glass surface with a spin coater, so that photoresist (PR) could be completely attached to the glass. PR AZ4620 coated the slide glass, which is aligned under a patterned mask film, was exposed to UV light (MDE-4000) with the intensity of 15 mW/cm^2 for 10 s. The PR was removed using AZ 400K developer and was etched for 45 min in 6:1 buffered oxide etching solution. Then gate reservoir and inlet and outlet hole of mainchannel were drilled. Lastly, a cover glass with the same size as the patterned glass was prepared and washed for 45 min with piranha solution before the thermal bonding process.

3.2.2 Positively and Negatively Charged Polyelectrolytic Gel Electrodes Fabrication.

In order to fabricate the charge-selective polyelectrolytes, we used photopolymerization technique, as shown in Figure 3.12. The monomer solutions comprised of positive and negative charged DADMAC, and

AMPSA respectively. The microchannel, coated with 0.5% 3-(trimethoxysilyl) propylmethacrylate (TMSMA), was filled with 65% DADMAC solution that contains photoinitiator (2%) and cross-linker (2%). The microfluidic chip was aligned under a patterned mask film and was exposed to UV light at 15 mW/cm^2 for 2 s. After polymerization, the DADMAC monomer solution remaining in the microchannel was removed with 1 M KCl. To create pAMPSA, the microchannel was filled with 2 M AMPSA solution that contains both photoinitiator (2%) and cross-linker (2%), and was exposed to UV light with same intensity for 3 s. The microfluidic chip with pDADMAC and pAMPSA were stored in 10 mM KCl solution.

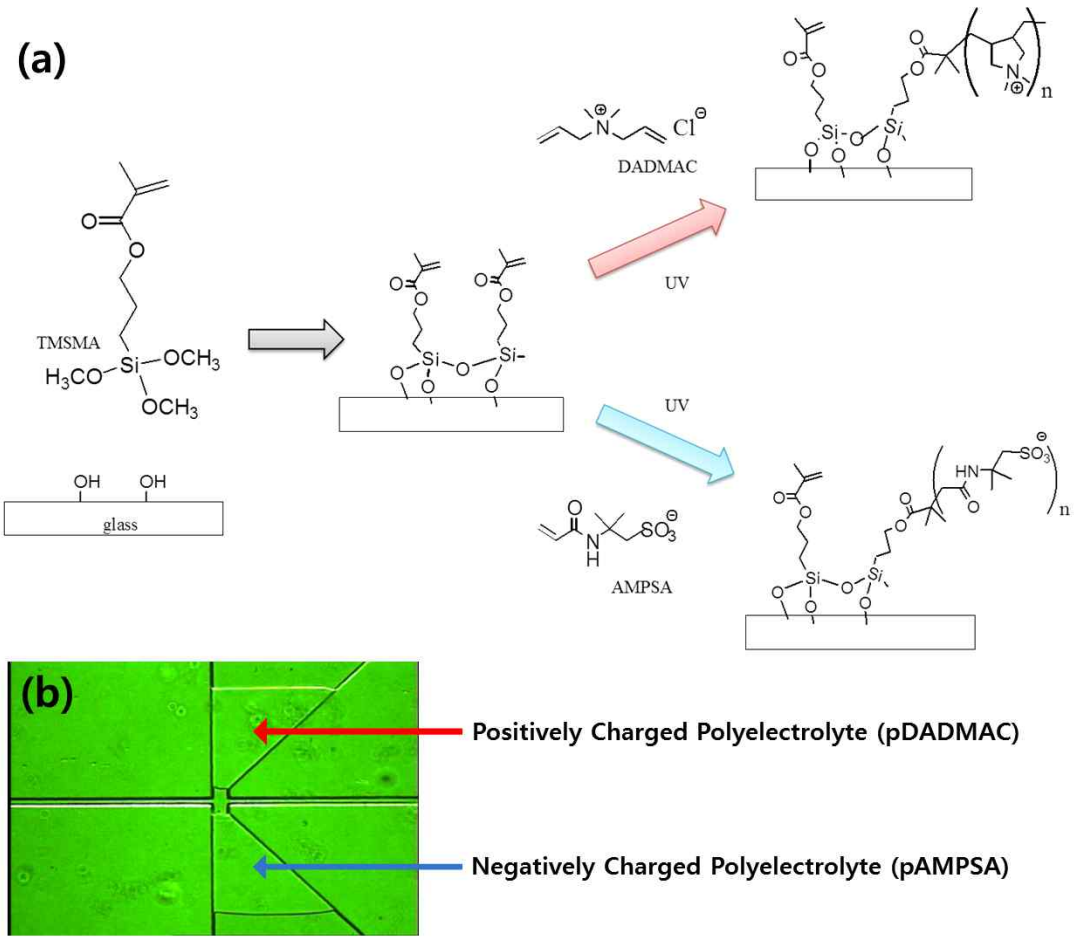

Figure 3.12 (a) The photopolymerization process for fabrication of charge-selective polyelectrolyte plugs in microchannel. (b) A pair of oppositely facing polyelectrolytes, pDADMAC, and pAMPSA, is positioned on the microchannel wall.

3.2.3 Instrumentation

To observe the distribution of the fluorescent dyes in the microchannel, a fluorescence microscope, TE-2000 (Nikon), mercury lamp, and 12-bit ProgRes C3 CCD camera (JENOPTIK) were used. Gate voltage generated by a dc power supplier was applied to source and drain electrodes that were connected to the microfluidic chip, while an electrochemical analyzer-CHI 750 (CH Instruments Inc.)- was used for measuring the change in the current, I_D.

3.2.4 Sample Preparation

All materials were used without additional purification. Rhodamine 6G, fluorescein, 3-(Trimethoxysilyl)propyl methacrylate (TMSMA), poly-2-acrylamido-2-methyl-1-propanesulfonic acid (pAMPSA), poly-diallyldimethylammonium chloride (pDADMAC), hexamethyl disilazane (HMDS), and platinum wire (0.05 mm thick, 99.9%) were purchased from Sigma (St. Louis, MO). The fluorescent dye was diluted in 10 mM KCl before use and impurities were removed using a syringe nanofilter.

3.3 Results and Discussion

3.3.1 Formation and Expansion of Ion-Depletion Region

When the gate voltage is not applied, cations and anions are equally distributed in the microchannel. To confirm this ionic flow, the behavior of anionic fluorescein and cationic rhodamine 6G dyes was monitored using a fluorescence microscope. As shown in Figure 3.13(a), 10 μM fluorescein molecules and 10 μM rhodamine 6G in 10 mM KCl solution are diffused into the positively charged pDADMAC and negatively charged pAMPSA, respectively. As a gate voltage was applied to the polyelectrolytes, pDADMAC and pAMPSA, fluorescein and rhodamine 6G are rapidly extracted from the microchannel, and the ion concentration between the polyelectrolytes decreases, thereby ion depletion is created in local area [Figure 3.13(b)]. As the gate voltage is increased, an ion depletion region appears in the middle of the mainchannel and subsequently expands, as shown in Figure 3.13(c). Thus, the charge-selective extraction of anions and cations through the pDADMAC and pAMPSA plugs generated ion depletion in the middle of the microchannel between the source and the drain.

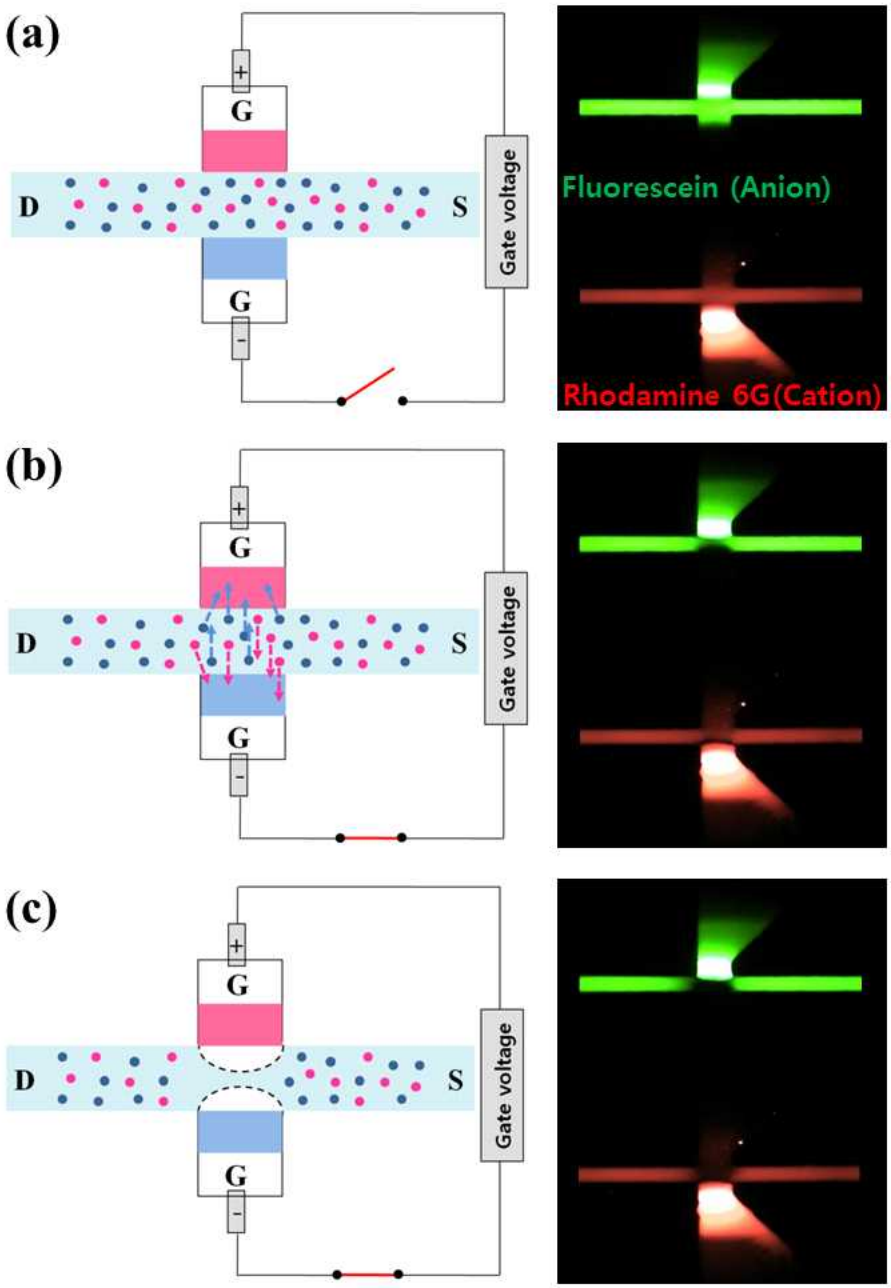

Figure 3.13 Ion control mechanism of the polyelectrolyte junction field effect transistor (pJFET).

3.3.2 Output Characteristics of a Polyelectrolyte Junction Field Effect Transistor

The source-drain current, I_D, of the in conventional JFETs is controlled by the gate voltage, V_G, which causes the depletion region to adjust the channel conductivity between the source and the drain. When a gate voltage was applied to the proposed pJFET system, an ion depletion region was formed in the aqueous solution, rather than in the semiconductors of the JFETs. This ion depletion causes a drop in the conductivity of the microchannel, which dependent on the equation, $R=\rho I/A$ (R is total channel resistance, ρ is the resistivity of the electrolyte, I is the length of the conducting path, and A is the cross sectional area of the conducting path) As shown in Figure 3.14, the source-drain current, I_D, is directly related to the ion depletion region formed by the gate voltage. When the gate voltage is increased from 0 V to 6 V, I_D decreased because of the large ion depletion region, which reduces the conductivity of the microchannel. Therefore, the behavior of the proposed pJFET system is similar to that of a conventional JFET; however, these two systems differ with respect to the charge carriers, the working principles, and the medium through which the current flows.

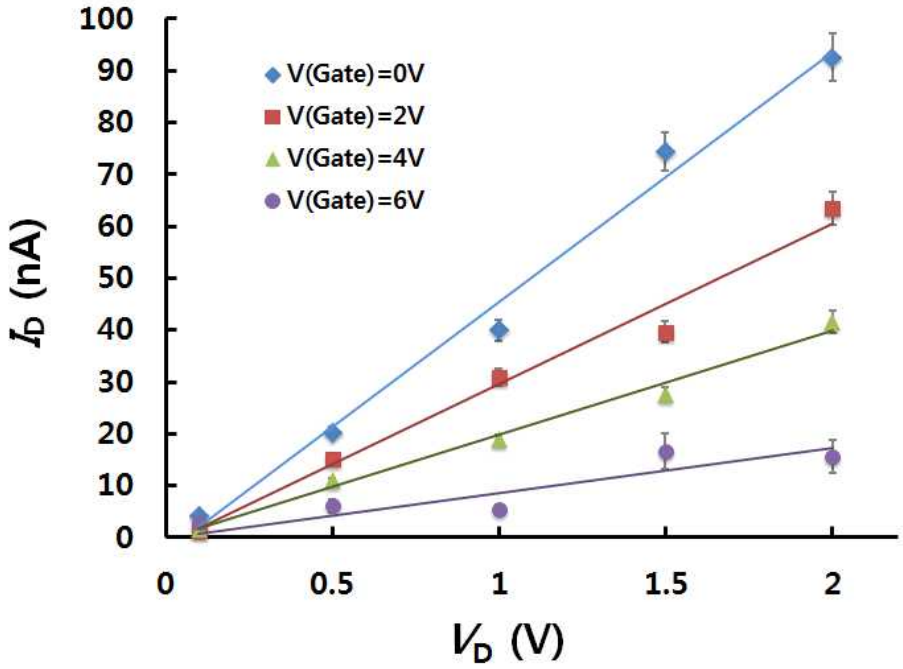

Figure 3.14 Output characteristics of a pJFET.

3.4 Conclusion

We have demonstrated a pJFET system that operates in an aqueous medium by reliably controlling the ionic flow through oppositely charged polyelectrolyte plugs. The applied V_G causes ion depletion in the middle of the main microchannel, which regulates I_D. This system does not require a complicated and sophisticated process

such as nanofabrication. Despite the simple structure and short fabrication process, the polyelectrolyte plugs are remarkably more effective tools for ion extraction than nanochannels. Hence, an ion depletion region can be rapidly created in the microfluidic networks. The pJFET has the great potential for evolving into more versatile utilities such as multi-functional ionic circuits by suggesting new opportunity to aqueous information processors.

Publications

Kwang Bok Kim, Ji-Hyung Han, Hee Chan Kim*, and Taek Dong Chung*, "Polyelectrolyte junction field effect transistor based on microfluidic chip", *Applied Physics Letters*, 2010, 96(14), 143506.

Chapter 4.

Application Ⅲ

Dynamic and Reversible Preconcentration of Gold Nanoparticles for Surface-enhanced Raman Scattering

4.1 Introduction

4.1.1 Label-Free Molecular Detection Methods

4.1.1.1 Surface Plasmon Resonance (SPR)

Surface plasmon resonance (SPR) is a phenomenon based on charge-density oscillations existing at the interface of two transparent

media with dielectric constant of different signs such as noble metals and glass. As shown in Figure 4.1(a), when a external light energy with specific resonant condition focus on the boundary between the media, the absorption of the incident light is increased, which causes electrons to have oscillatory motion. Therefore, the surface plasmon is generated by oscillation of the electron charge-density at the media interface, and the SPR is modulated with changing the light reflectance. The SPR have been used in optical biosensors without the need for labeling, thereby allowing real-time detection of protein, cells, carbohydrates, and DNA. As shown in Figure 4.1(b) when the antigen bind to antibody in the microchip, the changes of refractive index in the vicinity of the medium surface can be changed by mass of the biomolecules at the surface, thereby shifting the resonance angle [39].

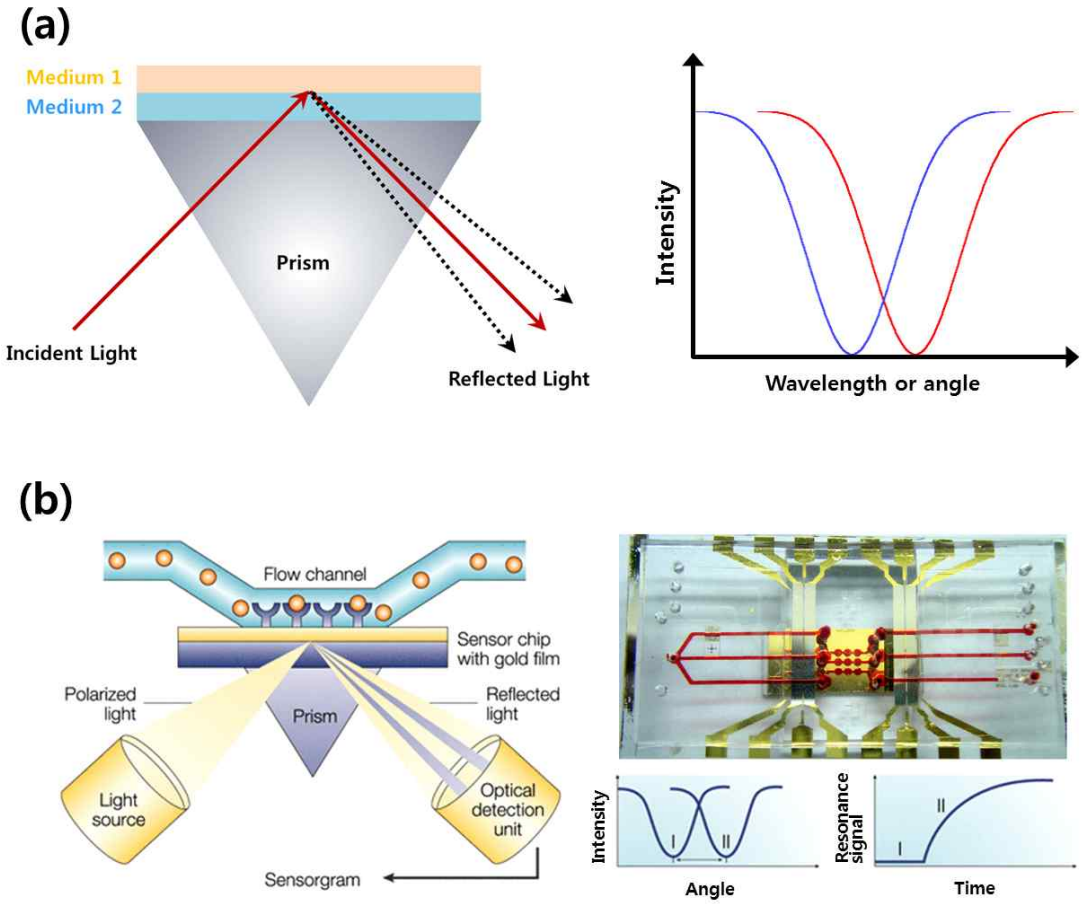

Figure 4.1 (a) Basic schematic of SPR. (b) Microfluidic chip-based SPR biosensor.

4.1.1.2 Piezoelectric Biosensor

Piezoelectric biosensors are generally based on a quartz crystal microbalance (QCM) for mass detection. The piezoelectricity is defined as the change of the charge when a quarts crystal is compressed, twisted, or distorted. Under an electric field with high frequency, the quartz crystals also oscillate in a mechanically resonant shear mode. The QCM is a acoustic wave mass sensitive detector, and an foreign mass of the surface affect the resonant frequency of an oscillating quartz. As mass is attached on the surface of the crystal, the thickness increases, thereby the frequency of oscillation decreases from the initial value [Figure 4.2(a)]. Some parameters including the density and the shear modulus of quartz crystals, and the properties of the media also influence the oscillation frequency. The QCM-based biosensors without labeling have been applied for monitoring affinity reactions, such as antigen-antibody and DNA hybridization, and it is easy to measure mass densities down to a level of below 1 μg/cm^2. Recently, the QCM integrated in a microfluidic systems. As shown in Figure 4.2(b), a nickel pilar array is fabricated on the QCM sensors for trapping and label-free detection of the target molecules. When magnetic field is applied, receptor protein-functionalized superparamagnetic micro-beads (SPMBs) are trapped on the nickel pillars, and suspended A549 cancer cells are captured by the WGA on the surface of the magnetic beads [40].

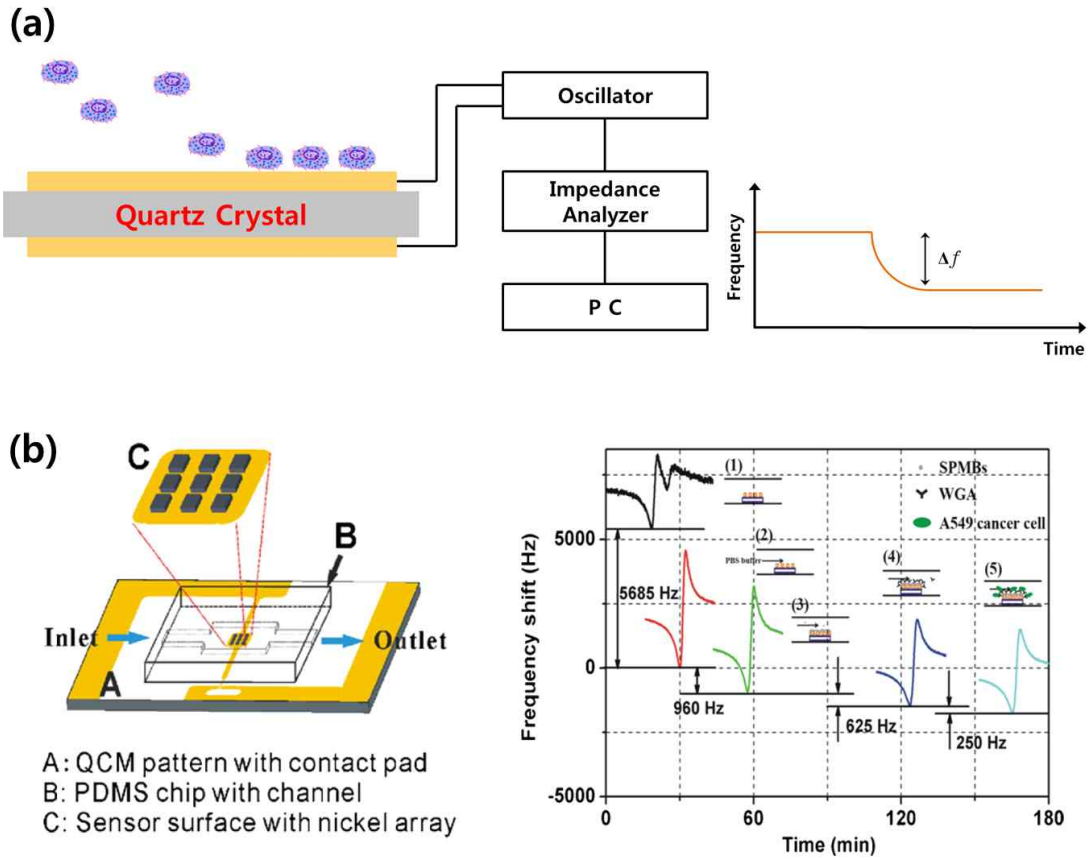

Figure 4.2 (a) QCM-based Piezoelectric biosensor. (b) Microfluidic system with QCM and nickel array for trapping and detecting of cancer cells.

4.1.1.3 Cantilever

A cantilever is a nanomechanical sensor, which originate from the scanning force microscope (SFM) and atomic force microscope (AFM). The advantages of cantilever biosensors is that the system do not need the labelling process, for example fluorescence and radioactive tags. Because the cantilever has intrinsic flexibility, it is possible to monitor the mass change directly. The end of cantilever can be coated with bioreceptors, such as antibody, therefore a differential surface stress that is induced by antigen binding to the surface of the cantilever cause the cantilever to bend in Figure 4.3(a) [41]. As shown in Figure 4.3(b), the most commonly used readout method for cantilever bending is the optical beam deflection [42]. A laser beam that focused on the end of the cantilever is reflected on the optical sensor, such as position-sensitive photodetector. The position of the reflection spot is changed as the additional mass on the cantilever surface. In addition, the changes of temperature and resonance frequency also used to detect the cantilever motion. The microfluidic systems have adopted the cantilever biosensor for detect and measure the biochemical reactions. To understand the cell cycle and identify cell type and state, a silicon cantilever is integrated in microchannel, Figure 4.3(c). The suspended microchannel resonator (SMR) measures the mass, volume, and density of cells [43]. Through these three basic physical parameters of cells, it is certified that the cell density increase requires energy, function of the protein

synthesis regulator target of rapamycin, passage through START (commitment to cell division), and an intact actin cytoskeleton.

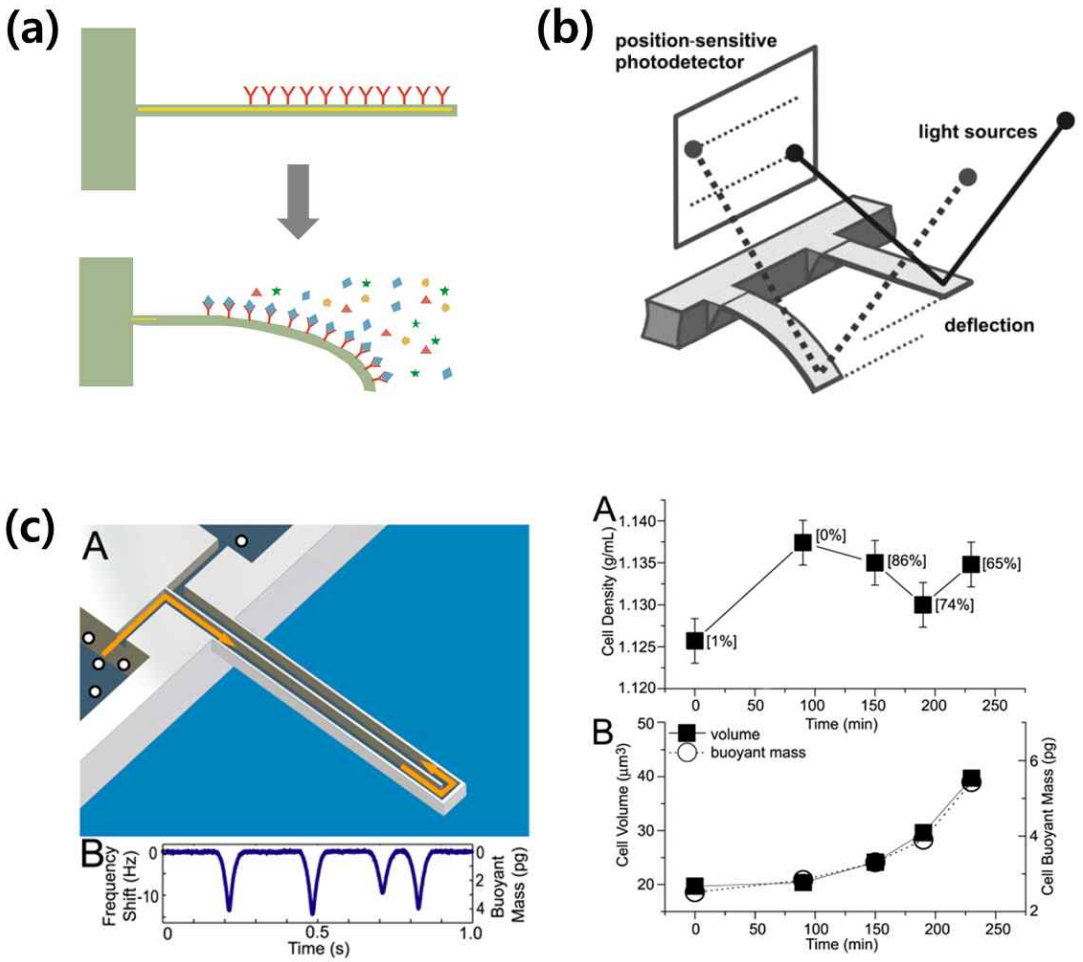

Figure 4.3 (a) Illustration of cantilever biosensor mechanism. (b) Cantilever readout system by optical beam defection. (c) The silicon cantilever with embedded microfluidic channel.

4.1.1.4 Transistor

Semiconducting nanowire and nanotube transistor-based biosensors are attracting considerable attention due to their high sensitivity, selectivity, and label-free detection capabilities. Furthermore, the semiconductor-based biosensors achieved the high-throughput and high-yield characteristics with multiple sensor array. As shown in Figure 4.4, the source and drain are connect with the semiconductor channel, such as nanowire and nanotube, and the gate electrode modulates the conductivity of the channel. The receptors for recognition of target molecules are immobilized on the semiconductor channel. When the target molecules with positively charge are bounded by the receptor, holes as majority carriers are depleted in the p-type nanowire, thereby the conductance decreases. On the other hand, the receptors binding with the negatively charged molecules accumulate the hores, leading to conductance increasing. The transistor-based biosensors have been applied to detect not only the peptide, protein-protein interaction, and DNA hybridization, but also mixtures with disease indicators for diagnosis of virus infection and cancer symptoms [44-46].

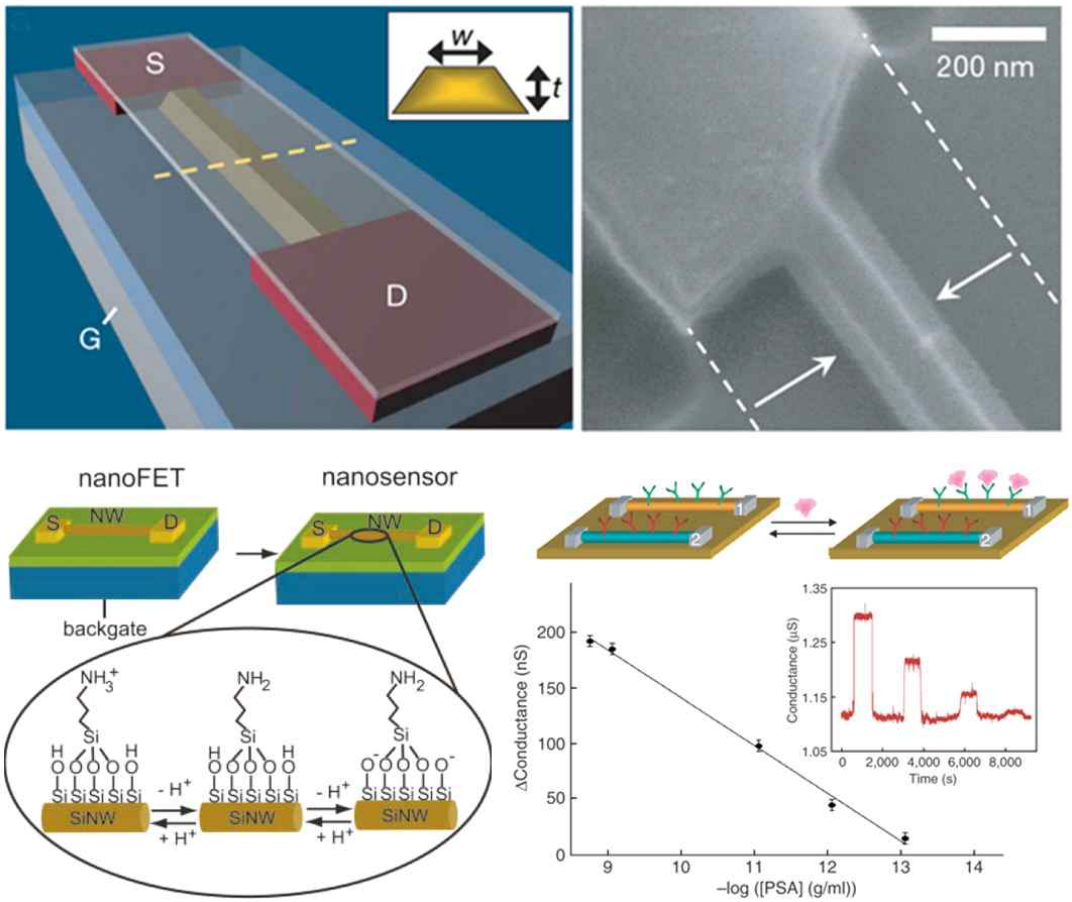

Figure 4.4 Semiconducting nanowire and nanotube transistor-based biosensors.

4.1.2 Surface-enhanced Raman Scattering (SERS)

4.1.2.1 The Origin and Mechanism of SERS

Raman spectroscopy, named after Chandrasekhara Venkata Raman, is a one of the spectroscopic techniques, which is based in inelastic scattering of monochromatic light, such as laser in the visible, near infrared, and near ultraviolet. As shown in Figure 4.5(a) Photons of the laser are absorbed by the samples and interact with molecular vibrations or excitations, and then reemitted. The Raman effect is that the frequency of the reemitted photons shift the original monochromatic frequency to stokes, Rayleigh, and anti-stokes lines. In addition, the frequency shift gives information about vibration, rotation, and other low frequency transitions in sample molecules, and the Raman spectroscopy measure these energy shift [47].

Surface-enhanced Raman scattering (SERS) was accidently discovered while Martin Fleschmann and his coworkers tried to do Raman on the roughened silver electrode in 1974. They observed that the surface of silver electrode with high roughness factor tremendously enhanced the intensity of Raman scattering in Figure 4.5(b). Although the exact mechanism of SERS is still a matter debate in the academia, there are two theories of surface enhancement. The first one is electrochemical enhancement. When the laser light collide on the metal or particle surface and resonance with the Raman scatted fields, localized surface plasmon resonance is

excited and enhanced, leading to increasing the Raman intensity. These electromagnetic enhancement can increase the scatted intensity by $\sim 10^4$. A second mechanism, referred to as the chemical enhancement, is that charge transfer effect and chemical bond formation between analyte molecules and metal surface create new electronic states, resulting in enhancing the scattering by a factor of ~ 100 [48].

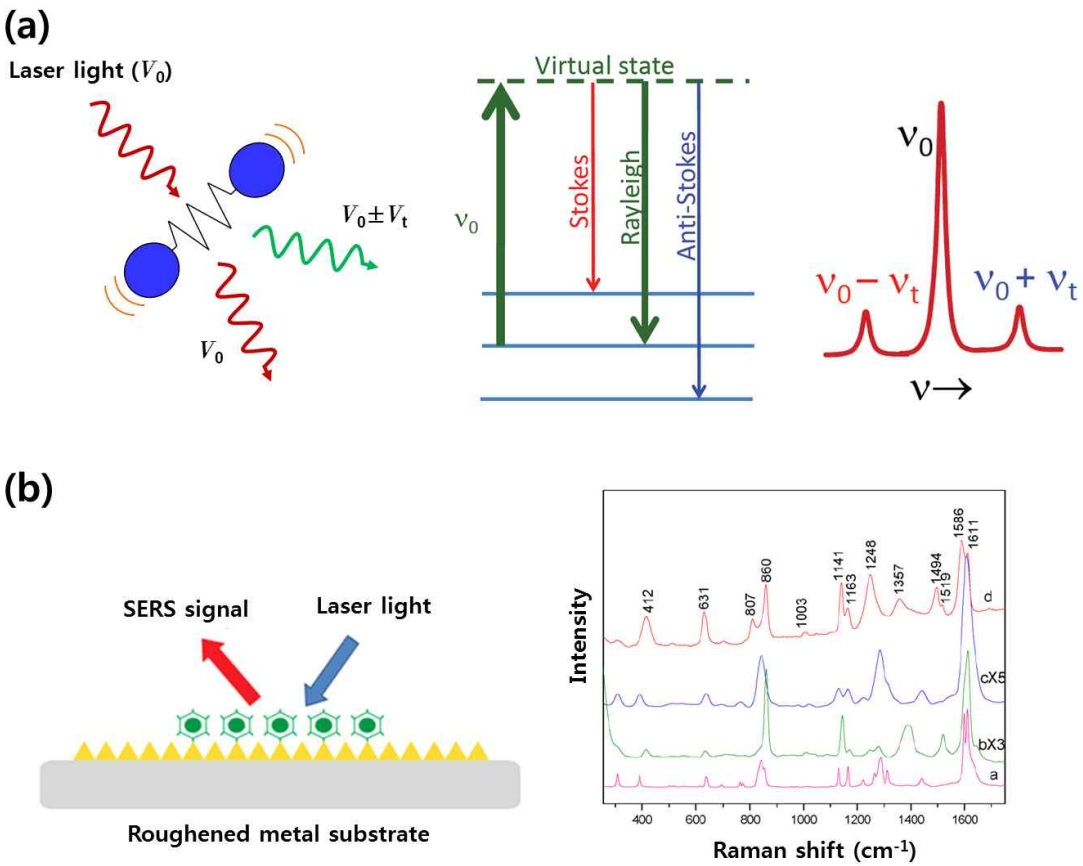

Figure 4.5 Illustration of (a) Raman Scattering and (b) SERS mechanism.

4.1.2.2 Enhancing Substrates for SERS

SERS in the wavelength of visible light is observed at nanoparticles, nanoshells or rough surfaces on nano scale of a few metals like Au, Ag or Cu, as well as narrow interstices among them, "hot spots". Since SERS phenomenon is originated from nanostructures per se, SERS intensity sensitively depends on the geometry, size and shape of the substrates [49]. In this regard, sophisticated engineering of nanomaterials have been a critical issue in nanoscience and recently significant progress was made in developing more sensitive SERS substrates, as shown in Figure 4.6 [50]. Many metallic nanostructures with highly elaborate morphology like Au nanorods as one dimensional nanostructures [51] and Ag nanowire monolayer close-packed and aligned in parallel on a silicon wafer [52] were reported. In addition, Au and Ag nanoparticles with well defined sizes and shapes are available for SERS-based molecular analysis.

In case of nanoparticle based SERS study, single nanoparticle or nanoshell by itself was reported to produce detectable SERS signals [53]. However, it is not enough to obtain the sufficiently strong SERS signals for practical analysis so that aggregation of nanoparticles into a form of cluster or film [54] is needed to produce hot spots giving the overlap of electromagnetic field besides local surface plasmon resonance [55, 56]. For instance, immunoassays using aggregation of nanoparticles are useful to not only confirm the

immune reaction but also quantify the target molecules [57, 58]. Tunable nanoparticle-film and metal doped nanowells were designed to attain strong SERS [59, 60].

However, previous SERS based techniques have intrinsic problems, which one of them is reproducibility. The hot spots among the aggregated nanoparticles are formed with serious uncertainty. SERS signals are very sensitive to how many nanoparticles are aggregated as well as how they are fixed on nano scale, hot spots. As for SERS substrates with closely-packed pattern of nanostructures, the hot spots with the gap as narrow as several nm are beyond control at the present stage. Even if precise fabrication technology in the range of a few nm is available, minute pores are presumably vulnerable to clogging or uncontrolled adsorption. More importantly, many SERS based analytical methods require irreversible treatments like tagging or silvering to intensify the signals so that there are severe limitations such as time consuming, nonspecific binding, and large sample volume. In order to utilize SERS in monitoring molecular species of interest in the middle of a reaction process, it is necessary to acquire strong SERS signals without any irreversible pretreatment, contamination, or loss of analytes.

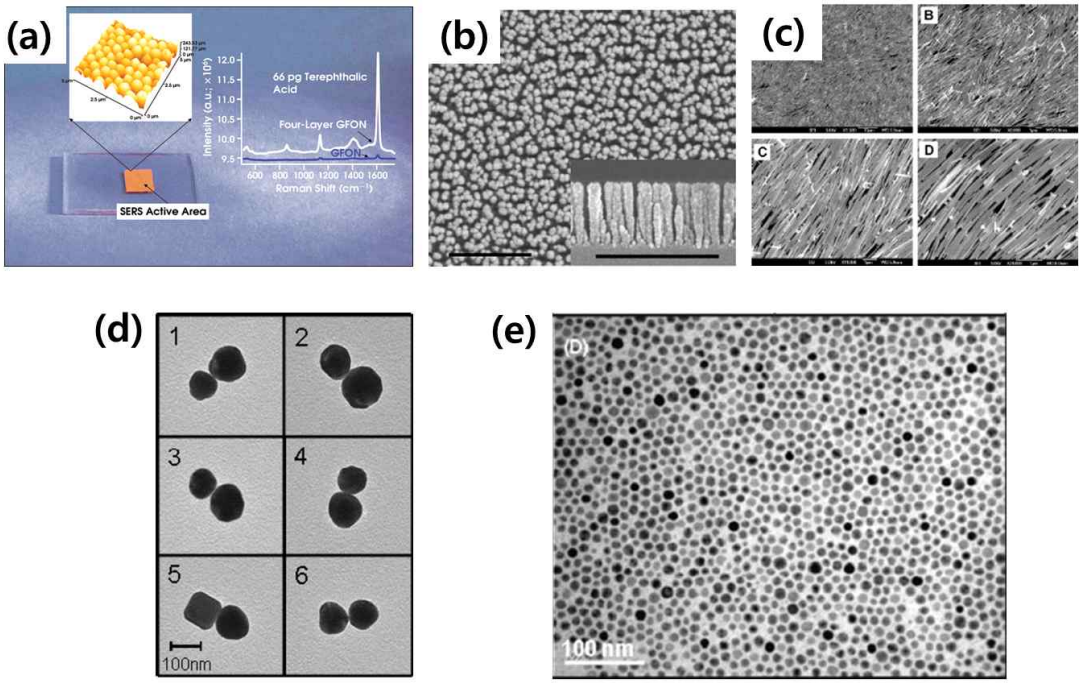

Figure 4.6 Enhancing substrate for SERS : (a) Noble metal with nanostructure, (b) Nanorod array, (c) Nanowire, (d) Nanoparticles, (e) Nanoparticle film.

4.1.3 SERS on a Microfluidic Chip

Recently, SERS-based molecular probing on a microfluidic chip increasingly attracts keen attention, since the Raman tags are free from possible quenching or bleaching unlike fluorescence detection. A number of the biological analytes themselves are Raman-active and thereby need no tags, Raman reporters. A few chips employing SERS analysis were reported [61-63]. Aggregation of metal nanoparticles is the most typical way to acquire strong SERS signals in microfluidic systems as well. The nanoparticles in the SERS-chip were aggregated by using special monolithic structures [Figure 4.7(a)], optical trapping [Figure 4.7(b)], or reagents such as chloride, nitrate, perchlorate, polylysine, and modified DNA [64-66]. However, reliable analysis based on SERS through irreversible aggregation is still challenging toward practical applications. Once the nanoparticles in the microchannel were aggregated, the SERS-chips were readily exposed to the risk of clogging, which is hardly recovered. The rapid advance in modern microfluidic technology has made good tools available to precisely control the local conditions for SERS generation and allow integration with other miniaturized units for sophisticated process monitoring [67-69]. Reversible generation of environments for stable and strong SERS without the addition of any chemical reagents or consumption of analyte is expected to offer great opportunities for the innovation of nano-bioanalysis on microfluidic chips.

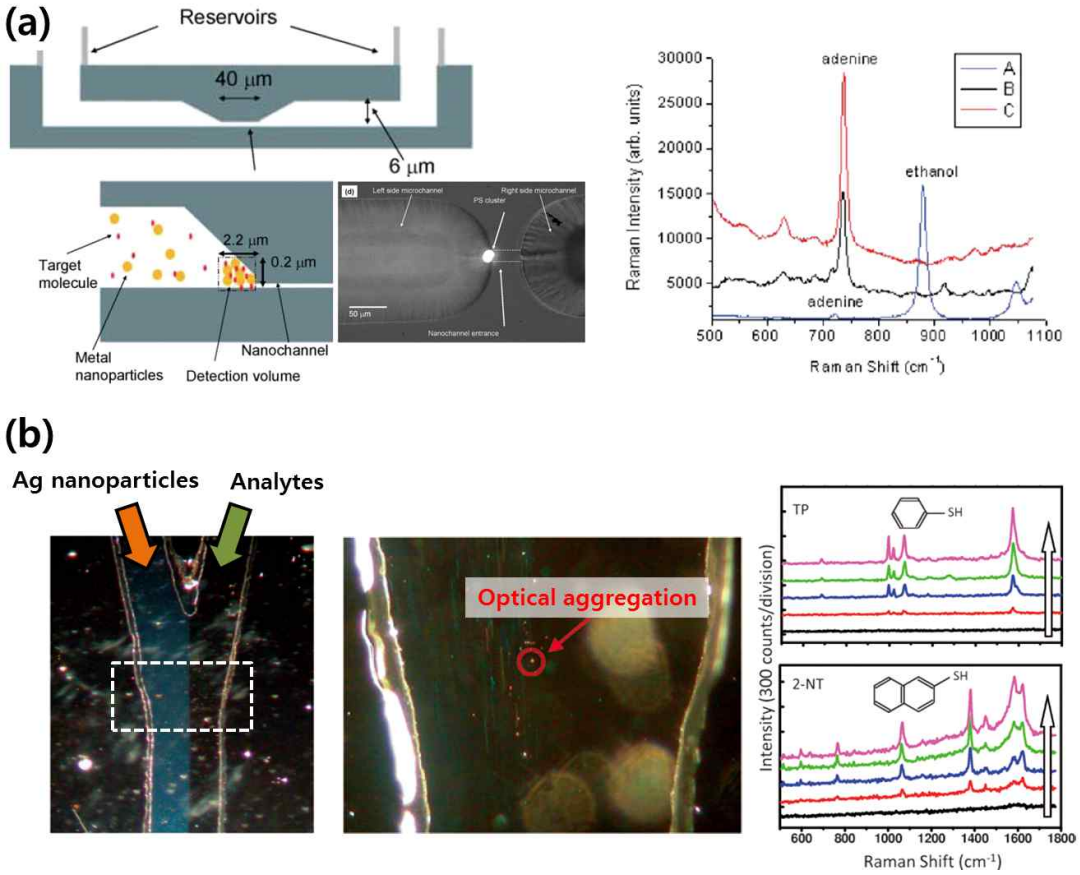

Figure 4.7 SERS on a microfluidic system using (a) the monolithic nano structure and (b) optical aggregation.

4.1.4 Goals of This Study

We propose dynamic reversible preconcentration of gold nanoparticles (AuNPs) to create SERS-active substrate in microfluidic system and let it disappear if not needed, as shown in Figure 4.8. A negatively charged polyelectrolyte membrane, poly-2-acrylamido-2-methyl-1-propanesulfonic acid (pAMPSA) was employed for electrokinetic trapping. In this system, the pAMPSA plugs facing to each other were photopolymerized in the microchannel. Due to the anionic charge fixed on the polyelectrolyte backbones, cations are selectively allowed to pass through the pAMPSA phases. When electric field is applied to the platinum electrodes across the two pAMPSA plugs, the cations in the microchannel near the region between the pAMPSA plugs are extracted to the reservoirs in which ground electrodes are immersed. Obviously, anions cannot go through the negatively charged polyelectrolyte membrane. When extraction of cations is faster than mass transport making charge balance, the local ionic charge balance breaks at the region between the pAMPSA plugs. As a consequence, ion depleted space appears and expands as a function of the applied voltage and time. Combining with the electroosmotic flow (EOF) coming in, the ion depletion produces a region where ions are preconcentrated. Therefore, the AuNPs with negative zeta potential in aqueous solution can be locally preconcentrated in the microchannel to generate SERS active substrate.

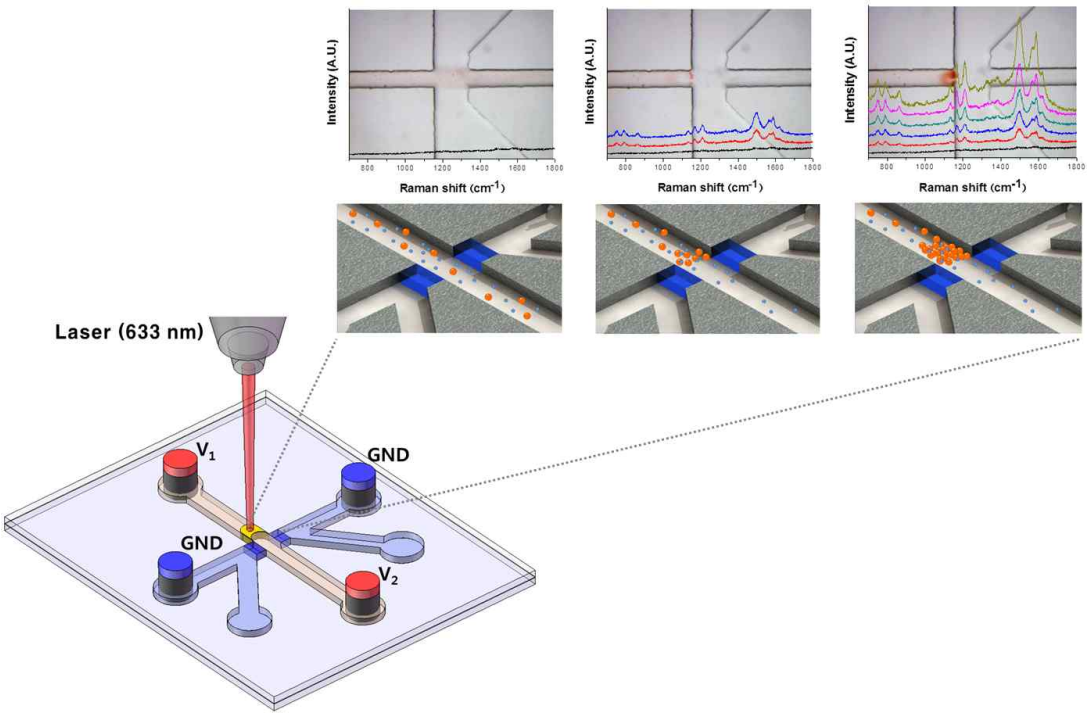

Figure 4.8 Schematic for detecting SERS signals based on the dynamic preconcentration of AuNPs.

4.2 Experimental Section

4.2.1 Microchannel Fabrication Process

Conventional photolithographic techniques were used to fabricate to microchannel with 70 μm wide and 30 μm [Figure 4.9]. A glass slide (Corning, USA) was washed with piranha solution (H_2O_2 : H_2SO_4 = 1:3) for 45 min. To remove the cleaning reagent, it was rinsed twice with deionized-water, acetone and methanol. The glass was dehydrated on a hot plate at 150 °C for 100 min, and then cooled to tepid at room temperature. The glass was coated with hexamethyldi silazane, HMDS (Clariant, Switzerland) using a spin coater (Won Corp., Korea) at 6000 rpm for 30 s to enhance the adherence of photoresist to its surface. Photoresist (PR) AZ4620 (Clariant, Switzerland) was then coated on the glass using a spin coater at 500 rpm for 7.5 s and at 6000 rpm for 30 s. The PR-coated slide glass was soft baked at 100 °C for 90 s and cooled to room temperature, before it was exposed to ultra-violet (UV) light with an intensity of 15 mW cm^{-2} for 10 s through a patterned mask film. The exposed PR was removed by AZ400K developer (Clariant, Switzerland). The glass was then hard baked on a hot plate of 150 °C for 15 min and etched by 6:1 buffered oxide etch solution (J.T.Baker, USA). Dust on the glass was removed by ultrasonic cleaning (351OE-DTH, Brasonic, USA) for 15 min. The reservoirs were drilled into the glass chip to introduce sample solutions and

apply the electric field in the microchannel. The etched surface of the glass was covered by a precleaned flat slide glass and heated at 600 °C for thermal bonding.

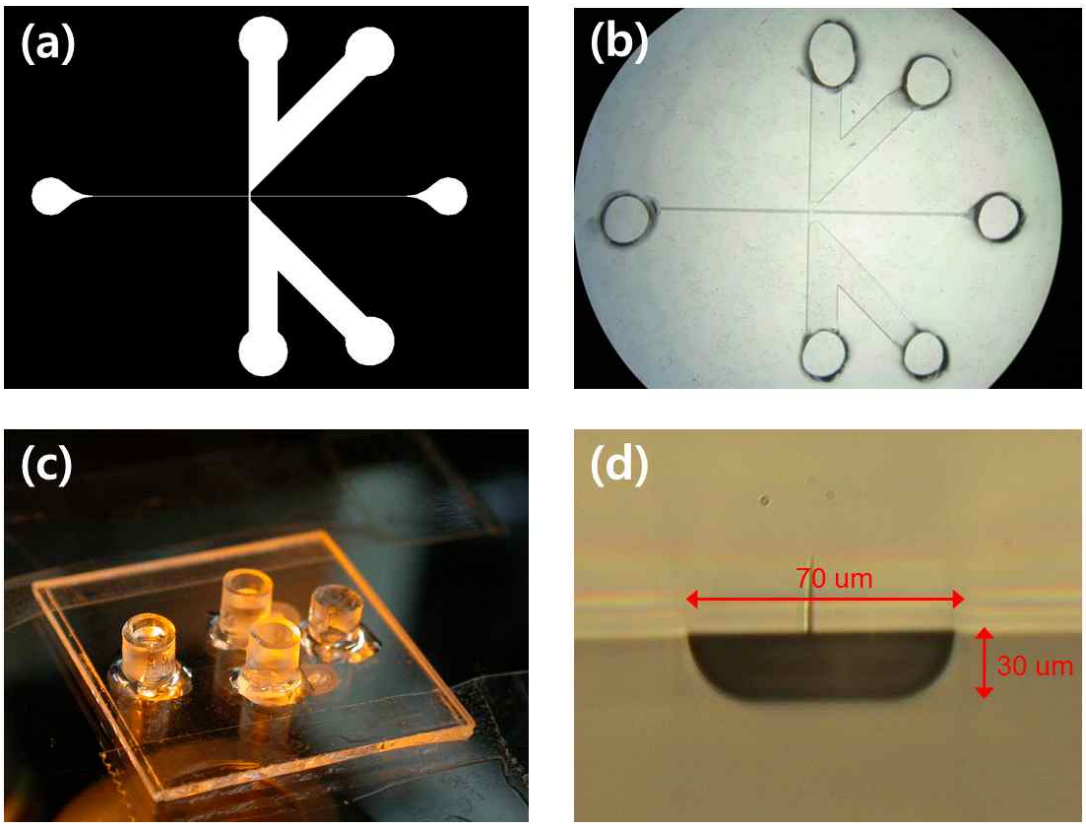

Figure 4.9 The fabricated microfluidic chip. (a) Mask design with AutoCAD. (b, c) The microfluidic chip is comprised of inlet, outlet and reservoirs for the electrode connection. (d) Cross-sectional image of microchannel.

4.2.2 Negatively Charged Polyelectrolytic Gel Electrodes Fabrication

As shown in Figure 4.10, a pair of polymer plugs was fabricated by UV photopolymerization. 2 M aqueous 2-acrylamido-2-methyl-1-propane sulfonic acid (AMPSA) was the monomer used to create the negatively charged polymer. It was prepared with a photoinitiator (2%) and a cross-linker (2%). Before polymerization, the microchannel was coated with 0.5% 3-(trimethoxysilyl) propylmethacrylate (TMSMA) to covalently link the polymer plugs and the glass surface at room temperature for 30 min. The TMSMA-coated microchannel was cleaned with deionized water and methanol, and was filled with the monomer solution. The microchannel was aligned under a patterned mask film to determine the desired location of the polymers and exposed to UV light at 15 mW/cm^2 for 2 s. The pAMPSA plugs in the microchannel were washed and stored in 10 mM KCl solution.

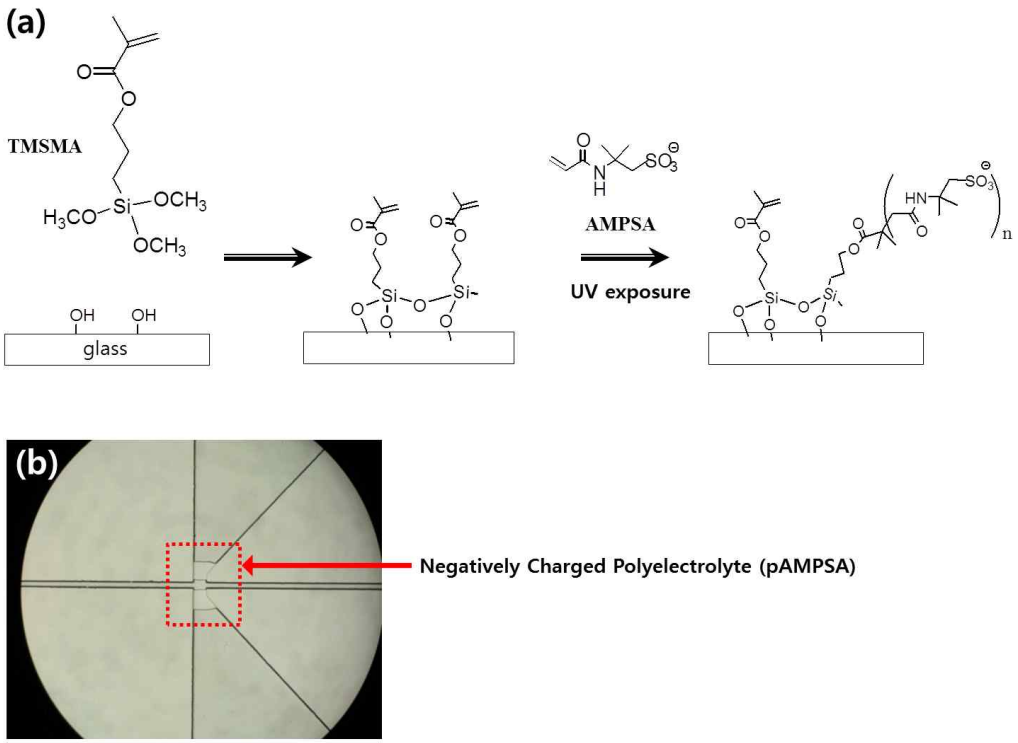

Figure 4.10 (a) The photopolymerization process for fabrication of negatively charged polyelectrolytic gel electrodes (pAMPSA) in microchannel. (b) A pair of oppositely facing pAMPSA plugs is positioned on the microchannel wall.

4.2.3 Instrumentation

To observe the distribution of the fluorescent dyes in the microchannel, a fluorescence microscope, TE-2000 (Nikon), mercury lamp, and 12-bit ProgRes C3 CCD camera (JENOPTIK) were used. A dc power supplier was applied to the Ag/AgCl electrodes that were connected to the microfluidic chip, while a customized micro-Raman spectroscopic system equipped with a microscope and 12-bit ProgRes C3 CCD camera (JENOPTIK) allowed monitoring of the distribution of AuNPs and SERS signals from the microchannel.

4.2.4 Sample Preparation

All materials were used without additional purification. Fluorescein, 3-(Trimethoxysilyl)propyl methacrylate (TMSMA), 2-acrylamido-2-methyl-1-propanesulfonic acid (AMPSA), hexamethyl disilazane (HMDS), and platinum wire (0.05 mm thick, 99.9%) were purchased from Sigma (St. Louis, MO). The fluorescent dye was diluted in 10 mM phosphate buffer at pH 7.0 before use and impurities were removed using a syringe nanofilter.

4.3 Results and Discussion

4.3.1 Preconcentration Mechanism

As shown in Figure 4.11, the preconcentrated AuNP plug that was created by electrokinetic trapping. When dc 20 V and 5 V were applied to V_1 and V_2, respectively, the 20 nm AuNPs with negative zeta potential (ξ) that varied from -10 to -25 mV at pH 4 to 12 in 10 mM phosphate buffer solution were driven by EOF in the glass microchannel [Figure 4.11(a)]. When the GND (chassis ground) electrodes were connected to the ground of the power supply, cations were instantly extracted through the negatively charged polymer, pAMPSA. At the same time, anions and AuNPs with negative zeta potential in 10 mm phosphate buffer at pH 7.0 were repelled from the region between the pAMPSA plugs [Figure 4.11(b)]. Consequently, an ion-depletion region clearly appeared between the pAMPSA plugs. The incoming anionic AuNPs were stacked near the ion depleted region, resulting in preconcentration [Figure 4.11(c)]. The trapped AuNPs appeared as a reddish spot that was easily observable with a conventional microscope coupled to the Raman spectrometer. When the GND electrodes were floated, the nanoparticles began to redisperse in the sample solution and flow along the microchannel [Figure 4.11(d)]. Therefore, by controlling the applied electric field across the two pAMPSA plugs, it was possible to regulate precisely the degree of AuNP preconcentration.

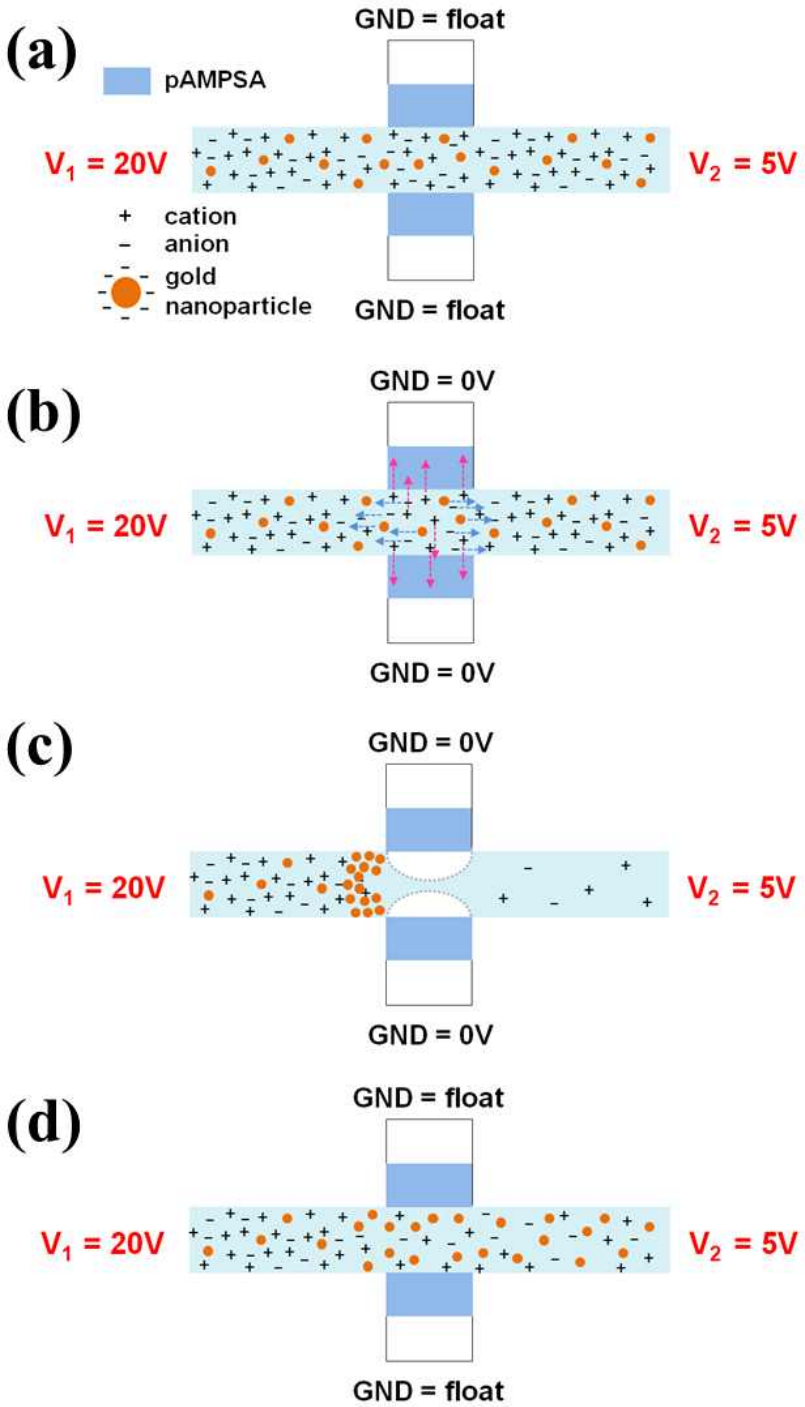

Figure 4.11 Preconcentration mechanism with negatively charged polymer, pAMPSA.

4.3.2 Preconcentration of Anionic Fluorescent Dye

To confirm sample preconcentration by electrokinetic trapping, the behavior of anionic fluorescein was monitored using a fluorescence microscope. Figure 4.12 shows that 10 μM fluorescein molecules in 10 mM phosphate buffer at pH 7.0 was preconcentrated in the microchannel. Under an applied electric field, cations in sample solution were rapidly extracted through the pAMPSA plugs. As a result, anions and anionic fluorescein molecules were expelled from around the polyelectrolytic plugs to maintain charge neutrality. As the sample solution was delivered into the microchannel by electro-osmotic flow (EOF), anions including the fluorescein molecules were preconcentrated near the ion depletion region that was generated between the pAMPSA plugs.

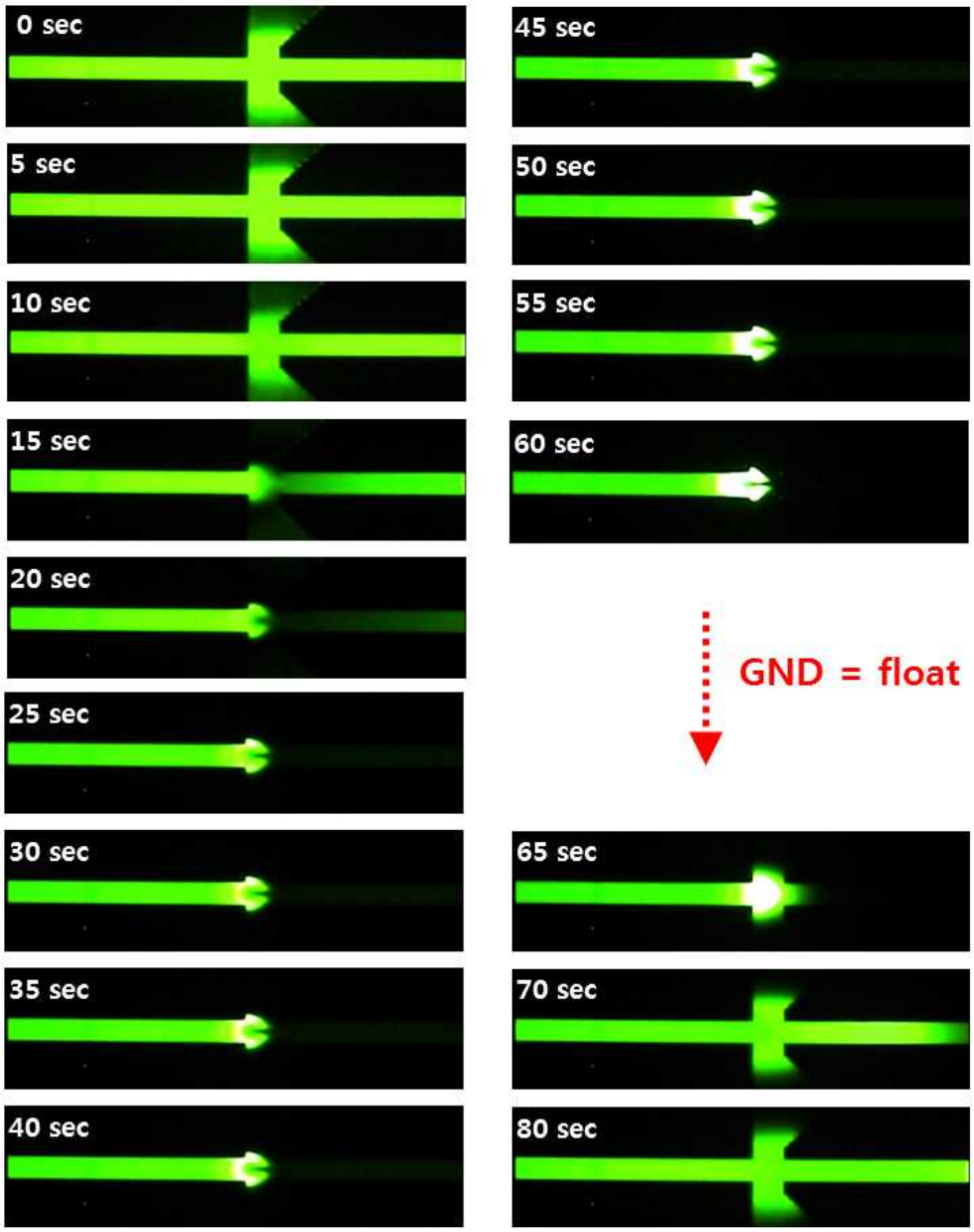

Figure 4.12 Fluorescence images of preconcentrated anionic dye. When V1, V2, and GND were 20 V, 5 V, and 0 V, respectively, anionic fluorescein was rapidly preconcentrated in the microchannel. The preconcentrated anionic molecules were redispersed into the sample solution by floating the electrode, GND.

4.3.3 Preconcentration of Gold Nanoparticles (AuNPs)

Figure 4.13 shows the preconcentrated AuNP plug. When the dc voltage was were applied, the AuNPs in 10 mM phosphate buffer solution were driven by EOF to move along the microchannel [Figure 4.13(a)]. As soon as the GND electrodes on the chip were set to the ground potential, cations in the solution instantly passed through the negatively charged polymer, pAMPSA [Figure 4.13(b)]. Consequently, anionic AuNPs were stacked near the ion depleted region, as shown in Figure 4.13(c). When the GND electrodes were floated, the nanoparticles began to redisperse into the sample solution and flow down along the microchannel [Figure 4.13(d)].

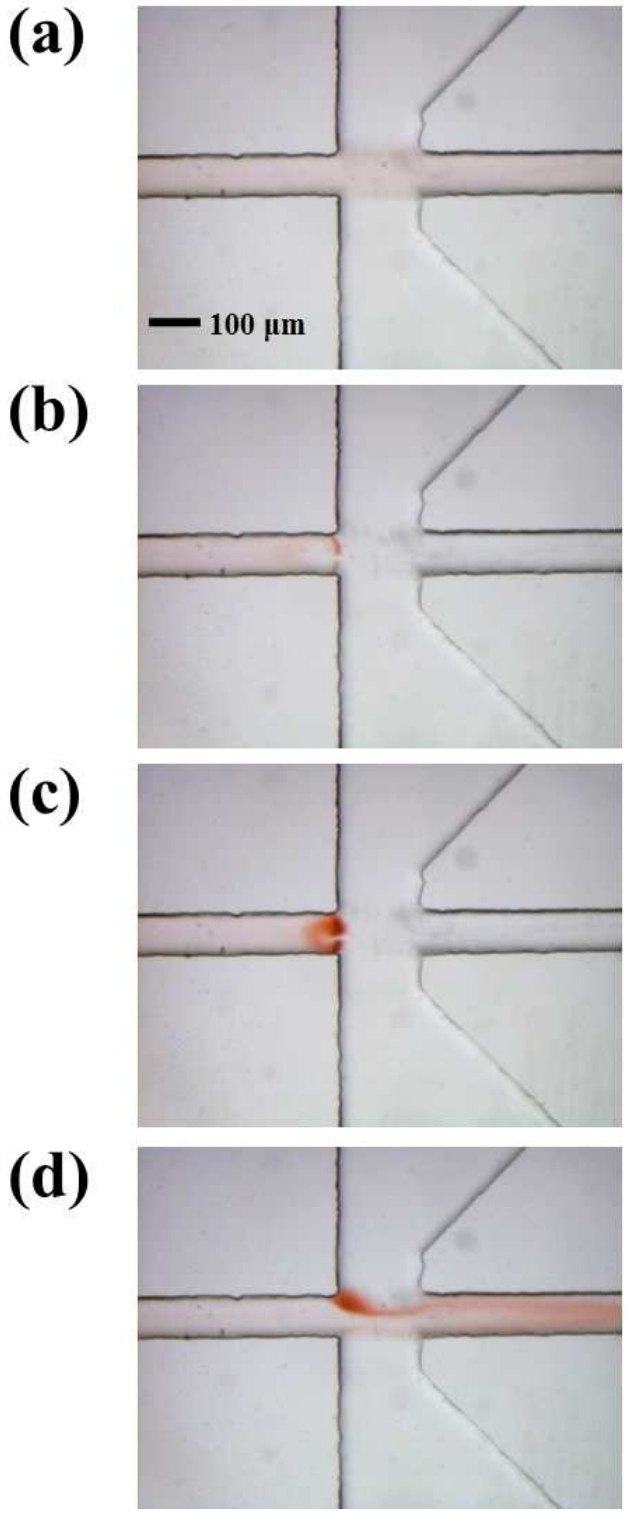

Figure 4.13 Optical images of preconcentrated AuNPs.

4.3.4 Average Inter-Particle Distance Between the Preconcentrated AuNPs

To estimate the concentration of AuNPs during preconcentration process, AuNP solutions of various concentrations (from 20 to 2500 times of the original concentration) were prepared by centrifugation. Each sample was introduced into the microchannel and the corresponding images were captured with a microscope, and 12-bit ProgRes C3 CCD camera (JENOPTIK). Image analysis using custom software written in Matlab 7 (The MathWorks, Natick, MA) revealed the absorbance data from the samples. Absorbance was assumed to be linearly dependent on the known concentrations of AuNPs suspensions, which were homogeneously dispersed in the solution, a calibration curve of absorbance and AuNP concentration was obtained and the dynamic concentration of the AuNPs during preconcentration was estimated [Figure 4.14(a)]. From the AuNPs concentration, the average distance among AuNPs can be calculated. Suppose that an individual AuNP occupies a space that can be regarded as an imaginary sphere of radius, dR. Given that a number density of 0.1% AuNPs is equal to 5.33×10^{12} AuNPs mL^{-1}, the radius (d_R) of the imaginary sphere can be expressed as:

$$d_{\mathrm{R}} = \sqrt[3]{\frac{V_{\mathrm{sol}}}{5.33 \times 10^{12}} \times \frac{3}{4\pi}}$$

where V_{sol} is the volume of solution containing 5.33×10^{12} AuNPs. From this consideration ratio, the inter-particle distance (D_{NP}) can be calculated according to the following equation:

$$D_{\mathrm{NP}} = 2 \times (d_{\mathrm{R}} - d_{\mathrm{r}})$$

where d_r is the radius of a single AuNP, 20 nm. As a result of preconcentration for 60 s, corresponding to over 2500 times higher concentration than the original, the average inter-particle distance was calculated to be about 12 nm [Figure 4.14(b)]. Considering the absorbance of the preconcentrated spot in the microchannel, the average space was predicted to be less than 12 nm, which is narrow enough to act as hot spots.

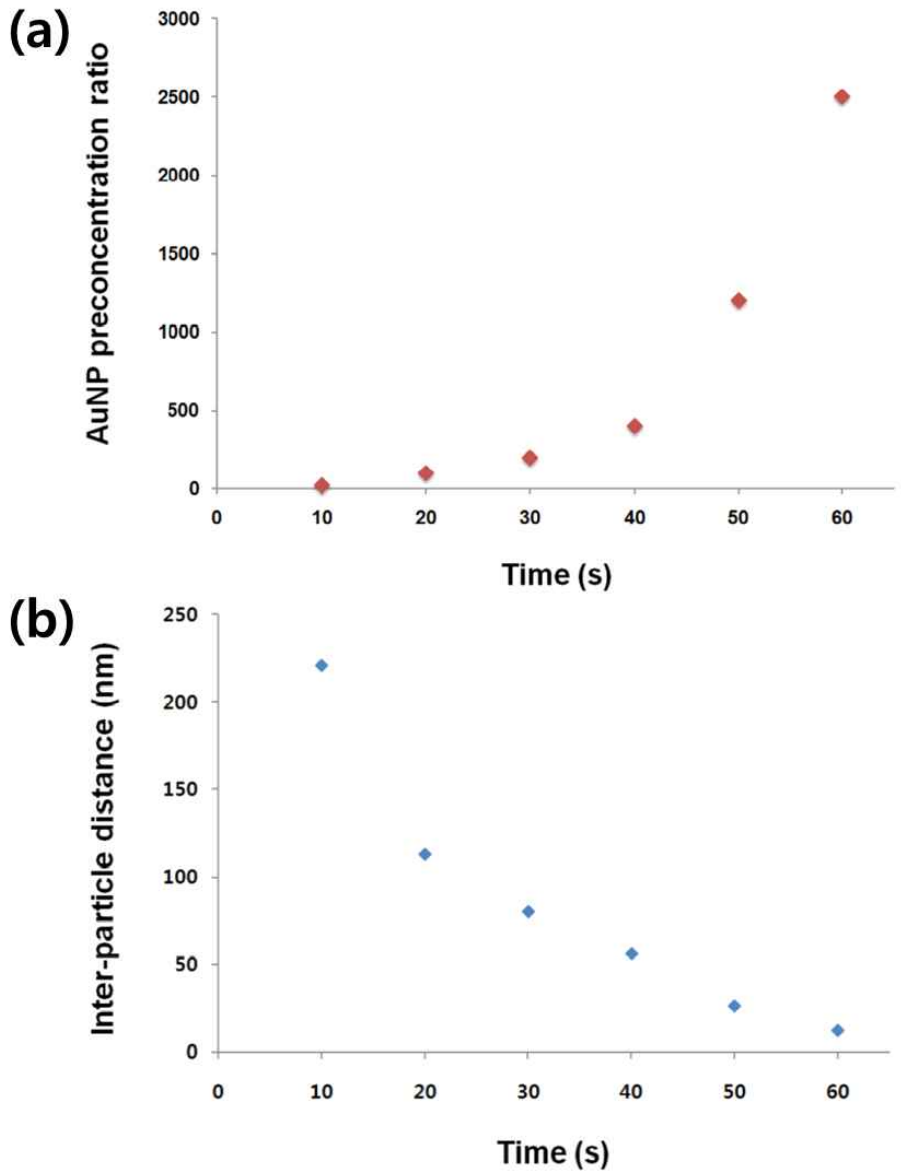

Figure 4.14 (a) The ratio of preconcentrated to original concentrations of AuNP suspensions in the microchannel as a function of preconcentration time. (b) Estimated average inter-particle distances among AuNPs resulting from the preconcentration process. As the concentration of the preconcentrated AuNPs exceeds 2500 times of the original, the average inter-particle distance is predicted to be about 12 nm.

4.3.5 SERS Signals of Raman Active Molecules

4.3.5.1 4-Aminobenzoic Acid (4-ABA)

4-aminobenzoic acid (4-ABA) with low pK_a values 2.41 and 4.87 was dissolved in 10 mM phosphate buffer at pH 4.0 to make the 4-ABA neutral charge and avoid preconcentration of analyte molecule itself. When the mixture of 0.01% AuNP and 10 μM 4-ABA was introduced into the microchannel and the electric fields were applied, the SERS signals of 4-ABA remarkably grew as the AuNPs were rapidly preconcentrated in the microchannel [Figure 4.15].

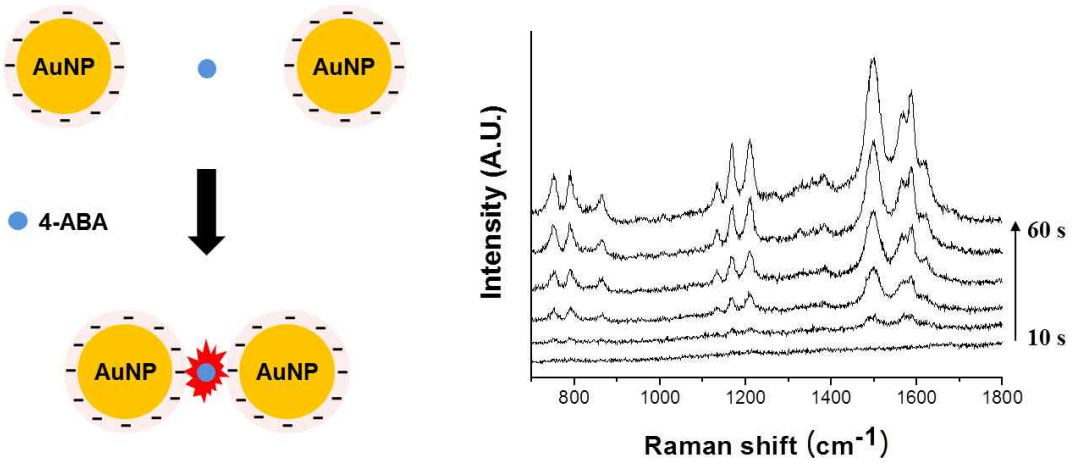

Figure 4.15 SERS spectra of 10 μm 4-aminobenzoic acid (4-ABA) which had neutral charge in 10 mm phosphate buffer at pH 4.0. The peak intensity increased as AuNPs were preconcentrated.

4.3.5.2 Pyridine

Pyridine (pK_a 5.25) was dissolved in 10 mM phosphate buffer at pH 8.0. When a mixture of 0.1% AuNP and 10 μM pyridine was introduced into the microchannel and the electric fields were applied, the SERS signals of pyridine grew remarkably. Figure 4.16 shows that SERS peaks corresponding to neutral pyridine molecules increased as the AuNPs were preconcentrated, similar to that observed with 4-ABA. As the average distance among the AuNPs kept decreasing during preconcentration, it is believed that effective hot spots appeared and intensified the SERS signals of the analytes.

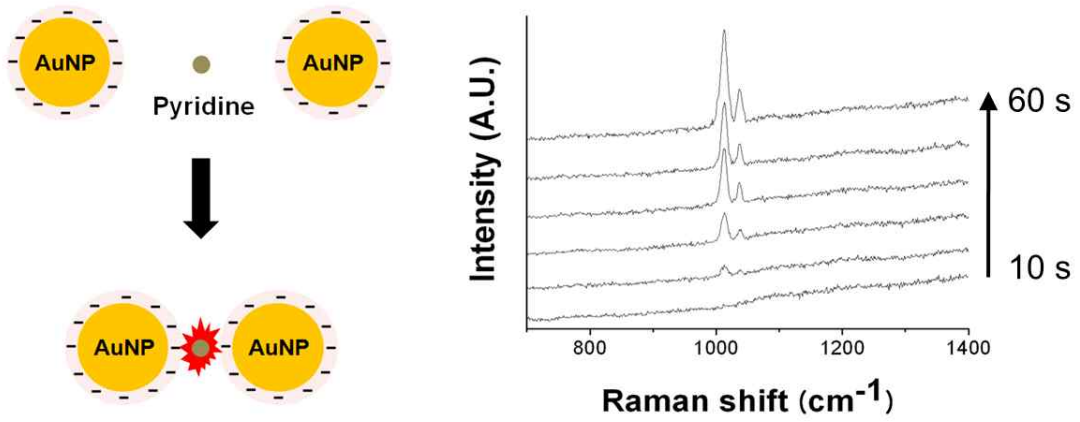

Figure 4.16 A series of SERS spectra of neutral pyridine that were acquired every 10 s from mixtures consisting of AuNPs and neutral 10 μM pyridine in 10 mM phosphate buffer at pH 8.0.

4.3.5.3 4-Mercaptobenzoic Acid (4-MBA)

To see if the distance between the preconcentrated AuNPs is short enough to significantly enhance the Raman scattering, the surfaces of AuNPs were functionalized with 4-Mercaptobenzoic Acid (4-MBA, pK_a 4.79) by dissolving 1 mM 4-MBA and 0.01% AuNPs in 10 mM phosphate buffer solution at pH 4.0. Spontaneous self assembly monolayer of 4-MBA was allowed to proceed for 16 h at room temperature with stirring. Then the 4-MBA modified AuNPs were centrifuged at 13,000 rpm for 30 min and redispersed in 10 mM phosphate buffer solution to remove excess 4-MBA molecules. The same procedure was repeated twice to obtain 0.01% 4-MBA-modified AuNPs, which was then injected into the microchannel by EOF. Under the electric field, the negatively charged 4-MBA-modified AuNPs in the 10 mM phosphate buffer at pH 7.0 were preconcentrated and produced the enhanced Raman signals corresponding to 4-MBA as time elapsed [Figure 4.17]. In general, the SERS activity was increased considerably when the hot spot or nano-gap width was less than 10 nm [70, 71]. To confirm whether distance of hotspot generated by preconcentration of AuNPs is near nm dimension, we calculated the distance between the preconcentrated AuNPs by image processing in section 4.3.4. As shown in Figure 4.14, it was estimated that the distance became narrow from 221 nm to 12 nm at 10 and 60 seconds, respectively. Therefore, the hot spot produced by preconcentration of AuNPs is a reasonable reason for

significantly enhanced SERS signal. Moreover, It was well known that the SERS intensity of single nanoparticle coated with a monolayer of SERS analytes was much smaller than dimers and trimers [72]. Accordingly, in our system, increasing the number of the hot spots between the preconcentrated nanoparticles were more dominant factor than sum of the SERS signal from individual AuNPs themselves in the enhanced SERS intensity.

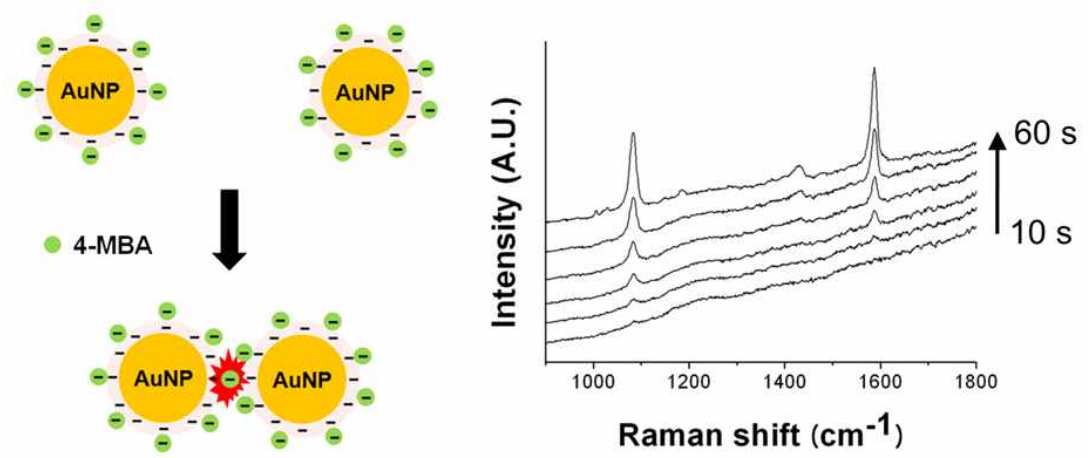

Figure 4.17 SERS spectra of 4-mercaptobenzoic acid (4-MBA) on the AuNPs in the middle of the preconcentration process.

4.3.6 SERS Signals of Neurotransmitter: Histamine

4.3.6.1 Histamine

The well-known neurotransmitter with an aromatic nitrogen base, histamine, was employed to probe the power of quantitative analysis using the proposed system. Detection of the histamine concentration is very important because it is directly relevant to immune response, central nervous system, and allergic reaction. Many different methods were proposed to quantify nanomolar histamines, for example capillary electrophoresis, liquid chromatography, and electrochemical methods [73].

4.3.6.2 SERS Analysis of Histamine

Histamine was employed to probe the limit of detection (LOD) of the propose system. Histamine solutions over a wide range of concentration (1 nM, 10 nM, 100 nM, 1 μM, 10 μM, 100 μM, 500 μM and 1 mM) were prepared by dissolving it in 10 mM phosphate buffer at pH 11.5. The pK_a value of histamine is 5.8 and 9.4; therefore, only the AuNPs should be negatively charged at pH 11.5. When electric field was applied across the two pAMPSA plugs, the preconcentrated nanoparticle plug was reproducibly maintained to be steady. Figure 4.18(a) shows the SERS spectra of histamine, which

were consistent with the previously histamine report [74]. The intensity of the histamine-characteristic peak at 1261, 1316, and 1567 cm^{-1} was measured 60 s after preconcentration began, and used for the quantitative evaluation. The peak intensity increases in proportional to the concentration of histamine [Figure 4.18(b)]. The limit of detection (signal-to-noise ratio of 3) was 10 nM. Statistical data processing was performed based on SERS data that had been acquired by 5 independent measurements, and each the experiment was conducted by repeating the reversible processes of preconcentration and redispersion on a single chip. Therefore, the SERS measurements from the proposed system enabled the quantitative analysis of Raman-active analytes such as histamine with low standard deviation and high sensitivity.

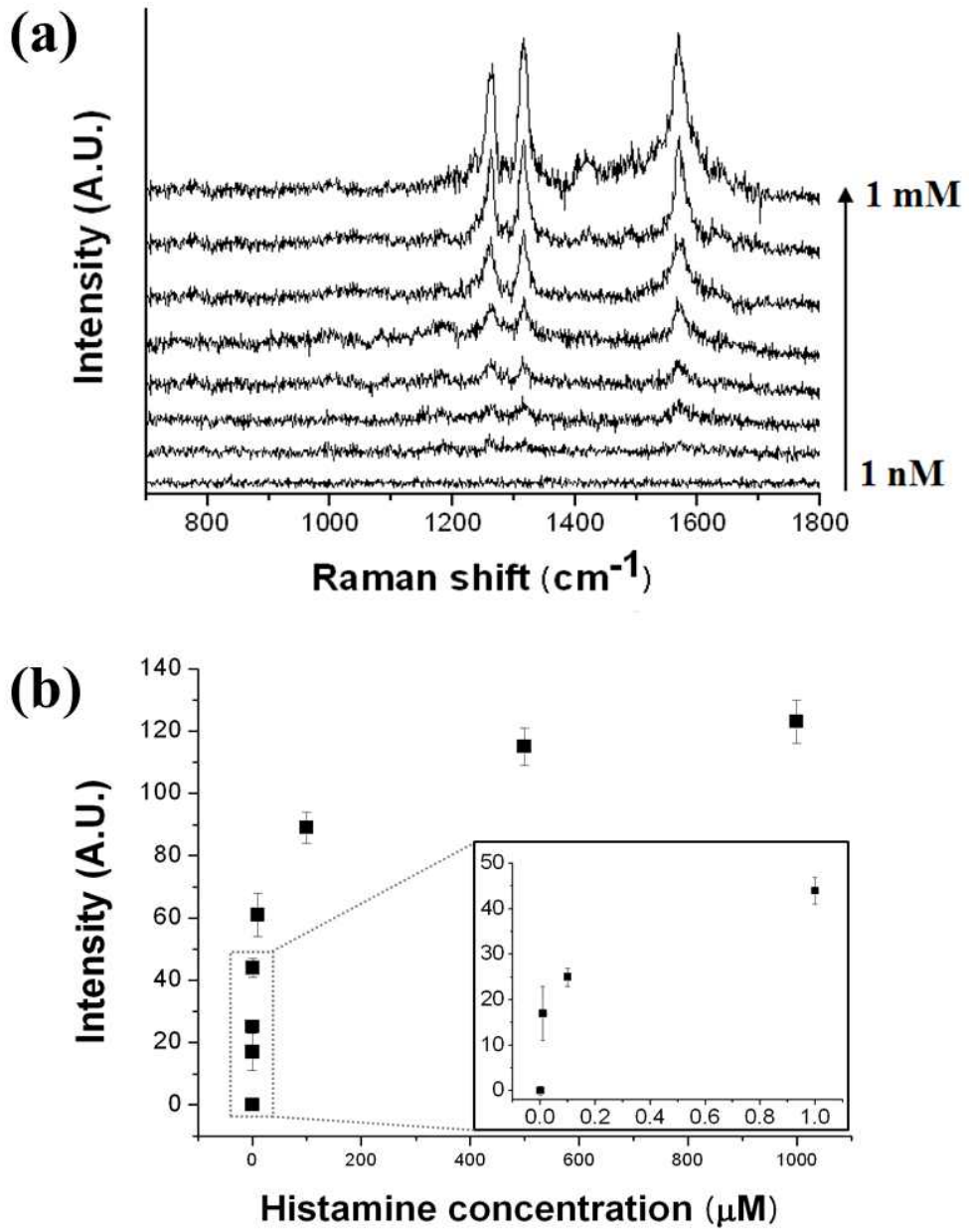

Figure 4.18 (a) SERS spectra for a variety of concentrations of histamine which was mixed with AuNPs in 10 mM phosphate buffer at pH 11.5. (b) The intensity of a characteristic peak of histamine versus the concentration of histamine.

4.4 Conclusion

In conclusion, the reversible preconcentrated AuNPs by the electrokinetic trapping in the microchannel acted as dynamic SERS-active substrate which needed no fabrication of the well defined nanostructures for strong SERS. The proposed microfluidic system can provide highly reproducible environment for SERS analysis without any clogging or memory effect. In addition, the system let us acquire strong SERS signals without any sampling, contamination, or loss of analytes. The repetitive measurements can substantially improve the reliability of SERS so as to enable quantitative SERS analysis as well as in situ molecular monitoring in a microfluidic system. It is expected to inspire many innovative ideas about evolution of nanotechnology toward even wider practical applications.

Publications

Kwang Bok Kim, Ji-Hyung Han, Hyoungseon Choi, Hee Chan Kim*, and Taek Dong Chung*, "Dynamic Preconcentration of Gold Nanoparticles for Surface Enhanced Raman Scattering in a Microfluidic System", Small, 2012, 8(3), 378-383.

Chapter 5.

Conclusion and Discussion

This dissertation is study of the polyelectrolytic gel electrodes in microfluidic chip for development of RBC counter, transistor, and AuNP preconcentrator integrated SERS-on-a-chip as biomedical, electrical, and analytical chemistry application, respectively.

We showed the technique of PGE-based cell counting using a low-voltage-biased dc impedance analysis as a new strategy for a chip-based cell counter in the second chapter. RBCs in human whole blood samples were counted with error approximately within 10% in comparison with a clinical hematoanalyzer. The required sample was 2 μL of whole blood diluted by a factor of more than 800 with a buffer and EDTA solution, which can be readily implemented in a microfluidic chip. The greatest advantage of the developed PGE-based system is that it requires no preprocessing, neither centrifugation nor

filtering, to separate blood cells. Furthermore, it can protect the blood cells from electrical damage and undesirable aggregation on the surface of electrodes because there is no direct contact between them. Although a number of miniaturized chip-type blood cell counters have been suggested, it is difficult to find one with practical clinical applications, mainly because most of them are based on relatively large and expensive optical equipment that often require sophisticated alignments and fine tunings. Our whole system, including the external electronic circuitry, is simple and compact enough to be a point-of-care testing-type cell counter. For this reason, the proposed PGEs-based system has sufficient potential for many valuable clinical applications in the near future.

In the third chapter, we demonstrated a pJFET system that operates in an aqueous medium by reliably controlling the ionic flow through oppositely charged polyelectrolyte plugs. The applied V_G causes ion depletion in the middle of the main microchannel, which regulates I_D. This system does not require a complicated and sophisticated process such as nanofabrication. Despite the simple structure and short fabrication process, the polyelectrolyte plugs are remarkably more effective tools for ion extraction than nanochannels. Hence, an ion depletion region can be rapidly created in the microfluidic networks. The pJFET has the great potential for evolving into more versatile utilities such as multi-functional ionic circuits by suggesting new opportunity to aqueous information processors.

Finally, in chapter four, the reversible preconcentration and

redispersion of AuNPs were realized by electrokinetic trapping in the microchannel. This unprecedented dynamic SERS substrate needed neither well-defined nanostructures nor irreversible treatments like silvering to obtain strong signals. The proposed microfluidic system provided a highly reproducible environment for SERS without clogging or memory effects. More significantly, the system allowed the acquisition of strong SERS signals without any sampling, contamination, or loss of analyte. Repetitive measurements in this platform allowed the statistical improvement in terms of the reliability of SERS intensity so as to enable quantitative analysis based on SERS as well as in-situ molecular monitoring in the microfluidic system. It is expected to inspire many innovative ideas about evolution of nanotechnology to even wider applications.

It is believed that the microfluidic platform with polyelectrolytic gel electrodes provides a way to regulate the ionic mobility and current without metallic electrodes in the microchannels. Using the ionic mass transportation with polyelectrolytic gel electrodes, various biosamples, such as protein, gene, lipid, and cell could be mixed, separated, and preconcentrated in single platform for post analysis, and in the near the future, each samples could be identified by barcoding technologies. Therefore, mixed biological samples from molecular level to cellular level could be totally separated and analyzed in the microfluidic systems. These microfluidic platform also has the potentials of proposing the solution to the worldwide water-shortage problem. Polyelectrolytes have been utilized in water

purification and desalination for at least four decades. The conventional methods for water treatment including filtration, reverse osmosis, and electrodialysis have required high power consumptions and costs due to low energy efficiency. For this reason, microfluidic chip system with polyelectrolytes plug would be realized in a portable device with low energy consumption to obtain drinkable water in underdeveloped countries. In addition, gel scientists have developed polyelectrolytes with soft and wet nature, which could serve biomechanical roles in blood vessels, articular cartilages, and muscles due to its good adhesion to cells and proper elastic modulus. Finally, microfluidic chip-based polyelectrolyte diode and transistor may open new intelligent microprocessor working in an aqueous solution, such as sea water and human body.

Bibliography

[1] D. A. Mortimer, Polym Int 1991, 25, 29-41.

[2] T. Boudou, T. Crouzier, K. Ren, G. Blin, C. Picart, Adv Mater 2009, 21, 1-27.

[3] Y. M. Chen, N. Shirashi, H. Satokawa, A. Kakugo, N. Tetsuharu, J. P. Gong, Y. Osada, K. Yamamoto, J. Ando, Biomaterials 2005, 26, 4588-4596.

[4] Y. Osada, J. P. Gong, Adv Mater 1998, 10, 827-837.

[5] P. J. Norris, E. S. Rosenberg, J. Mol. Med. 2002, 80, 397 - 405.

[6] T. Hanscheid, Clin. Lab. Haem. 1999, 21, 235 - 245.

[7] C. Lancaster, M. Kokoris, M. Nabavi, J. Clemmens, P. Maloney, J. Capadanno, J. Gerdes. et al., Methods 2005, 37, 120 - 127.

[8] W. B. Gross, J. Am. Vet. Med. A 1984, 185, 343 - 343.

[9] L. K. Nielsen, G. K. Smyth, P. F. Greenfield, Biotechnol. Progr. 1991, 7, 560 - 563.

[10] L. A. Herzenberg, D. Parks, B. Sahaf, O. Perez, M. Roederer, Clin Chem 2002, 48, 10, 1819-1827.

[11] J. K. Nicholson, D. Stein, T. Mui, R. Mack, M. Hubbard, T. Denny, Clin. Diagn. Lab. Immunol. 1997, 4, 309 - 313.

[12] U. D. Larsen, G. Blankenstein, J. Branebjerg, Transducers 97 1997, 2, 1319 - 1322.

[13] O. A. Saleh, L. L. Sohn, Rev. Sci. Instrum. 2001, 72, 4449 - 4451.

[14] G. M. Whitesides, Nature 2006, 442, 27, 368-373.

[15] J. Zhe, A. Jagtiani, P. Dutta, J. Hu, J. Carletta, J. Micromech.

Microeng. 2007, 2, 304 - 313.

[16] S. Gawad, L. Schild, P. H. Renaud, Lab Chip 2001, 1, 76 - 82.

[17] D. Satake, H. Ebi, N. Oku, K. Matsuda, H. Takao, M. Ashiki, M. Ishida, Sens. Actuators B Chem. 2002, 83, 77 - 81.

[18] M. G. Ormerod, Flow cytometry: A Practical Approach, Oxford University Press, Oxford 2000.

[19] S. Gawad, K. Cheung, U. Seger, A. Bertsch, A., P. Renaud, Lab Chip 2004, 4, 241 - 251.

[20] H. Tang, Y. F. Gao, IEEE Sens. J. 2005, 5, 1346 - 1352.

[21] J. Kruger, K. Singh, A. O'Neill, C. Jackson, A. Morrison, P. O'Brien, J. Micromech. Microeng. 2002, 12, 486 - 494.

[22] A. Y. Fu, H. P. Chou, C. Spence, F. H. Arnold, S. R. Quake, Anal. Chem. 2002, 74, 2451 - 2457.

[23] D. Huh, W. Gu, Y. Kamotani, J. B. Grotberg, S. Takayama, Physiol. Meas. 2005, 26, R73 - R98.

[24] T. D. Chung, H. C. Kim, Electrophoresis 2007, 28, 4511 - 4520.

[25] H. Chun, T. D. Chung, H. C. Kim, Anal. Chem. 2005, 77, 2490-2495.

[26] H. Chun, H. C. Kim, T. D. Chung, Lab Chip 2008, 8, 764-771.

[27] D. Li, Electrokinetincs in microfluidics, Elsevier 2004.

[28] R. C. Lo, V. M. Ugaz, Lab Chip 2008, 8, 2135-2145.

[29] T. Glawdel, C. L. Ren, Mech Res Commun 2009, 36, 75-81

[30] S. Joo, T. D. Chung, H. C. Kim, Sensor Actuat B-Chem 2007, 123, 1161-1168.

[31] M. H. Oddy. J. G. Santiago, J. C. Mikkelsen, Anal Chem 2001,

73, 5822-5832.

[32] H. Chun, H. C. Kim, T. D. Chung, Lab Chip 2008, 8, 764-771.

[33] Y-C. Wang, A. L. Stevens, J. Han, Anal Chem 2005, 77, 4293-4299.

[34] H. Chun, T. D. Chung, J. M. Ramsey, Anal Chem 2010, 82, 6287-6292.

[35] L-J. Cheng, L. J. Guo, ACS Nano 2009, 3, 575-584.

[36] J-H. Han, K. B. Kim, H. C. Kim, T. D. Chung, Angew Chem Int Edit 2009, 121, 3888-3891.

[37] G. Maltezos, R. Nortrup, Appl Phys Lett 2003, 83, 2067.

[38] R. Karnik, R. Fan, M. Yue, D. Li, P. Yang, A. Majumdar, Nano Lett 2005, 5, 943-948.

[39] M. A. Cooper, Nat Rev Drug Discov 2002, 1, 515-528.

[40] K. Zhang, L-B. Zhao, S-S. Guo, B-X. Shi, T-L. Lam, Y.-C. Leung, Y. Chen, X-Z. Zhao, H. L. W. Chan, Y. Wang, Biosens Bioelectron 2010, 26, 935-939.

[41] N. R. Frometa, Biotecnologia Aplicada 2006, 23, 320-323.

[42] J. Fritz, Analyst 2008, 133, 855-863.

[43] A. K. Bryan, A. Goranov, A. Amon, S. R. Manalis, P Natl Acad Sci USA 2010, 107, 999-1004.

[44] E. Stern, J. F. Klemic, D. A. Routenberg, P. N. Wyrembak, D. B. Turner-Evans, A. D. Hamilton, D. A. LaVan, T. M. Fahmy, M. A. Reed, Nature 2006, 445, 519-522.

[45] Y. Cui, Q. Wei, H. Park, C. M. Lieber, Science 2001, 293, 1289-1292.

[46] G. Zheng, F. Patolsky, Y. Cui, W. U. Wang, C. M. Lieber, Nature Biotech 2005, 23, 1294-1301.

[47] K. Kneipp, M. Moskovits, H. Kneipp, Surface-Enhanced Raman Scattering: Physics and Applications, Springer 2006.

[48] P. Kambhampati, C. M. Child, M. C. Foster, A. Campion, J Chem Phys 1998, 108, 5013-5026.

[49] S. Lal, N. K. Grady, J. Kundu, C. S. Levin, J. B. Lassiter, N. J. Halas, Chem Soc Rev 2008, 37, 898-911.

[50] R. J. C. Brown, M. J. T. Milton, J Raman Spectrosc 2008, 39, 1313-1326.

[51] J. G. Fan, Y. P. Zhao, Langmuir 2008, 24, 14172-14175.

[52] A. Tao, F. Kim, C. Hess, J. Goldberger, R. He, Y. Sun, Y. Xia, P. Yang, Nano Lett 2003, 3, 1229-1233.

[53] M. Yang, R. N. Alvarez-Puebla, H-S. Kim, P. Aldeanueva-Potel, L. M. Liz-Marzan, N. A. Kotov, Nano Lett 2010, 10, 4013-4019.

[54] D. R. Whitcomb, B. J. Stwertka, S. Chen, P. J. Cowdery-Corvan, J Raman Spectrosc 2008, 39, 421-426.

[55] A. M. Michaels, J. Jiang, L. Brus, J Phys Chem B 2000, 104, 11965-11971.

[56] H. Xu, E. J. Bjerneld, M. Kall, L. Borjesson, Phys Rev Lett 1999, 83, 4357.

[57] J-W. Chen, Y. Lei, X.-J. Liu, J.-H. Jiang, G.-L. Shen, R.-Q. Yu, Anal Bioanal Chem 2008, 392, 187-193

[58] D-K. Lim, K-S. Jeon, H. M. Kim, J-M. Nam, Y. D. Suh, Nat Mater 2010, 9, 60-67.

[59] Y. Lu, G. L. Liu, L. P. Lee, Nano Lett 2004, 5, 5-9.

[60] G. L. Liu, L. P. Lee, Appl Phys Lett 2005, 87, 074101.

[61] T. Park, S. Lee, G. H. Seong, J. Choo, E. K. Lee, Y. S. Kim, W. H. Ji, S. Y. Hwang, D-G. Gweon, S. Lee, Lab Chip 2005, 5, 437-442.

[62] G. Wang, C. Lim, L. Chen, H. Chon, J. Choo, J. Hong, A. de Mello, Anal Bioanal Chem 2009, 394, 1827-1832.

[63] S. Lee, S. Joo, S. Park, S. Kim, H. C. Kim, T. D. Chung, Electrophoresis 2010, 31, 1623-1629.

[64] M. Wang, N. Jing, I. H. Chou, G. L. Cote, J. Kameoka, Lab Chip 2007, 7, 630-632.

[65] L. Tong, M. Righini, M. U. Gonzalez, R. Quidant, M. Kall, Lab Chip 2009, 9, 193-195.

[66] A. M. Schwartzberg, C. D. Grant, A. Wolcott, C. E. Talley, T. R. Huser, R. Bogomolni, J. Z. Zhang, J Phys Chem B 2004, 108, 19191-19197.

[67] L. Chen, J. Choo, Electrophoresis 2008, 29, 1815-1828.

[68] L. X. Quang, C. Lim, G. H. Seong, J. Choo, K. J. Do, SK. Yoo, Lab Chip 2008, 8, 2214-2219.

[69] W. Wang, C. Yang, X. Cui, Q. Bao, C. Li, Microfluid Nanofluid 2010, 9, 1175-1183.

[70] S. J. Lee, Z. Guan, H. Xu, M. Moskovits, J Phys Chem C 2007, 111, 17985-17988.

[71] J-H. Tian, B. Liu, X. Li, Z-L. Yang, B. Ren, S-T. Wu, N. Tao, Z-Q. Tian, J Am Chem Soc 2006, 128, 14748-14749.

[72] G. Chen, Y. Wang, M. Yang, J. Xu, S. J. Goh, M. Pan, H. Chen,

J Am Chem Soc 2010, 132, 3644-3645.

[73] R. Kurita, K. Hayashi, T. Horiuchi, O. Niwa, K. Maeyama, K. Tanizawa, Lab Chip 2002, 2, 34-38.

[74] K. L. Davis, M. L. McGlashen, M. D. Morris, Langmuir 1992, 8, 1654-1658.

국문 초록

본 논문은 양전하성 pDADMAC (poly-diallyldimethylammonium chloride) 폴리머와 음전하성 pAMPSA (poly-2-acrylamido-2-methyl-1-propanesulfonic acid) 폴리머를 이용하여 마이크로 유동칩에 직접이 가능한 폴리머 전극을 개발하고, 폴리머 전극이 집적된 마이크로 유동 시스템의 디자인 및 제작 방법 그리고 다양한 응용 사례 및 대체 전극으로서의 가능성에 대해 연구한 논문이다.

첫째, 폴리머 전극이 집적된 마이크로 유동칩의 응용 연구를 위하여 양극성 폴리머인 pDADMAC가 집적된 적혈구 계수 시스템을 개발하였다. 제안된 마이크로 유동칩 기반의 세포 계수 시스템은 마이크로 채널 양단에 제작된 폴리머 전극 사이로 적혈구가 지나 갈 때 발생하는 직류 임피던스의 변화를 감지하도록 설계되었으며, 이 때 발생하는 임피던스 변화의 크기와 개수를 통하여 우리는 세포의 크기 및 개수 정보를 획득할 수 있었다. 크기가 다른 3가지 마이크로 형광 비드 (7.2, 10.0, and 15.0 μm)를 이용하여 세포 크기에 따른 시스템의 임피던스 정보를 확인 및 보정하였으며, 적혈구 크기와 유사한 7.2 μm 형광 비드를 다양한 농도로 준비하여 개발된 시스템과 상용 동물용 혈구 계수기에 동시에 테스트함으로서 시스템의 데이터 획득 정확도를 검증하였다. 마지막으로 사람으로부터 채혈된 전혈을 이용한 실험을 진행하였으며 획득된 적혈구 계수 결과를 임상용 혈구 계수기와 비교함으로서 개발된 시스템의 임상 적용 가능성을 확인해 보았다.

둘째, 폴리머 전극을 이용한 이온 제어 가능성 및 응용 연구를 위하여 본 연구에서는 폴리전해질을 이용한 접합형 전계 효과 트랜지스터 (Polyelectrolyte Junction Field Effect Transistor, pJFET)을 개발하였다.

반대 극성을 지닌 pDADMAC와 pAMPSA 폴리머를 마이크로 채널 벽면에 제작하였으며, 이를 통해 전해질 용액이 채워진 마이크로 채널의 국소 부위에 양이온과 음이온을 효과적으로 제어하고 이온 공핍 영역을 발생 시킬 수 있었다. 폴리머 전극의 이온 추출 정도를 제어하는 게이트 전압을 통하여 이온 공핍 영역을 확장 혹은 축소시킬 수 있었으며, 이에 따라 소스-드레인 사이에 흐르는 이온 전류를 제어할 수 있음을 밝혔다.

마지막 응용 연구로서 네 번째 챕터에서는 라만 스케터링의 증강 효과(Surface-enhanced Raman Scattering, SERS)를 마이크로 유동칩에서 구현하기 위하여 폴리머 전극 기반의 금나노 입자 농축 시스템을 개발하였다. 마이크로 채널에 고루 부유하고 있는 금나노 입자는 음전하성 폴리머 전극의 이온 선택적 추출 현상에 의해 발생한 이온 공핍 영역 전단부에서 농축이 가능하다. 따라서 금나노 입자가 농축된 마이크로 채널에 레이저를 조사하면 금나노 입자 사이의 'Hot spot' 영역에 존재하는 샘플의 라만 신호를 증강된 형태로 관찰이 가능함을 알 수 있었다. 분석화학적 적용 사례를 보고하기 위하여 본 연구에서는 대표적인 신경전달물질로 알려진 히스타민의 검출 테스트를 진행하였다.

키워드: 폴리전해질, 동전기학, 미세유체공학, 세포 계수기, 폴리머 접합형 전계 효과 트렌지스터 (pJFET), 표면 강화 라만 산란 (SERS)

Student Number : 2007-21272

Acknowledgement

감사의 글

학위 논문을 마무리 하면서 6년 동안의 대학원 과정을 회상해 봅니다. 2006년 11월 교수님을 따라 병원에서 여전도회관에 위치한 MELab 연구실을 방문했을 때 그 초조함과 설레임은 지금도 기억에 남아있습니다. 기대에 부응하듯 실험 기자재로 가득한 실험실과 분주하게 실험하고 계셨던 선배님들의 모습이 여전히 생생합니다. 본 받고 싶고 후배들에게 귀감이 되시는 선배님들이 많았던 MELab에서의 대학원 생활은 저에게 제 2의 도약의 힘을 만들어 주었습니다. 그 동안 받았던 후광을 앞으로 학계 및 사회에 계신 선배님들과 후배님들을 위해 더 멀리 비출 수 있는 그런 사람으로 거듭 날 수 있도록 불철주야 최선을 다하겠습니다.

입학부터 박사 졸업심사까지 누구보다 걱정하시고 신경써주신 김희찬 지도 교수님께 무한한 감사의 말씀을 드립니다. 입학도 하지 않은 저에게 파격적으로 일본 도쿄에서 열리는 2006 마이크로타스 학회를 보내주신 덕분에 누구보다 빨리 제가 해야 할 연구에 대해서 개괄할 수 있었고 그 눈높이를 높게 잡을 수 있었습니다. 무엇보다 지난 학위기간동안 보여주신 저에 대한 믿음과 신뢰는 그 어떤 칭찬보다 저에겐 힘과 용기가 되었습니다. 그 믿음에 보답하고자 대학원 생활동안 스스로 마음속 중심을 잡으려고 노력했었고 후회 없이 최선을 다해 연구에 몰입했습니다. 부끄럽지 않은 제자가 되기 위해 가슴속에 교수님을 품고 힘들 때 마다 회상하며 살아가겠습니다. 감사하고 존경합니다 교수님.

저에게 마이크로플루이딕 시스템의 모든 것을 전수해주신 화학부 정택동 교수님께 이 글을 빌어 다시 한 번 감사의 말씀을 드립니다. 성신여대 화학부 제직하실 때부터 서울대 화학부 정교수 진급하시기까지 교수님 옆에 있으면서 전공 지식뿐만 아니라 훌륭한 연구자가 되기 위해서는 어떻게 해야 하는가?에 대한 해답을 주셨습니다. 교수님의 박학다식함을 늘 존경했고 본받고 싶었습니다. 그동안 직속 제자가 아님에도 불구하고 항상 불러주셔서 실험 디자인과 논문 교정 그리고 화학과 학생들과 함께 할 수 있게 배려해주셔서 감사합니다. 졸업 이후에도 자주 찾아 뵙고 인사 드리겠습니다 교수님.

졸업 1년전부터 저희과에 부임하신 허동은 교수님 미국에서 좋은 연구로 국위선양 하시고 돌아오셨을 때 허교수님과 랩을 구성하면서 정말 많은 경험을 할 수 있었습니다. 허교수님을 모실 수 있었던 1년이 저에게는 더할나위 없이 소중한 경험이었습니다. 섹시한 발표자료! 훌륭한 연구의 기준을 한층 더 높일 수 있었던 기회였습니다. 감사합니다 교수님.

그리고 두 분의 연구실 출신 교수님이신 천홍구 교수님, 주세경 교수님 저에게 희망과 자신감을 주셔서 감사합니다. 칩 팀의 양대 산맥이신 두 분의 선배님이 계셨기에 제 연구에 자부심을 가질 수 있었고 그 가치를 더 높일 수 있었습니다. 박사학위 기간동안 두 선배님을 모실 수 있었던 건 행운이었다고 생각합니다. 존경합니다 홍구형, 세경형 ^^

우리 MELab 식구들에게 어떻게 감사의 말씀을 드려야할지요. 먼저 연구실 살림을 위해 불철주야 연구비 관리와 월급을 챙겨주신 백지영 목소리의 이진경 비서님 감사드려요. 저의 롤 모델이셨던 강재민 박사님 첫 논문을 쓸 때 분야가 다름에도 불구하고 첨삭과 온라인 제출 그리고 리비전까지 도와주셔서 감사합니다. 첫 논문 작성 때 형의 도움에 눈물을 좔좔 흘렸습니다. 훈남 카리스마 김동우 박사님 졸업 시기에 바쁘신 와중에도 커피 한잔과 진로 상담 시간을 내주셔서 너무 감사해요. 근데 어쩜 그렇게 여전히 훈남이세요?^^ 그동안 누구보다 연구실을 위해 헌신하신 공현중 교수님 곧 현중 주니어가 세상에 나온다고 들었습니다. 형수님 그리고 아기와 행복하시길 바래요. 자주 찾아뵐께요 형^^ 작년에 진급하신 이정찬 교수님 늘 웃음과 학문적 열정으로 학생들과 함께하는 모습이 너무 보기 좋았습니다. 서울대 의공학과의 대들보라 감히 자신합니다. 예전 종로의 그 곳에서 교수님과 술 한잔 또 하고 싶습니다. 지금 열심히 창업중이신 이규진 박사님 억대 매출의 그날이 오면 꼭 쏘시는거 아시죠? 어얼리 어댑터 현석이 형, 진정한 연구자 우리 우영 형님, 만물박사 일형 형님, 얄라용~대구 사나이 김선권 박사님, 조각 미남 덴티스트 훈기 형님, MBA 유학 준비하고 있는 종호, 좐스 홉킨스 정민양, 박선미 부부, 천경우, 차재평에게 이 글을 빌어 감사의 말씀을 전합니다. 곧 연구실로 컴백하는 내 친구 구윤서 박사학위 입학을 진심으로 축하하고 영실이와 함께 자주 보자꾸나 알았지? 칩 팀의 첫 후배였던 우리 기현이 너와의 그 날밤은 아직도 생생하다 알지? 유학 꼭 잘 되길 진심으로 형은 바란다. 칩 팀의 맏형 종민 형님 사업 준비하시는거 꼭 대박

나세요. 그리고 저의 정신적 지주 박상윤 박사님 그리고 형수님이신 호선누나 두 분이 계셨기에 대학원 생활이 너무 행복했어요. 평생 두 분과 함께할 수 있으면 좋겠습니다. 상윤형 촉오로 사랑합니다~!!! 그리고 “있어요~” 치열이 다부진 연구 열정과 따뜻한 마음에 형과 연구실 식구들은 너에게 빠져들고 있단다 고마워 치열아. 우리 연구실 3호 커플 노승우, 조인아 내가 감사의 글에 도장 빡~! 찍었으니깐 이제 빼도 박도 못하는겨 언능 결혼해라 알았지? 승우야 형 잘했어? 아산병원으로 파견가신 우리 똑똑이 장표형, 고려대에 열연구 중인 내 친구 “만지지만” 지만이 진행중인 연구 대박 터트리길 바래요. 지만아 협주곡 연주칩은 언제 나와? 사이언스, 네이쳐 늘 모니터링하고 있다. 귀염이 우리 병욱이 지난해 전문연구요원 준비할 때 얼굴이 반쪽이 되서 놀랬다. 멀리서 학교 다니느라 힘들텐데 형들한테 늘 살갑게 웃어주고 너의 매력에 흠뻑 빠지겠어. 나이는 1살 어리지만 인생 선배 우리 충희 힘들 때마다 옆에서 위로해줘서 고맙고 충희가 있어 늘 활력이 되었다. 쓰고 있는 논문 술술 잘 풀리길 바라고 자주 연락할게 충희야. 1년동안 이벤트 핸들러 하느라 고생한 지흠이, 겸둥이 긍정맨 중우, 그리고 똑똑이 능력가 ROTC 후배 은제에게 감사의 말을 전합니다. 박사 졸업 동기 우리 지원이 제주도 학회 때의 너의 포스를 오빠는 잊을 수가 없다 알지? 졸업하고 자주 연락하자꾸나. 이사 다니느라 고생이 많은 우리 만승이 초집중하고 있는 너를 보니 조만간 뭔일이나도 나겠구나 라는 생각이 든다. 대박 논문 기대할게. 새신랑 사람이 졸업 준비와 결혼으로 많이 정신없지? 대만 공항에서 형과 이야기했던 것 잊지말고 지금처럼 프로페셔널하게 성공의 탄탄대로가 함께하기를 간절히 바랄게. 마지막으로 칩 팀의 대들보 칩팀장겸 유일한 칩팀원인 형선아 간다 간다 했는데 형이 정말 졸업을 해서 이곳을 떠나게 됐구나. 형이 형선이 너에게 무한 애정을 준거 알지? 생각만큼 못해준거 같아 못내 아쉽다. 마지막 칩팀 후배이지만 그동안 보여준 너의 능력은 역시 기대에 부응했다. 한번도 칭찬을 안했지만 이글을 빌어 말해주고 싶구나. 이제는 형보다 칩도 더 잘 만들고 실험 디자인도 잘하고 논문도 잘쓰고 너무 대견하다. 그동안 형 믿고 따라와줘서 고맙다 형선아. 그리고 바쁜 회사일에도 불구하고 학구열을 불태우고 계시는 준형이형, 새로운 신입생 이동헌, 권치헌의 앞날에 기쁨과 성공이 함께 하길 바랍니다.

저에게 화학 실험과 관련하여 무한 애정을 아끼지 않으신 화학부 정택동 교수님 EChem Lab 식구분들에게 감사의 말씀을 드립니다. 매주 금요일 밤 녹두와 낙성

대, 서울대 입구 맛집 탐방과 생화학 공부를 시켜주신 박학다식 황인성 박사님, 한국 전기화학계의 두 거장이신 노마디엔의 존경하는 박세진 박사님, 부한길 박사님 그리고 다정다감 친누나 같은 란아 누나, 이쁜 정민 누나 그동안 도와주셔서 감사합니다. 칩팀 원년 멤버이셨던 공진 팀장님과 찬우형 그리고 연구비 관리뿐만 아니라 여학생들의 정신적 지주가 되어주신 이혜정 비서님께 감사의 말씀을 전합니다. 지금은 MIT에서 열심히 연구하며 국위선양하고 있을 한지형 박사 그동안 논문 및 실험 디자인에 도움을 줘서 고맙습니다. 삼성전자에서 열심히 군것질중인 송연주, 정현주 그리고 라이벌 회사 LG전자의 5등신 미녀 김지연에게 감사의 말을 전하며 그들의 깨방정이 여전히 그립습니다. 정현주, 김지연 트리오의 브아걸 춤은 당대 최고! 중국에서 홀로 유학와서 좋은 논문 많이 쓰면서 당차게 연구실 생활하고 있는 청초미인 려림이, 연구실에서 유일하게 Fab과 싸워서 승리하신 듬직하고 우직한 충무형, 스마일 배방장 제현이, 성신여대 원년 멤버인 최강동안 범진이, 연구실 맏언니 진영누나, 진짜 싸나이 동훈이, 얼굴도 마음도 이쁜 은중이, 당찬 포부를 가지고 연구와 사랑에 빠진 창수, 반쪽 장혁 연구실 최강 훈남 성열이, 긍정의 마인드와 따뜻한 마음을 가진 승룡이, 동훈이의 운명 솔지, 똑똑이 동협이, 누나들의 타겟 수홍이, 그리고 신입생 우혁이와 소영이에게 감사의 인사를 드립니다.

그리고 1년 동안 허동은 교수님 BioLines Lab 셋업에 너무나 고생이 많았던 코넬대학의 수재 듬직한 랩장 진우, 그리고 심지가 올곧은 이쁜 정윤이 그동안 부족한 저를 믿고 따라와 줘서 너무 고맙습니다. 그리고 신입생 도윤이와 지수, 인턴연구원 서연이 오래 함께 지내지 못해 아쉽지만 진우와 정윤이를 도와 멋진 연구 결과 얻으리라 기대합니다.

끝으로 정신적 지주 사랑하는 아버지, 힘든 새벽 식당일 하시면서 나아주시고 길러주신 어머니에게 지금의 박사 학위의 모든 영광을 돌립니다. 아버지, 어머니 진심으로 감사하고 존경하고 사랑합니다. 그리고 주말마다 찾아와서 비타민같이 식구들에게 기쁨을 주셨던 우리 매형, 누나, 조카 예림이, 예준이, 매부, 여동생, 조카 병준이에게 감사의 말을 전합니다. 그리고 지난 10년동안 가진 것 없는 만년 학생이었던 저에게 세상에서 제일 멋지고 잘난 사람이라고 한결같이 말해줬던 한 사람, 사랑하는 나의 용순이에게 이 논문을 바칩니다.

- 2013년 2월 김 광 복 드림 -